Development and Validation of a System Thermal-Hydraulic/CFD Codes Coupling Methodology for Multi-Scale Transient Simulations of Pool-Type Reactors

Antonio Toti

Promotoren: prof. dr. ir. J. Vierendeels, dr. F. Belloni
Proefschrift ingediend tot het behalen van de graad van
Doctor in de ingenieurswetenschappen: werktuigkunde-elektrotechniek

UNIVERSITEIT
GENT

Vakgroep Mechanica van Stroming, Warmte en Verbranding
Voorzitter: prof. dr. ir. J. Vierendeels
Faculteit Ingenieurswetenschappen en Architectuur
Academiejaar 2017 - 2018

ISBN 978-94-6355-142-7
NUR 950
Wettelijk depot: D/2018/10.500/60

Members of the examination committee

Chair

prof. dr. ir. Filip De Turck	Ghent University

Reading Committee

prof. dr. Nicola Forgione	University of Pisa
dr. Angel Papukchiev	Gesellschaft für Anlagen- und Reaktorsicherheit (GRS)
ir. Katrien Van Tichelen	SCK•CEN
prof. dr. ir. Joris Degroote	Ghent University
prof. dr. ir. Geraldine Heynderickx	Ghent University

Other members

prof. dr. ir. Jan Vierendeels	Ghent University
dr. Francesco Belloni	SCK•CEN

Preface

This dissertation is submitted for the doctoral degree at the Department of Flow, Heat and Combustion Mechanics of Ghent University in Belgium. The research was carried out in the Nuclear Systems Physics (NSP) expert group at the Belgian Nuclear Research Centre SCK•CEN, and received financial support by the project MYRTE, established within the Euratom research and training programme 2014–2018 under grant agreement No 662186.

In the first place, I would like to express my deepest gratitude to my advisor Professor Jan Vierendeels for his constant support, guidance and advice. His explanations on computational fluid dynamics and the inputs on code coupling algorithms have been crucial for the success of the project. He has been the best supervisor I could wish for.

Complementary, I would like to express my sincere gratitude for the daily support of my SCK•CEN supervisor Francesco Belloni, always available to provide guidance and insights. I am also deeply grateful to Gert Van den Eynde, Head of NSP and PhD co-supervisor, and Michèle Coeck, Head of the SCK•CEN Academy for Nuclear Science and Technology, for providing me with the opportunity and the means to perform my doctoral research.

I would like to extend my gratitude to all the colleagues at SCK•CEN for creating a very enjoyable work environment, that enriched my professional and personal experience from many perspectives. Particular thanks go to the colleagues of the MYRRHA team, especially the members of the reactor safety analysis group Guy Scheveneels, Diego Castelliti, Tewfik Hamidouche and Dario Bisogni for the countless insightful discussions and interactions. A warm thanks goes to Katrien Van Tichelen and to Steven Keijers for their collaboration and support on the work performed within the European projects MYRTE and SESAME. With regard to those, I would like to thank all the colleagues from the partner

organizations for sharing so many enriching experiences around Europe in occasion of the project meetings.

I am grateful also to the colleagues at Ghent University, particularly to Joris Degroote for his precious inputs on high performance computing and to Yves Maenhout for promptly helping me in sorting out any issue related to the use of the computer clusters.

I would like to thank also the Jury members for accepting the commitment of evaluating my research work and this dissertation.

I also acknowledge the support received from the Commissie Wetenschappelijk Onderzoek (CWO) at Ghent University, which funded my participation to two major international conferences.

Before my last personal acknowledgment, I would like to express the deep sense of gratitude that I feel particularly towards Francesco, Joris and Katrien for the personal support I have been able to rely on during the last, challenging phase of my PhD. Thank you!

Finally, I would like to thank the members of my family for their unconditional support, and for motivating me throughout these years. A very special thank you to Veronica, for believing in me and staying always by my side during this adventure.

Antonio Toti
June 24, 2018

Contents

Nomenclature

Greek Letters

α	Volume fraction	(-)
β	Thermal expansion coefficient	$(^{\circ}C^{-1})$
Δ	Difference	(-)
δ	Perturbation	(-)
δ_{ij}	Kronecker delta	
ϵ	Convergence criterion	
ϵ	Surface roughness	(m)
ϵ	Turbulent kinetic energy dissipation rate	$(J \cdot kg^{-1} \cdot s^{-1})$
Γ	Boundary	
Γ	Volumetric mass transfer rate	$(kg \cdot m^{-3} \cdot s^{-1})$
γ	Porosity	(-)
λ	Wall laminar friction factor	(-)
μ	Dynamic viscosity	$(kg \cdot m^{-1} \cdot s^{-1})$
ν	Degree of freedom	(-)
ν	Kinematic viscosity	$(m^2 \cdot s^{-1})$
Ω	Domain	
ω	Specific turbulence dissipation rate	(s^{-1})
ω	Under-relaxation factor	(-)
ϕ	Solver global operator	
ρ	Density	$(kg \cdot m^{-3})$
σ	Turbulent Prandtl number	(-)
τ	Stress tensor	$(kg \cdot m^{-1} \cdot s^{-2})$

Symbols

$\mathbf{I}$	Identity matrix	
$\mathbf{J}$	Jacobian matrix	
$\mathbf{R}$	Coupling residual vector	
$\mathbf{U}$	Coupling input vector	
$\mathbf{Y}$	Coupling output vector	
$\dot{m}$	Mass flow rate	$(kg \cdot s^{-1})$
A	Surface	(m^2)

C_p	Specific heat	$(J \cdot kg^{-1} \cdot K^{-1})$
D	Diameter	(m)
D_h	Hydraulic diameter	(m)
$DISS$	Energy dissipation function	$(W \cdot m^{-3})$
E	Fluid specific energy	$(J \cdot kg^{-1})$
Eu	Euler number $= \frac{p}{\rho u^2}$	(-)
f	Body force	$(N \cdot m^{-3})$
f	Wall turbulent friction coefficient	(-)
FIF	Interphase drag coefficient for liquid phase	(s^{-1})
FIG	Interphase drag coefficient for vapor phase	(s^{-1})
Fr	Froude number $= \frac{u^2}{\rho \Delta H}$	(-)
FWF	Wall drag coefficient for liquid phase	(s^{-1})
FWG	Wall drag coefficient for vapor phase	(s^{-1})
g	Gravitational acceleration	$(m \cdot s^{-2})$
h	Fluid specific enthalpy	$(J \cdot kg^{-1})$
h	Heat transfer coefficient	$(W \cdot m^{-2} \cdot K^{-1})$
k	Thermal conductivity	$(W \cdot m^{-1} \cdot K^{-})$
k	Turbulent kinetic energy	$(J \cdot kg^{-1})$
L	Length	(m)
Nu	Nusselt number $= \frac{hD}{k}$	(-)
P	Rod pitch	(m)
p	Pressure	(Pa)
Pe	Péclet number $= \frac{C_p \rho u D}{k}$	(-)
Q	Power	(W)
q''	Surface heat flux	$(J \cdot m^{-2} \cdot s^{-1})$
r	Residual vector term	
Re	Reynolds number $= \frac{\rho u D}{\mu}$	(-)
Ri	Richardson number $= \frac{g \beta \Delta H \Delta T}{u^2}$	(-)
S	Volumetric heat source	$(J \cdot m^{-3} \cdot s^{-1})$
s	Wetted perimeter	(m)
T	Temperature	$(^{\circ}C)$
t	Time	(s)
U	Specific internal energy	$(J \cdot kg^{-1})$
u	Generic coupling vector term	
u	Velocity	$(m \cdot s^{-1})$
u^+	Dimensionless velocity	(-)
V	Volume	(m^3)
X	Quality	(-)
x	Space coordinate	(m)
y^+	Dimensionless wall distance	(-)

Superscripts

$j, j-1, j+1$	Spatial noding indices for junctions
k	Coupling iteration
n	Time step counter
w	Quantity at wall

Subscripts

b	Boron
c	Core
c_in	Core inlet
c_out	Core outlet
f	Liquid phase
fr	Friction
g	Vapor/gas phase
hx	Heat exchanger
hyd	Hydraulic
m	Mixture property
n	Non condensable
phx	Primary heat exchanger
pp	Primary pump
r	Rod
t	Turbulent
th	Thermal
w	Wire
wg, wf	Wall to vapor/gas, wall to liquid

Acronyms

1D	One-Dimensional
3D	Three-Dimensional
ACS	Above Core Structure
ADS	Accelerator-Driven System
ANL	Argonne National Laboratory
ASTRID	Advanced Sodium Technological Reactor for Industrial Demonstration
BC	Boundary Condition
BPG	Best practice guideline
BWR	Boiling Water Reactor
CEA	Commissariat à l'énergie atomique et aux énergies alternatives
CFD	Computational Fluid Dynamics
CR	Control Rod
DHR	Decay Heat Removal
ENEA	Agenzia nazionale per le nuove tecnologie, l'energia e lo sviluppo economico sostenibile

ESNII European Sustainable Nuclear Industrial Initiative
FA Fuel Assembly
GCR Gas Cooled Reactor
GEN-IV Generation-IV
GFR Gas Fast Reactor
GRS Gesellschaft für Anlagen- und Reaktorsicherheit
HLLW High Level Long-lived Waste
HWR Heavy Water Reactor
HX Heat Exchanger
INEEL Idaho National Laboratory and Environmental Laboratory
INL Idaho National Laboratory
IPS In-Pile Section
IVFHM In-Vessel Fuel Handling Machine
IVFS In-Vessel Fuel Storage
KAERI Korean Atomic Energy Research Institute
KTH Kungliga Tekniska Högskolan
LBE Lead-Bismuth Eutectic
LDC Local Defect Correction
LES Large Eddy Simulation
LFR Lead Fast Reactor
LLFP Long-lived Fission Products
LMFR Liquid Metal-cooled Fast Reactor
LOF Loss Of Flow
LOOP Loss Of Offsite Power
LP Lower Plenum
LWR Light Water Reactor
MA Minor Actinide
MOC Method of Characteristics
MOX Mixed OXide
MSLB Main Steam Line Break
MTR Material Testing Reactor
MYRRHA Multi-purpose hYbrid Research Reactor for High-tech Applications
NPP Nuclear Power Plant
NRC Nuclear Regulatory Commission
PCT Peak Cladding Temperature
PDE Partial Differential Equation
PHX Primary Heat Exchanger
PIRT Phenomena Identification and Ranking Table
PP Primary Pump
PSI Paul Scherrer Institute
PTS Pressurized Thermal Shock

PVM	Parallel Virtual Machine
PWR	Pressurized Water Reactor
RANS	Reynolds-Averaged Navier Stokes
ROM	Reduced Order Model
SFR	Sodium Fast Reactor
SNETP	Sustainable Nuclear Energy Technology Platform
STH	System Thermal-Hydraulic
TRU	TRansUranic
UDF	User Defined Function
UP	Upper Plenum
UQ	Uncertainty Quantification
VHTR	Very High Temperature Reactor
VOF	Volume Of Fluid

Samenvatting

Voor het MYRRHA (Engelse afkorting voor Multi-purpose hYbrid Research Reactor for High-tech Applications, ofwel multifunctionele hybride onderzoeksreactor voor hoogtechnologische toepassingen) project werkt het Belgisch studiecentrum voor kernenergie SCK•CEN aan het ontwerpen en ontwikkelen van een flexibele bestralingsfaciliteit dat wordt aangedreven door een deeltjesversneller (Accelerator Driven System of ADS) waardoor de reactor zowel met een kritische als met een sub-kritische kern kan werken. Naast materiaaltesten en onderzoek naar nucleaire brandstof, is het doel van de reactor om de haalbaarheid van de ADS technologie aan te tonen voor de transmutatie van langlevend nucleair afval alsook om een demonstratiereactor te zijn voor vierde generatie reactoren met koeling op basis van zware gesmolten metalen. De MYRRHA reactor is van het pooltype en maakt gebruik van koeling met gesmolten lood-bismuth.

De innovatieve configuratie van het primaire circuit zorgt ervoor dat er nieuwe modellerings- en simulatietools nodig zijn om het ontwerp en de veiligheidsanalyses te ondersteunen. Het gebruik van een pooltype primair koelsysteem, wat typisch isvoor een loodgekoelde reactor, gaat gepaard met complexe koelvloeistofstromingsvelden en driedimensionale stromingseffecten, zoals menging en thermische stratificatie in grote plena, die mogelijk van invloed zijn op het integrale systeemgedrag tijdens plotselinge overgangen zoals het verlies van stroming,asymmetrische condities en andere fenomen en bijgevolg een impact kunnen hebben op relevante veiligheidsparameters. In het bijzonder kan lokale stromingsmenging en een driedimensionaal gedrag van het temperatuursprofiel de evolutie van de koelstroming gedurende de transitie van gedwongen naar natuurlijke convectie beïnvloeden en de ontwikkeling van een thermische stratificatie kan de doeltreffendheid van het passieve noodkoelingssysteem ondermijnen. Deze bovengenoemde fenomenen zijn moeilijk te voorspellen met standaard industriële thermisch-hydraulische systeemcodes (System Thermal-Hydraulic of STH) die voor

veiligheidsbeoordelingen van kernreactoren gebruikt worden. Deze codes die gebaseerd zijn op ééndimensionale lumped parameterformuleringen waren oorspronkelijk ontwikkeld voor de analyse van looptype systemen en zijn niet gevalideerd voor de simulatie van de fysische fenomenen in een pooltype reactor. Moderne numerieke simulatiecodes voor stromingsanalyses (Computational Fluid Dynamics of CFD codes) zijn daarom van bijzonder belang als het gaat om het verkrijgen van een realistischer weergave van complexe stromings- en warmteoverdrachtsfenomenen. Daarom is het gebruik hiervan in thermisch-hydraulische en veiligheidsanalyses voor nucleaire reactoren sterk toegenomen. Echter het gebruik van dergelijke hulpmiddelen voor integrale systeemanalyses is rekenintensief en vaak niet praktisch voor industriële toepassingen.

Het doctoraatsonderzoek dat in dit proefschrift wordt gepresenteerd is gericht op het ontwikkelen, de verificatie en voorlopige validatie van een nieuwe code, dat gebaseerd is op het geïntegreerde gebruik van de STH- en CFD-codes specifiek voor simulaties van hoge betrouwbaarheid voor geavanceerde kernreactoren. De multi-scale methode die hier wordt voorgesteld koppelt RELAP5-3D, een 1D systeemcode, met Ansys Fluent, een CFD-code en is gebaseerd op een domain decompositie techniek en dynamische uitwisseling van randvoorwaarden aan de koppelingsinterfaces tussen beide codes. Er is een uitgebreid onderzoek verricht naar numerieke koppelingsalgoritmen. Zoals verwacht leidde het gebruik van expliciete koppelingsschema's tot problemen met numerieke instabiliteit, meer bepaald bij de berekening van snelle transienten in incompressibele stromingstoepassingen, door de imbalans van de druk-snelheidskoppeling tussen de verschillende domeinen. De implementatie van impliciete schema's zorgde voor numerieke stabiliteit en een significante verbetering van de resultaten. Om het convergentiegedrag te verbeteren en de berekeningskost te reduceren werden dynamische relaxatiealgorithmes onderzocht waaronder de implementatie van een quasi-Newton koppelingsalgorithme wat tot een significante verbetering heeft geleid. Een nieuwe numerieke techniek voor de toepassing van dit koppelingsalgorithme op multi-domein gekoppelde problemen werd ontwikkeld en succesvol toegepast op verschillende cases. Een verdere extensie van de multischaal modelleringscapabiliteit werd bekomen door te implementatie van thermische koppelingsinterfaces voor de berekening van gekoppelde warmteoverdrachtsfenomenen.

Een eerste validatie van de numerieke methode is gebeurd op basis van resultaten van een experimentele campagne met een LBE lus van de TALL-3D faciliteit op de Koninklijke Technische Hogeschool (KTH) in Zweden. Het ontwerp van de experimentele faciliteit was speciaal gedaan

om mutuele feedback te induceren tussen natuurlijke convectie in de loop en complexe 3D menging en stratificatie in een pooltype testsectie om de verificatie en validatie van gekoppelde multischaal berekeningsmethodes toe te laten. De analyse die in dit doctoraat wordt behandeld, is gedaan voor een test met verlies van stroming, waarbij er een oscillerende overgang van gedwongen naar natuurlijke convectie plaatsvindt. In vergelijking met de resultaten van volledige systeemcodemodellen lieten de gekoppelde berekeningen een hogere nauwkeurigheid zien, zowel voor het voorspellen van het globale dynamische gedrag, waarbij werd gekeken naar de karakteristieke frequentie en amplitude van de stromings- en temperatuursoscillaties als voor de voorspelling van de lokale parameters die beïnvloed worden door de 3D stromingen. De verschillen die werden opgemerkt waren hoofdzakelijk te wijten aan tekortkomingen in de codes afzonderlijk wat uiteraard duidelijk maakt dat de validatie van de gebruikte STH en CFD codes een nodige voorwaarde is voor deze gekoppelde berekeningen. Met het oog op de toepassing van de code voor veiligheidsanalyses en het vergunnen van toekomstige reactoren, is er een validatie met een representatievere configuratie nodig die het verder onderzoeken van relevante verschijnselen toestaat. Daarvoor is er een schaalmodel van het primaire systeem van de MYRRHA reactor, een pooltype reactor genaamd E-SCAPE (momenteel in de inbedrijfstellingsfase), ontworpen en gebouwd op het SCK•CEN. Een gekoppeld 1D-3D simulatiemodel is ontwikkeld voor deze faciliteit waarmee een aantal pretest LOF simulaties werden uitgevoerd en vergeleken met simulatieresultaten van 1D systeemcodes. De resultaten van de simulaties bevestigen de validatie van de geïmplementeerde numerieke methode en benadrukt de potentiële onnauwkeurigheid van de 1D modellen wanneer er bepaalde stromingscondities worden ontwikkeld in geval van natuurlijke circulatie. Dit bevestigt dat 3D modelleren wellicht nodig is voor bepaalde transiënte simulaties van snelle reactor. De experimentele testdata die nog moet gegenereerd worden zal eerst moeten gebruikt worden voor de validatie van de codes afzonderlijk, speciaal gericht op de gebieden en fenomenen die voor elk van deze codes relevant zijn. Nadien kunnen integrale testdata gebruikt worden voor de validatie van de koppelingstool.

In het laatste deel van het onderzoek staat het gebruik van de code voor de analyse van de MYRRHA reactor centraal. Het doel was om de prestaties van de code op een eerste toepassing op reactorschaal te beoordelen én relevante thermisch-hydraulische overgangsverschijnselen in de reactor te bestuderen, alsook het bepalen van limieten en mogelijke modelverbeteringen voor de STH-codes. Een transient met verlies van

stroming en reactorstop (LOF) is geanalyseerd en de gevonden resultaten zijn in goede overeenstemming met die van het E-SCAPE schaalmodel. Dit suggereert dat de 3D effecten geen significante impact zullen hebben op het integraal gedrag van de LOF in het huidige ontwerp van MYRRHA, ondanks dat er enkele tegenstrijdigheden waren opgemerkt op bepaalde parameters vanwege de 3D effecten.

Abstract

Within the MYRRHA (Multi-purpose hYbrid Research Reactor for High-tech Applications) project, the Belgian Nuclear Research Centre SCK•CEN is currently developing and designing a flexible irradiation facility, configured as an Accelerator Driven System (ADS) able to operate in critical and sub-critical modes. In addition to material testing and fuel research, the objectives of the reactor are to prove the feasibility of the ADS technology for the transmutation of long-lived nuclear waste as well as to represent a demonstration plant for Generation IV heavy liquid metal-cooled reactors. The current system design features a compact pool-type primary cooling system operating with molten Lead-Bismuth Eutectic (LBE).

The innovative primary system configuration brings along the need of new modeling and simulation capabilities to support the design and safety analyses. The pool-type primary cooling system, typical of liquid metal-cooled fast reactor designs, implies the presence of complex coolant flow fields and three-dimensional effects which might have an impact on the integral system behavior during accidental transients such as loss of flow events, dissymmetric conditions among others, and therefore on safety-relevant parameters. In particular, local flow mixing and a three-dimensional temperature profile distribution can affect the evolution of the coolant mass flow during the transition from forced to natural convection, and the development of thermal stratification may worsen the effectiveness of the passive emergency cooling systems.

The aforementioned phenomena are of difficult prediction for industry-standard System Thermal-Hydraulic (STH) codes, reference tools for nuclear power plants safety assessments. These codes, based on one-dimensional lumped parameters formulation, were originally developed for loop-type systems analysis, and are not validated to correctly simulate the physics of the phenomena occurring in a pool-type reactor. Modern Computational Fluid Dynamic (CFD) codes, on the other side, are of particular interest for more realistic representation of complex

fluid flow and heat transfer phenomena, therefore their use in nuclear reactor thermal-hydraulic and safety analyses is constantly increasing. However, the use of CFD codes for integral system analyses is computational intensive and often not practical for industrial applications.

The PhD research project presented in this dissertation is focused on the development, verification and preliminary validation of novel code infrastructure based on the integrated use of STH and CFD codes, specifically conceived for high-fidelity transient simulations of advanced nuclear reactors. The proposed multi-scale methodology couples the 1D system thermal-hydraulic code RELAP5-3D to the CFD code FLUENT, and is based on the domain decomposition technique and dynamic exchange of boundary conditions at coupling interfaces. An extensive investigation of coupling numerical algorithms was performed. As expected, the use of explicit schemes led to numerical stability issues, especially in the computation of fast transients in incompressible fluid systems, due to imbalance of pressure-velocity fields between the domains. The implementation of implicit schemes led to numerical stability and a significant improvement of the results. To accelerate convergence rates and reduce computational costs, dynamic relaxation algorithms have been investigated; among them, the implementation of a Quasi-Newton coupling algorithm has shown significant improvements of the performance of the tool. A novel numerical technique for the application of this coupling algorithm to multi-domain coupled problems has been developed and successfully applied on a number of cases. A further extension of the multi-scale modeling capabilities has been achieved through the implementation of thermal coupling interfaces for the computation of conjugate heat transfer phenomena.

A first validation of the numerical method against experimental data has been carried out on the basis of the experimental campaign at the TALL-3D facility, a LBE loop in operation at the Royal Institute of Technology (KTH) in Sweden. The design of the experimental facility was specifically conceived to induce mutual feedback between natural circulation in the loop and complex 3D mixing and stratification phenomena in a pool-type test section, in order to support the verification and validation of multi-scale codes coupling approaches. The analysis discussed in this dissertation focused on a loss of flow experimental test, characterized by an oscillating transition from forced to natural circulation. Compared to full system code models, the multi-scale approach showed higher accuracy in the prediction of the dynamic behavior of the system, in terms of characteristic frequency and amplitude of mass flow and temperature oscillations, and of local parameters affected by 3D flows.

The discrepancies observed were mostly attributed to deficiencies in the single codes, confirming that the use of well validated STH and CFD codes is fundamental pre-requisite for accurate coupled analyses. In view of the application of the tool on the safety analysis and licensing of future nuclear reactors, the validation on a more representative configuration which allows for the investigation of relevant phenomena and transient conditions is needed. To this purpose, the pool-type mock-up E-SCAPE (European SCAled Pool Experiment), a scale model of the MYRRHA primary cooling system, has been designed and built at SCK•CEN and is currently in the phase of commissioning tests. A coupled model for the facility has been developed and applied to a number of pre-test loss of flow transient simulations, and assessed against full 1D models. The results of the simulations confirmed the validity of the implemented numerical method, and highlighted potential inaccuracy of 1D models when particular flow conditions in natural circulation establish, confirming that 3D modeling might be required for certain fast reactor transient simulations. The experimental data-set to be generated will be used first for the validation of the stand-alone codes in relation to the regions and phenomena relevant to them, and integral test data will be successively used for the validation of the coupling tool.

The final part of the research was centered on the application of the tool to the analysis of the MYRRHA reactor. The purpose of this activity was twofold: from one side, it aimed at the assessment of the tool performance on a first reactor-scale application, and on the other side, it allowed investigating relevant thermal-hydraulic transient phenomena in the reactor and identifying limitations and potential model improvements of STH codes. A reference protected loss of flow transient was analyzed and the results, similarly to the work on E-SCAPE, were found in good overall agreement. This suggests that no significant impact of 3D effects on the integral behavior in loss of flow conditions is expected in the current MYRRHA design, although some discrepancy on certain parameters was observed due to 3D effects.

List of publications

Papers published in peer-reviewed Journals

- A. Toti, J. Vierendeels, F. Belloni, "Improved numerical algorithm and experimental validation of a system thermal-hydraulic/CFD coupling method for multi-scale transient simulations of pool-type reactors", *Annals of Nuclear Energy*, **103**, 36-48 (2017)
- A. Toti, J. Vierendeels, F. Belloni, "Extension and application on a pool-type test facility of a system thermal-hydraulic/CFD coupling method for transient flow analyses", *Nuclear Engineering and Design*, **331**, 83–96 (2018)
- A. Toti, J. Vierendeels, F. Belloni, "Coupled system thermal-hydraulic/CFD analysis of a protected loss of flow transient in the MYRRHA reactor", *Annals of Nuclear Energy*, **118**, 199-211 (2018)

Papers published in International Conference Proceedings

- A. Toti, J. Vierendeels, F. Belloni, "Development and Preliminary Validation of a STH-CFD Coupling Method for Multiscale Thermal-Hydraulic Simulations of the MYRRHA Reactor", *Proceedings of 24th International Conference on Nuclear Engineering*, Charlotte, North Carolina, USA, June 26–30, 2016.
- A. Toti, J. Vierendeels, F. Belloni, "Numerical analysis of a dissymmetric transient in the pool-type facility E-SCAPE through coupled system thermal-hydraulic and CFD codes", *Proceedings of 17th International Topical Meeting on Nuclear Reactor Thermal Hydraulics*, Xi'an, Shaanxi, China, Sept. 3-8, 2017.

Chapter 1

Introduction

1.1 Innovative nuclear power technologies

As of 31 December 2016, 448 nuclear reactors were in operation worldwide, with a net capacity of 391 GW of electricity, and about 60 new reactors were under construction [1]. At present, the share of nuclear power in the total global electricity generation is about 11%, a fraction that raises to about 18% in the OECD member countries [2]. The majority of the Nuclear Power Plants (NPP) under operation belong to the so-called generation II of nuclear technology, and are mostly based on Light Water Reactors (LWR), specifically in the two categories of Pressurized Water Reactors (PWR) and Boiling Water Reactors (BWR) (Figure 1.1). Intensive efforts were made in the last decades to improve the performances and safety features of these systems, evolving in the current third generation (Gen III "Advanced LWRs") of nuclear power technology. LWRs rely upon thermal neutron spectrum and Uranium dioxide (UO2) fuel enriched to 3-5wt % of 235U, or in some cases a mixture of UO2 and PuO2 (Mixed OXide (MOX)) fuel. The remaining portion of nuclear reactors include natural uranium fueled Heavy Water Reactors (HWRs) and a number of Gas-Cooled Reactors (GCRs). At present, only a very limited number of fast neutron spectrum reactors are in operation.

Current NPPs have proven to represent a mature and reliable technology for large-scale energy supply, with over 17000 reactor-years of operating experience [1]. However, a number of issues related to the current technologies and the associated fuel cycles remain open. Among them, the resource utilization and the management of the spent fuel are certainly of primary relevance. It is known that, even with the reprocessing of the

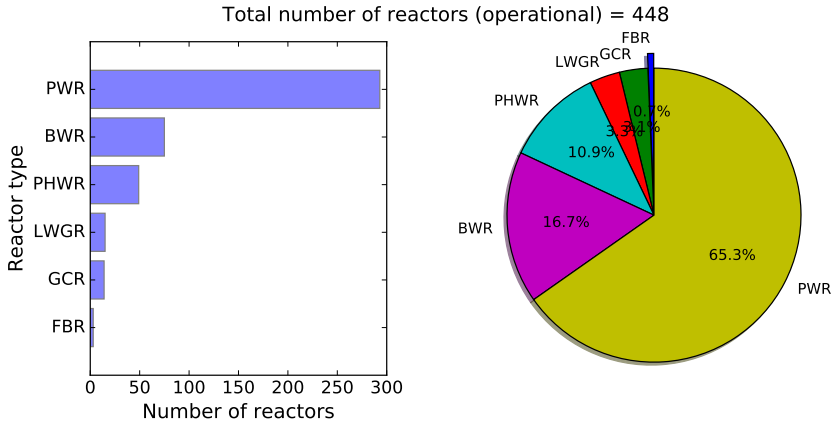

Figure 1.1: Operational reactors by type (*Data source: IAEA PRIS* [1]).

spent fuel and the recycling of fissile material, the energy content of the original resource can be only partially extracted with the use of thermal spectrum systems [1]. Moreover, despite its relatively small volume, the spent fuel inventory remains highly radio-toxic for hundreds of thousands of years before reaching the level of natural uranium. The accumulation of transuranic elements (TRansUranic (TRU)) [2] is the main responsible for the long-term radio-toxicity, which poses technical challenges and public concerns for the waste management and final disposal.

The nuclear industry has from its inception recognized the potential of fast spectrum reactors, and the possible fuel cycle options associated with them, to ensure a long-term, sustainable use of nuclear energy. The original interest in this technology was mainly driven by the possibility to reach breeding break-even, virtually enabling, through multiple recycling of the spent fuel, the full conversion of the fertile isotope 238U into fissile material. In the past decades, a significant number of Sodium-cooled Fast Reactors (SFRs) were designed, built and operated worldwide [3]. In Europe, experimental demonstration and prototype reactors such as Rapsodie, Phenix and Superphenix in France, DFR and PFR in the United Kingdom, SNR-300 in Germany were designed and built. Other demonstrative fast reactors were operated in Japan, Russia and USA. Only few prototypes of Lead-cooled Fast Reactors (LFRs) systems were built in Russia, and only for nuclear submarines propulsion application.

1. Reactors that use neutron moderators to reduce the neutron kinetic energy to that due to thermal motion
2. Pu and Minor Actinides (MA) (neptunium (Np), americium (Am), and curium (Cm))

At present, the need to reach a sustainable solution for the High Level Long-lived Waste (HLLW) is agreed at international level. Towards this goal, advanced fuel cycle strategies that envisage the use of Partitioning and Transmutation (P&T) processes have been pointed out to reduce the radiological hazard of long-term waste (in terms of magnitude and duration), to weaken the decay heat evolution history (e.g. by eliminating long lived heat producing actinides) and to reduce the quantities of the fissile and/or fertile radionuclides that pose proliferation concerns [4]. These goals can be achieved through critical fast reactors or by a "double strata" fuel cycle option, with a first stratum dedicated to electricity production using "clean fuel" containing only U and Pu plus a second stratum of systems devoted to transmutation. Sub-critical fast reactors (Accelerator Driven System (ADS)), which can be loaded with homogeneous fuels with significant content of MA, are particularly suitable for the last purpose.

Since 2000, the Generation IV International Forum (GIF) has selected six systems of which three are based on the fast spectrum technologies, namely the SFR, LFR and the Gas Fast Reactor (GFR) [5]. The goal of the initiative was to establish an international collaborative effort to develop next generation nuclear energy systems, characterized by higher performances in terms of sustainability (natural resource usage and reduction of waste production), economic competitiveness, safety and reliability, physical protection and proliferation resistance. The European Commission in 2010 launched the European Sustainable Nuclear Industrial Initiative (ESNII), which will support three Generation IV fast reactor projects as part of the EU's plan to promote low-carbon energy technologies. Through its Sustainable Nuclear Energy Technology Platform (SNETP), it has defined its own strategy and priorities for the fast neutron reactors that are the most likely to meet Europe's energy needs in the long term in terms of security of supply, safety, sustainability and economic competitiveness [6]. These systems are:

- The SFR as a first track aligned with Europe's prior experience;
- Two alternative fast neutron reactor technologies to be explored on a longer timescale: the LFR and the GFR.

Within this international framework, a high-priority research infrastructure is represented by the Multi-purpose hYbrid Research Reactor for High-tech Applications (MYRRHA) project, established at the SCK•CEN and aimed at designing and building a flexible fast spectrum irradiation facility that will replace the Material Testing Reactor (MTR) BR2 [7].

1.2 The MYRRHA project

The objective of the MYRRHA project is to design an experimental fast reactor, operated with Lead-Bismuth Eutectic (LBE) coolant and able to operate in both sub-critical and critical modes. In addition to material testing, the objectives of the reactor are to prove the feasibility of the ADS technology as MA burner as well as to represent a demonstration plant for Generation IV heavy liquid metal-cooled reactors (LFR).

A conceptual scheme of the installation and its major components i.e. proton accelerator, spallation target and reactor, is shown in Figure 1.2.

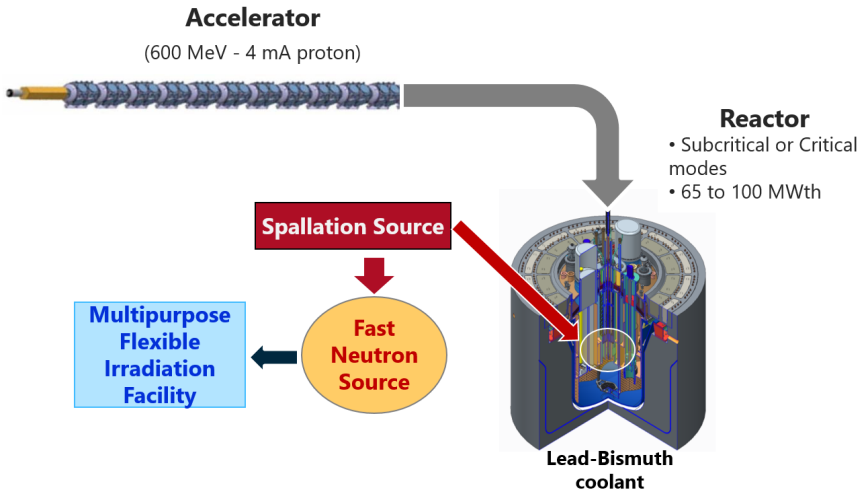

Figure 1.2: Conceptual scheme of the MYRRHA ADS.

The development of the system and the design of the reactor have been evolving throughout several stages, originating from the ADONIS project (1995), in which the coupling between an accelerator, a spallation target and a subcritical core has been studied for the first time, up the MYRRHA-FASTEF design [7]. These efforts led to the current reactor design (MYRRHA Design Version 1.6), which features a 100 MWth MOX fueled core and a LBE primary cooling system completely enclosed in the primary vessel (pool-type system). The design, whose detailed description will be given in chapter 6, is still under evolution and is supported by a broad research and development programme, undertaken at national level and within EU Framework Programs, to address the critical technological issues and to support the safety assessment of the

installation. At present, the major areas for research and innovation actions in support of the facility design can be summarized as follows:

- Lead-bismuth chemistry control and conditioning;
- Lead-bismuth component testing and thermal-hydraulics;
- Lead-bismuth instrumentation;
- Material qualification;
- Fast reactor MOX driver fuel qualification;
- Technology for coupling accelerator and subcritical core;
- High intensity proton accelerator performance and reliability.

As for the reactor thermal-hydraulics and safety, an important objective of the R&D programme is, among others, the assessment of the LBE primary system behavior in normal operation and transient conditions, and the demonstration of passive Decay Heat Removal (DHR) via natural circulation. Towards this objective, large-scale experimental programmes are established to investigate the thermal-hydraulic characteristics of a LBE pool-type system. In parallel to experimental investigations, these tests are also aimed at supporting the development, verification and validation (V&V) of advanced numerical tools for their use in thermal-hydraulic and safety analyses.

1.3 Thermal-hydraulics and safety analyses

The safety of nuclear installations certainly represents a further central element of public concerns on nuclear power, which gained revitalized attention in the aftermath of the accident at the Fukushima Daiichi plant (Japan, 2011). The accurate evaluation of NPPs performances during accident conditions has been a major objective of the research in the nuclear field. Deterministic safety assessments are usually carried out by using sophisticated modeling and simulation tools known as System Thermal-Hydraulic (STH) codes, which have been extensively used to support the design, licensing and operation of NPPs in the last decades. The role of these tools has become even more central with the establishment of modern "best-estimate (BE)" analysis procedures, aimed at predicting as accurately as possible the evolution of a certain accidental transient [8].

The development of new reactor concepts brings along the need of new modeling and simulation methodologies. Best-estimate STH codes such as RELAP [9], TRACE [10], ATHLET [11], CATHARE [12] etc., are generally based on equations for two-phase flows typically resolved in Eulerian coordinates. The two-phase flow field is described by mass, momentum, and energy conservation equations for the liquid and vapor phases separately and mass conservation equations for non-condensable gas present in the mixture (six equations formulation). The models are mainly suitable for 1D system simulation even if, for some NPP components (e.g., the vessel), some code has the capability to solve 3D system equations. Numerous empirical correlations are required to close the set of governing equations.

The lumped parameters formulation of STH codes may be in certain situations inadequate for the analysis of scenarios characterized by pronounced three-dimensional (3D) phenomena, including local flow mixing, dissymmetric conditions as well as others. Typical LWR scenarios of this nature are boron dilution problems, pressurized thermal shock (PTS), main steam line breaks (MSLB), situations involving the use of natural circulation and passive heat removal systems. In the analysis of liquid metal-cooled fast reactors (LMFRs), even more severe limitations may be introduced by the typical pool-type configuration of the primary cooling system, which induces complex coolant flow fields in the reactor plena and three-dimensional effects that may impact the short- and long-term system response to operational and accidental transients such as Loss Of Flow (LOF), Loss Of Offsite Power (LOOP) among others. Three-dimensional velocity and temperature profile distributions can affect the evolution of the coolant mass flow during the transition from forced to natural convection, with the possible generation of flow instabilities and local dissipating flows, and the development of thermal stratification may worsen the effectiveness of the passive emergency cooling systems. Furthermore, the presence of dead volumes can influence the characteristic time scale of perturbations propagation through the primary system.

In response to the need of more realistic predictions of fluid flow and heat transfer phenomena in nuclear reactor cooling systems, the use of Computational Fluid Dynamic (CFD) codes is constantly increasing in nuclear safety investigations, thanks to their capability to simulate complex flow fields by more detailed physical modeling, and to the continuous increase of the available computational power [13, 14]. However, even using modern supercomputers, performing integral transient simulations using CFD codes requires very large run-times and imple-

mentation efforts, which is often not practical for industrial projects.

This has led, over the past years, to the establishment of research and development projects to develop and validate advanced multi-dimensional computational approaches capable of simulating plant-scale transients including the resolution of complex 3D phenomena at acceptable computational costs. The need of such high-fidelity computational tools is recognized to be a key element for the design and safety analysis of advanced reactors at the international level [15, 16]. It is in this context that the PhD research activity presented in this dissertation, whose scope and objectives are discussed in the following paragraph, is framed.

1.4 Framework and objective of the PhD

The main objective of the PhD project was to investigate multi-scale modeling and simulation capabilities for high-fidelity thermal-hydraulic simulations of pool-type reactors, with particular focus on loss of flow accidents. The most relevant outcome of the work is the development, verification and preliminary validation of a computational methodology coupling the STH code RELAP5-3D to a commercial CFD code for 3D flow analyses. The work mainly aims at supporting the safety assessment of the MYRRHA reactor, in particular at identifying relevant transient 3D phenomena in plena and assessing their impact on the system response to off-normal conditions. Nevertheless, the developed computational technique has potential application on different reactor systems, and can be used for the analysis of a wide range of operational and accidental conditions.

A verification and validation programme has been outlined for the developed tool, which is strongly linked to two EC-funded international projects on advanced reactors thermal-hydraulic and safety, the H2020 EURATOM projects SESAME (Thermal-hydraulic simulations and experiments for the safety assessment of metal cooled reactors) and the thermal-hydraulic work package (WP3) of MYRTE (MYRRHA Research and Transmutation Endeavour) [17]. The project SESAME supports the development of liquid metal-cooled reactors by addressing their pre-normative, fundamental and safety-related challenges through [18]:

- The development and validation of advanced numerical approaches for the design and safety evaluation of advanced reactors;

- The achievement of a new or extended validation base by creating new reference data;

- The establishment of best practice guidelines (BPGs), verification & validation methodologies, and uncertainty quantification (UQ) methods for LMFR thermal-hydraulics;

The fundamental and generic nature of the SESAME project will also provide results of relevance to the safety assessment of contemporary LWRs. The SESAME project is complementary to the thermal-hydraulic work package of the project MYRTE, which focuses on MYRRHA-specific thermal-hydraulic challenges. A major focus of the MYRTE thermal-hydraulic package is pool-thermal hydraulics and integral system behavior, which is being investigated both experimentally and numerically. With regard to the numerical activities and methods development, the PhD project provided a direct contribution to MYRTE WP3. A scheme showing the synergies between the two projects and their location in the international context introduced above is shown in Figure 1.3.

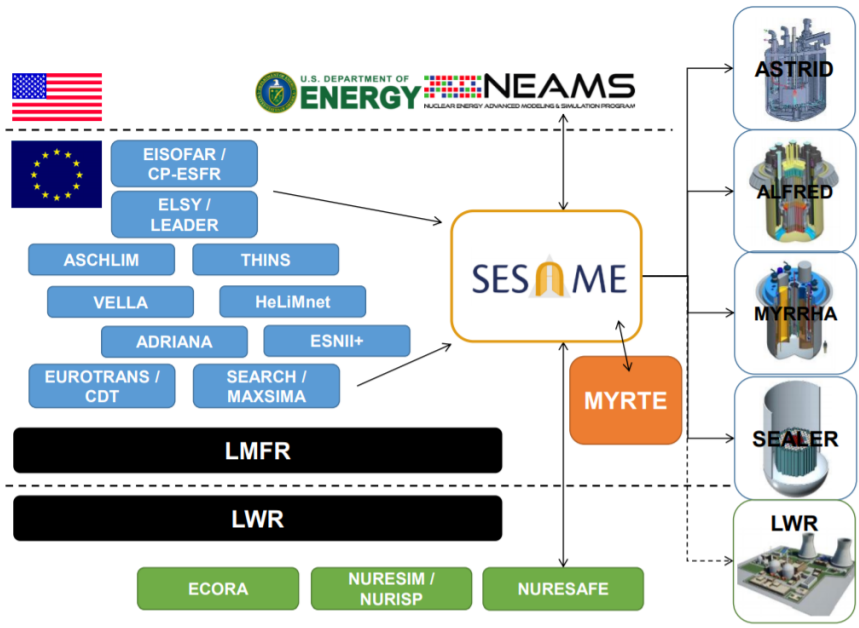

Figure 1.3: The SESAME and MYRTE projects and the international framework [18].

1.5 Outline of the research work

The work carried out can be conceptually structured into four sub-activities, which represent successive phases of work and reflect its logical and time progression.

Part 1 of the project focused on an extensive literature review on the subject, aimed at building knowledge basis on multi-dimensional simulation techniques and generating the necessary input to establish a code development strategy. To this purpose, the theoretical background, methods and applications of numerous nuclear and non-nuclear related developments have been analyzed.

Part 2 of work was centered on the implementation of the method, based on domain decomposition technique and dynamic exchange of interface boundary conditions (BCs). A new code infrastructure consisting of a supervisor code, written in Python language, FLUENT input files and User Defined Functions (UDFs) has been developed. An extensive investigation of numerical schemes has been carried out; in parallel to and supported by the verification and first validation assessments, novel coupling algorithms have been implemented to improve the performance of the tool and reduce computational costs. These developments represent one of the most valuable achievements and original scientific contribution of the PhD.

A multi-steps procedure of increasing complexity was established (part 3) within the verification and validation programme outlined for the tool. A first validation case was performed against the on-going experimental campaign at the test facility TALL-3D, operated by the Royal Institute of Technology (KTH) in Sweden. This choice relied on the main achievements of a completed EC-funded project (THINS), which provided a framework for the comparison of the developed method with different coupling approaches, as well as its validation against the available high-quality set of experimental data. A second set of validation analyses based on the pool-type experimental facility E-SCAPE, operated at SCK•CEN, is established and is currently ongoing.

The last part of the project (part 4) focused on the application of the codes coupling methodology on the MYRRHA reactor, which represented the ultimate objective of the project. The specific technical goals of this activity were:

- The demonstration of the applicability of the computational method on full pool-type system simulations;

- The identification of thermal-hydraulic phenomena occurring during LOF events in MYRRHA;
- The assessment of stand-alone STH models and the identification of possible model improvements.

A conceptual diagram illustrating these parts of the project and their mutual interconnection is shown in Figure 1.4:

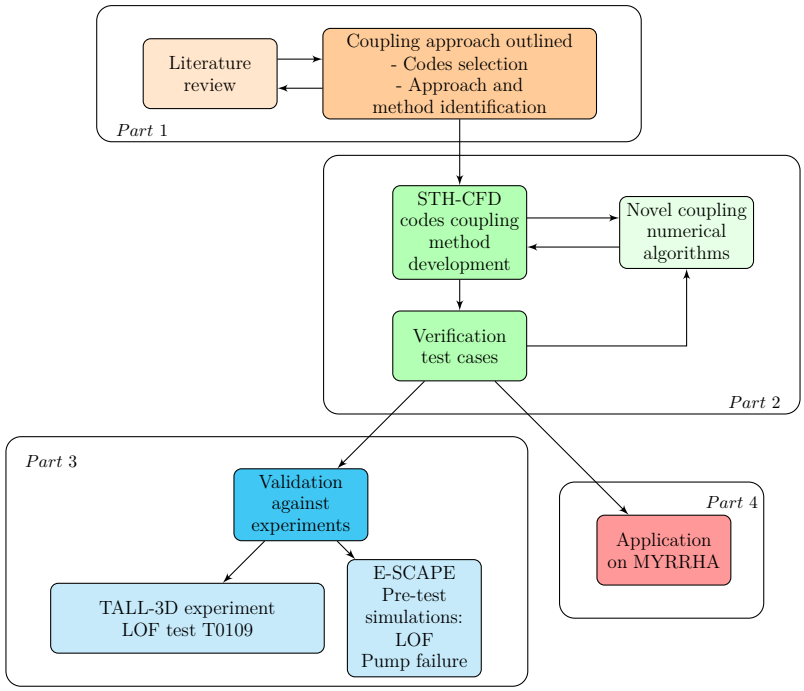

Figure 1.4: Overview of the different phases and activities of the PhD research project.

1.6 Structure of the thesis

The above discussed progression of the work is well reflected in the structure of this dissertation, which is based on and extends a number of papers published in peer-reviewed journals and international conference proceedings.

The state-of-art of multi-scale methodology development and validation for thermal-hydraulic analyses is discussed in chapter 2. Some theoret-

ical background of the reviewed methods is presented, along with their applications and, when available, validation efforts.

Chapter 3 describes the coupling methodology elaborated in this work. In particular, it provides an overview of the adopted calculation codes and their governing equations, the developed coupling technique, numerical schemes and verification tests on simple flow configurations.

In chapter 4, a first validation study against the LBE-loop TALL-3D is presented. Chapter 5 and chapter 6 present the application of the computational methodology on pool-type configurations, specifically the experimental scaled facility E-SCAPE and MYRRHA, for which loss of flow transients are mainly studied.

A summary of the work, its main conclusions and possible future developments are reviewed in chapter 7.

Chapter 2

Literature overview

This chapter reviews the state-of-art of multi-scale modeling and simulation tools developed for high-fidelity analysis of nuclear power plants, with particular focus on partitioned code coupling methods and techniques. General information on modeling approaches and techniques is provided, along with an overview of different applications and validation efforts available in literature.

2.1 General considerations

A coupled system consists of two or more distinct sub-systems, each one governed by its own set of differential equations but with some of the variables shared so that the sub-systems cannot be solved separately [19]. Typical coupled problems in the nuclear field are encountered when dealing with multi-physics e.g. fluid/structure interaction, neutronics/thermal-hydraulic coupling, thermal/structure interaction, etc. and multi-scale problems, of which the coupling between a fine fluid domain and a system-scale domain represents a typical instance.

Two main approaches can be envisaged to tackle such problems, which are referred to as the monolithic and partitioned techniques [20]. The first option implies that the two or more sets of governing equations are solved simultaneously, thus the mutual feedback between the domains is directly accounted for during the solution process. Such an approach is evidently efficient, but the development of new software infrastructure is usually demanded. In partitioned implementations, independent solvers are used and coupled through some form of data transfer which allows representing the mutual feedback between the domains. Performance

may be reduced with respect to monolithic methods; on the other hand, this approach is inherently modular and new models and numerical schemes can be easily introduced [21]. In the area of nuclear reactor thermal-hydraulics and safety, the first step in the development of a partitioned multi-scale code consists in the identification of the phenomena of interests, and the related space and time scales in order to select the appropriate simulation tool for each part of the domain of interest. Methodologies such as the Phenomena Identification and Ranking Table (PIRT) are usually adopted to support such process [22]. In general terms, once the simulation tools are identified, the following physical and numerical issues are to be addressed in the implementation of the multi-scale coupling tool:

- Space coupling;
- Data exchange;
- Time coupling and synchronization;
- Numerical scheme;
- Programming architecture and coupling execution.

With regard to space coupling aspects, the so-called domain decomposition method involves the subdivision of the original computational domain into two or more sub-domains, coupled via exchange of boundary conditions at the coupling interfaces during the solution process. The theoretical framework of the domain decomposition method is quite straightforward, which certainly represents an advantage of this coupling technique. The idea behind the so-called domain overlapping method is to use the CFD code, which computes only a limited region of the system where a fine resolution is required, to correct the solution of the system-scale code, which resolves the whole domain. On the contrary, the theoretical background of domain overlapping methods is more variegated, and different approaches can be identified. A conceptual scheme of the two coupling methods is represented in Figure 2.1.

For what concerns the choice of variables to be exchanged between the codes, both the above introduced coupling approaches may involve transferring surface variables. In such a case, the paradigm for data exchange should be such to assure the conservation of flow-transported quantities, in particular mass and energy. Transferring data from a 3D to a 1D domain necessarily implies a loss of information. On the other hand, translating 1D data to 3D profiles may require up-scaling

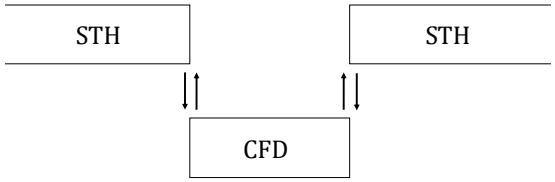

(a) Domain decomposition

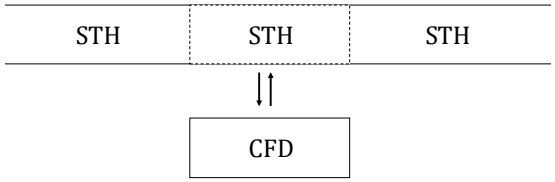

(b) Domain overlapping

Figure 2.1: Domain overlapping and domain decomposition coupling approaches.

choices which have be carefully assessed. These issues, in particular for domain decomposition methods, will be discussed in more details in chapter 3. Domain overlapping techniques, depending on the chosen modeling approach, may require transferring volume averaged data.

A crucial aspect of partitioned techniques is related to the time coupling and synchronization of the solvers, which is translated into the choice of the time steps in the codes and the data exchange frequency. A straightforward choice is to set an identical time step in both the solvers, and execute the exchange of boundary data at each time step. Sub-cycling options, with the coupled codes advancing to the same data exchange point using their own internal time step is also possible, and suitable especially when the resolved time scales are different. Indeed, with the use of sub-cycling strategies, each code can run with a size of the time step that optimizes accuracy, computational costs and numerical stability.

The scheme for the data exchange is strictly related to the coupling numerical scheme. Data can be generally exchanged in a parallel or sequential fashion, as represented in Figure 2.2. With a parallel scheme, if data is exchanged once per time step, the adopted coupling numerical scheme is purely explicit, and both the solvers compute a new time step using interface data from the previous time step. The explicit scheme is relatively of easy implementation, however it is often prone to numerical instability, as it will be discussed in chapter 3. Some implicitness can

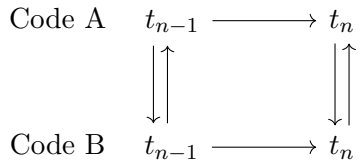

(a) Parallel data exchange scheme

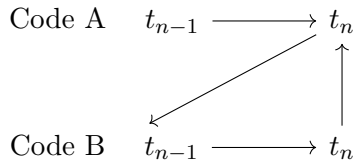

(b) Sequential data exchange scheme

Figure 2.2: Data communication patterns.

be added by using a sequential scheme, in which one code advances first to a new time level using data from the previous time level, whilst the second solver uses data calculated at the current time level. Full implicit schemes require the data exchange to be repeated within a time step until a converged solution is achieved. These schemes should theoretically lead to the same solution that would be obtained using a monolithic implementation. It is worth remarking that the above definitions of explicit and implicit schemes are not to be confused with the numerical schemes for the solution of ordinary Partial Differential Equations (PDEs) implemented in the coupled codes to solve their own governing equations. In partitioned methods, such terms are specifically related to the additional level of solution introduced by the exchange of data between the codes.

2.2 Literature overview

2.2.1 Domain decomposition methods

The first efforts to develop multi-dimensional modeling capabilities reported in the literature focused on nearly-monolithic implementations, mainly based on domain decomposition. These methodologies were originally targeted to LWRs analyses [23, 24]. The first work, carried out at the Korean Atomic Energy Research Institute (KAERI), focused on integrating the three-dimensional code COBRA-TF into the STH code RELAP5/MOD3. The purpose was to combine a realistic three-

dimensional reactor vessel hydrodynamic model of COBRA-TF with the features of RELAP5/MOD3, thus to develop high-fidelity modeling capabilities for LWR analyses. Both codes use a semi-implicit, finite-difference method based on a staggered-grid mesh and donor cell scheme. The system pressure matrices are coupled via the momentum modeling at the interfaces and solved simultaneously. The tool was assessed against the LOFT L2-3 large-break loss-of-coolant experiment [25]. The two solvers were later completely merged into a single code renamed MARS (Multi-dimensional Analysis of Reactor Safety) [26]. A similar approach was considered in the second work, carried out at Idaho National Laboratory (INL); a first implementation of an explicit coupling scheme between RELAP5-3D and the CFD code CFX was tested on a simple proof-of-principle calculation, namely the Edwards-O'Brien depressurization experiment. With the tested explicit scheme, the coupling information are exchanged between the solvers at the beginning of the solution of each time step. As expected, numerical stability issues were observed and attributed to the use of explicit coupling time stepping scheme. To address this issue, a semi-implicit coupling method was later developed [27]. With this scheme, in the master process (RELAP5-3D) the pressure changes in all the volumes of the sub-domain are expressed as linear functions of the yet unknown mass and energy fluxes at the coupling interfaces. Coefficients in these linear relations at the interfaces are transmitted to the slave process in order to solve simultaneously the flow field and the exchanged fluxes in its own sub-domain. Finally, the exchanged fluxes are used to solve the flow field in the master sub-domain.

A more recent body of work at INL to couple the RELAP5 code to the CFD code FLUENT is available in the literature [28–30]. The coupling tool has been used to simulate the flow in the outlet plenum of a Very High Temperature Reactor (VHTR), using the semi-implicit scheme and the Parallel Virtual Machine (PVM) message-passing technology to increase the computational speed.

The same codes, RELAP5-3D and FLUENT, were coupled using similar approaches in [31] and [32]. In the first work, carried out at the University of Illinois at Urbana-Champaign, the coupling is executed through FLUENT User Defined Functions. The same author presented a semi-implicit coupling method in [33], in which the importance of the coupling numerical scheme is stressed. Verification of the code is pursued through a simple unsteady pipe flow problem and with an application to a typical transient scenario of a PWR. The second development is performed at the Xi'an Jiaotong University in China, and makes use of

DLL (Dynamic Link Library) technology and FLUENT UDF and the same above mentioned Edwards–O'Brien pipe blowdown problem has been used for validation purposes.

An analogous domain decomposition implementation, using the 1D best-estimate code TRACE and the 3D CFD code CFX, was performed at the Paul Scherrer Institute (PSI) for the application on boron dilution problems. Both explicit and semi-implicit schemes have been tested, and constant under-relaxation factor is used to improve numerical stability. The tool was assessed against a simple single-phase mixing experiment [34], which showed clear advantages of a 3D simulation over a 1D approximation to capture the complexity of the mixing phenomena in a double T-junction. The code was also validated against a scaled down, simplified, two-dimensional vertical slice of a LWR vessel (FLORIS) [35]. Even in these validation efforts, the coupled simulations provided a noticeable improvement over stand-alone TRACE simulations. A similar approach to couple the system code ATHLET to CFX, using both explicit and semi-implicit schemes, was developed at the Gesellschaft für Anlagen- und Reaktorsicherheit (GRS) in Germany, and is reported in [36]. A satisfactory validation exercise on the tool has been carried out on a PTS experimental test performed at the Japanese LSTF PWR scaled facility [37].

In the last years, analogous codes coupling methods have been developed to improve the modeling capabilities of the coolant flow field in pool-type liquid metal-cooled reactors, in particular for what concerns the analysis of three-dimensional phenomena in large plena. These works are carried out in the general attempt to improve the accuracy in the prediction of SFR and LFR system behavior during accidental events such as loss of flow transients. Particular focus is on the evaluation of the transition from forced to natural circulation, whose evolution may be directly impacted by three-dimensional temperature profiles, of difficult prediction for 1D system codes. At the University of Pisa, a tool integrating the RELAP5-3D code and FLUENT is developed for the application on LFR system analyses [38]. The coupling method is being validated on the basis of the loop-type heavy liquid metal facility NACIE and the pool-type installation CIRCE, operated by the Italian National Agency for New Technologies, Energy and Sustainable Economic Development (ENEA). The development of domain decomposition techniques for SFR simulations have been object of research also at AREVA [39] and Argonne National Laboratory (ANL) [40].

A number of works on domain decomposition for non-nuclear application were also reviewed. In [41], a 1D system and 3D component domain

decomposition co-simulation method based on the Method of Characteristics (MOC) and CFD was proposed to study the interaction between valve-induced water hammer and pump during the rapid closing of the valve. The CFD code is used to model the regions where 3D effects are important, whereas the MOC code is mainly used to model all regions where the flow is expected to remain largely 1D. An implicit scheme is implemented, with sub-iteration until the defined convergence criterion is satisfied. Transient simulation demonstrated that MOC-CFD coupling analysis was closer to real conditions because of considering the effect of fluid inertia. A coupling methodology based on the MOC is also presented [42]. The method couples the OpenWAM code, a one-dimensional gas dynamic model able to calculate the air and gas flows within the intake and exhaust systems of internal combustion engine, with the CFD code FLUENT. In order to validate the coupling procedure, it was applied on the well-known analytical test case Sod's problem and on a configuration equivalent to an impulse test rig. An application of a multi-scale tool on internal combustion engines is also given in [43]. A relevant number of works on 1D/3D domain decomposition multi-scale methods for the simulation of the blood flow in the cardiovascular system are also available in the literature [44–46].

2.2.2 Domain overlapping methods

As it was introduced earlier, a second coupling approach that can be identified is based on domain overlapping, for which different modeling strategies can be envisaged. The methodology developed at the University of Michigan, reported in [47], couples the CFD code STAR-CCM+ and the system code TRACE and aims at equaling the total pressure difference at the boundaries of the coupling region in both the codes. To this purpose, the friction term in the 1D momentum equation is replaced, only in the coupled sub-domain, by a pressure drop calculated on the basis of a CFD-based friction factor f_{CFD}:

$$f_{CFD} = \frac{1}{2} \frac{D_h}{\rho_{TRC} (V^n_{j+1/2})^2} \frac{\Delta p_{CFD}}{L_{LP}} \tag{2.1}$$

$V^n_{j+1/2}$ refers to the velocity at the old time step defined at the edge between cells j and $j+1$, and L_{LP} is the lumped parameter length scale. For the application of this method to transient calculations, the inertial pressure drop has to be considered. This can be achieved by computing a non-inertial pressure gradient based friction factor through appropriate modification of the total pressure difference across the CFD

domain.

$$f_{CFD} = \frac{1}{2}\frac{D_h}{\rho_{TRC}(V^n_{j+1/2})^2}\Big[\frac{\Delta p^{n+1}_{CFD}}{L_{LP}} - \frac{1}{\Delta t}\Big(\frac{1}{V}\iiint \rho v^{n+1}\cdot\hat{n}_{fp}dV - \frac{1}{V}\iiint \rho v^{n}\cdot\hat{n}_{fp}dV\Big)\Big] \tag{2.2}$$

This method is being extended to 3D domain coupling.

The same condition of equal pressure difference at the domains boundaries can be achieved by using artificial momentum source/sink terms. In the technique presented in [48], developed at the French Atomic Energy and Alternative Energies Commission (CEA) to integrate the STH code CATHARE and the CFD code Trio_U, the 1D code imposes mass flow rates at every hydraulic boundary of the CFD domain, and the pressure-velocity fields coupling is achieved through a momentum source in the STH code to obtain the same pressure difference Δp across the coupled domain. The momentum source is derived from the following:

$$[p(O_{ref}) - p(O_i)]_{STH} - [p(O_{ref}) - p(O_i)]_{CFD} = 0 \tag{2.3}$$

where $p(O_{ref})$ is the pressure at a reference point in the overlap subdomain and $p(O_i)$ the pressure at the boundary i. As for thermal BC, fluid enthalpy calculated by the STH code is converted into a temperature and passed to the CFD code. The energy feedback from the CFD code is taken into account by modifying the energy balance equation in the STH code at each boundary of the coupled region, in order to equal the enthalpy flow-rate through the boundaries. This is achieved by replacing in the CATHARE code the enthalpy at the boundary of the coupling region with enthalpy calculated by the CFD code. The validation of the coupling methodology has been focused on the Phenix end-of-life tests campaign, a series of experiments performed at the prototype SFR before its definitive shut-down. In particular, the post-test analysis of the sodium natural convection test confirmed the complexity of the transition from forced to natural circulation in SFRs, and led to an improved numerical vs. experimental agreement when compared to the stand-alone STH model. Based on these development efforts, CEA recently extended its multi-scale modeling capabilities by implementing a new platform named MATHYS (Multi-Scale Astrid Thermal-Hydraulic Simulation), more flexible and versatile compared to the previous implementation, which is being validated against several experiments [49]. A similar approach, both in terms of methodology and application, can be found in [50].

An alternative domain overlapping approach is based on the Local Defect Correction (LDC) technique [51]. Supposing that the STH system equations can be expressed as follows:

$$AX = B \tag{2.4}$$

and that a solution $\widetilde{X}$ is computed using the CFD code in the overlapped sub-domain. The LDC method applies a simple correction via truncation of the global operator A:

$$AX = B - \lambda(B - A\widetilde{X}) \tag{2.5}$$

This method has been preliminary tested at CEA on a two-phase CATHARE3/CATHARE3 coupled calculation, and efforts to set up a single-phase coupled calculation using TrioCFD and CATHARE are ongoing.

In some domain overlapping techniques, the focus is only on the energy terms feedback from the CFD domain to the STH code, and no balance in the momentum terms is achieved. An example is provided in [52], which describes a coupling technique developed at the Royal Institute of Technology (KTH) in Sweden conceived for transient analyses of heavy liquid metal-cooled systems. The method is based on a CFD-based correction of the STH code energy equation through the implementation of a "virtual heater", in order to reach converged inlet and outlet temperatures between the codes. The STH code provides inlet boundary temperature and mass flow rate to the CFD code, which in turn calculates outlet boundary temperature. The STH model is then iteratively corrected until its solution is converged with the CFD solution.

2.2.3 Methods comparison and validation benchmarks

Some comparative studies and validation analyses on multi-scale modeling and simulation tools have been performed over the past years. In [47], domain decomposition and domain overlapping methods are compared on a number of test cases. The results showed that the domain overlapping method tends to exhibit superior convergence and numerical stability when compared to the domain decomposition approach, given the absence of interruptions in the STH nodalization and the weaker coupling between the pressure-velocity fields. However, no numerical techniques to improve numerical stability in domain decomposition techniques have been investigated.

In the field of pool-type liquid metals-cooled reactors analysis, for which the development of coupled codes is of particular interest, several international benchmarks at the European level and within IAEA initiatives have been established to perform code-to-code comparisons and V&V against experimental data. A comparison between the two space coupling approaches has been carried out within the THINS (Thermal-hydraulics of Innovative Nuclear Systems) project, specifically with the blind simulations of the TALL-3D LBE loop [53]. Post-test analyses were performed later on, and revealed that both the domain decomposition-based ATHLET/CFX and the domain overlapping-based RELAP5/STAR CCM+ coupled codes perform better than the respective ATHLET and RELAP5 stand-alone models [54]. Recently, further collaborative frameworks are established on pool scaled experiments as well as plant data (e.g. EBR-II, Phenix) [55, 56].

It is worth mentioning that in advanced coupling implementations, domain decomposition and overlapping methods can also be used simultaneously. For instance, at CEA a STH/subchannel/CFD coupling method was developed, and uses domain overlapping between STH and subchannel/CFD, but domain decomposition between subchannel and CFD [57].

2.3 Conclusions

A considerable amount of work performed in the last years on the development and validation of multi-dimensional thermal-hydraulic simulation tools is available in literature, focused on the attempt to enhance the accuracy of nuclear power plant transient analyses by combining system modeling with the resolution of 3D flow fields at reasonable computational costs. Although the first developments were based on nearly-monolithic implementations, most of the available research efforts are based on partitioned approaches, thus on the use of independent solvers coupled through mutual exchange of solution variables. With regard to the treatment of the computational domain, coupling techniques can be grouped into two main categories, namely the domain decomposition and domain overlapping techniques.

All the studies on domain decomposition confirmed the validity of this approach, although numerical stability issues mainly related to the numerical scheme were commonly identified. These issues, of particular importance in incompressible fluid system computations, confirmed the strict limitations in the coupling time step size in explicit schemes.

Implicit schemes with coupling iterations within each time step have been implemented in some studies to address those issues and relax the constraints on the time step size, although no attempts to improve numerical performances through more advanced numerical algorithms were found.

Domain overlapping methods have also been investigated and developed, and generally found to show favorable numerical stability characteristics. However, modeling strategies can be different and the pressure-velocity coupling can be weaker compared to domain decomposition methods. Moreover, modification of the codes' governing equations is usually required in such implementation strategies.

Originally applied to the simulation of LWRs, important activities are nowadays devoted to the development of multi-dimensional thermal-hydraulic simulation tools for more accurate prediction of transient heat transfer and fluid flow phenomena in pool-type LMFRs. Such developments are supported by a large number of international benchmarks that allow for the comparison of the different modeling approaches and their validation against experimental data.

Chapter 3

RELAP5-3D/FLUENT coupling method development and verification

This chapter presents the developed multi-scale computational methodology, and its testing on simple pipe flow calculations. The technique is based on a partitioned approach and makes use of proprietary codes, namely the best-estimate system thermal-hydraulic code RELAP5-3D and the CFD code FLUENT, whose a general overview is provided. The content of this chapter is an extension of a conference proceeding contribution [58] and the first part of a paper published in a peer-reviewed journal [59].

3.1 Codes governing equations and models

3.1.1 CFD code FLUENT

I. Governing equations

CFD codes numerically solve the governing equations for fluid flow. Conservation of mass and momentum are the fundamental equations solved in the code. The energy conservation equation is included in problems involving heat transfer or compressible flow. The mass conservation

equation for both compressible and incompressible flows is [60]:

$$\frac{\partial \rho}{\partial t} + \nabla \cdot (\rho \vec{u}) = 0 \tag{3.1}$$

where ρ is the fluid density and $\vec{u}$ the velocity. The momentum equation in a non-inertial reference system, known as the Navier-Stokes equation, is written as follows:

$$\frac{\partial (\rho \vec{u})}{\partial t} + \nabla \cdot (\rho \vec{u} \vec{u}) = -\nabla p + \nabla \cdot \bar{\bar{\tau}} + \rho \vec{f} \tag{3.2}$$

where p is the static pressure, $\bar{\bar{\tau}}$ is the stress tensor and $\rho \vec{f}$ is the generic body force. The energy equation is:

$$\frac{\partial (\rho E)}{\partial t} + \nabla \cdot (\rho \vec{u} E) = -\nabla \cdot (\vec{u} p) + \nabla \cdot (k \nabla T) + \nabla \cdot (\bar{\bar{\tau}} \cdot \vec{u}) + S \tag{3.3}$$

where k is the thermal conductivity and S is the generic volumetric heat source. The fluid total specific energy E is defined as:

$$E = h - \frac{p}{\rho} + \frac{u^2}{2} \tag{3.4}$$

where h is the sensible enthalpy. To close the set of equations, a constitutive equation for the fluid density $\rho = f(p, T)$ is needed.

II. Turbulence modeling

It is known that all flows become unstable above certain values of the Reynolds (Re) number, which is a dimensionless parameter equal to inertial forces over the viscous forces:

$$Re = \frac{\rho u L}{\mu} \tag{3.5}$$

in which L is a characteristic linear dimension and μ is the dynamic viscosity. Turbulent flows are characterized by fluctuating velocity fields and, as a consequence, fluctuating transported quantities such as momentum, energy, species concentration etc. The resolution of all time and space scales of these fluctuations in industrial flows is beyond the currently available computational power. Moreover, in most engineering applications these small fluctuations are not of interest, and only averaged values need to be known.

The instantaneous governing equations can be therefore time averaged, ensemble-average, or otherwise manipulated to remove the resolution of

small scales, resulting in a modified set of equations that are computationally less expensive to solve. However, such operations introduce additional unknowns, therefore turbulence models are needed to determine these variables.

Two alternative methods can be employed to avoid resolving all the small scales: Reynolds-averaging (or ensemble-averaging) and filtering. Both these methodologies require models to achieve a closure of the equations. The Reynolds-averaged Navier-Stokes (RANS) equations govern the transport of averaged flow quantities, with the whole range of scales of turbulence being modeled. Large Eddy Simulations (LES) provide an alternative approach in which only large eddies are resolved in a time-dependent simulation using "filtered" Navier-Stokes equations. The idea behind LES technique is to reduce the error introduced by turbulence models by modeling less turbulence and only the small scales that tend to be isotropic and less case-dependent. Filtering removes the eddies whose characteristic dimension is smaller than the applied filter, which is usually related to the mesh size.

In Reynolds averaging, the instantaneous variables are decomposed into mean and fluctuating components:

$$u_i = \overline{u}_i + u_i' \tag{3.6}$$

where $\overline{u}_i$ and u_i' are the mean and fluctuating velocity components. Likewise, for the generic scalar ϕ:

$$\phi = \overline{\phi} + \phi' \tag{3.7}$$

For an incompressible flow, substituting expressions of this form for the flow variables into the instantaneous conservation equations and taking a time (ensemble) average yields the ensemble-averaged equations:

$$\frac{\partial \rho}{\partial t} + \frac{\partial}{\partial x_i}(\rho \overline{u}_i) = 0 \tag{3.8}$$

$$\frac{\partial}{\partial t}(\rho \overline{u}_i) + \frac{\partial}{\partial x_j}(\rho \overline{u}_i \overline{u}_j) = \frac{\partial}{\partial x_j}\Big[- \overline{p}\delta_{ij} + \mu\Big(\frac{\partial \overline{u}_i}{\partial x_j} + \frac{\partial \overline{u}_j}{\partial x_i}\Big) - \rho\overline{u_i' u_j'}\Big] + \rho \overline{f}_i \tag{3.9}$$

The term $\overline{u_i' u_j'}$ in the right side of Equation 3.9 is referred to as the Reynolds stress, which accounts for the effect that turbulent motion has on the mean quantities. Different closure approaches of the RANS governing equations set lead to different turbulence models. Two-equation

models are most commonly used in engineering applications. In this work, the $k-\epsilon$ and $k-\omega$ models are considered. These models are based on the the eddy-viscosity concept proposed by Boussinesq, which assumes the turbulent stresses to be proportional to the mean-velocity gradients:

$$\overline{u_i{'}u_j{'}} = \frac{\mu_t}{\rho}(\frac{\partial \overline{u}_j}{\partial x_i} + \frac{\partial \overline{u}_i}{\partial x_j}) - \frac{2}{3}k\delta_{ij} \tag{3.10}$$

where μ_t is the eddy viscosity, k is the turbulent kinetic energy, and δ_{ij} is the Kronecker delta. The turbulent kinetic energy k is defined as:

$$k = \frac{1}{2}\overline{u_i{'}u_i{'}} \tag{3.11}$$

The standard $k-\epsilon$ model is a semi-empirical model based on model transport equations for the turbulence kinetic energy k and its dissipation rate ϵ. The assumption behind the model is that the flow is fully turbulent, and the effects of molecular viscosity are negligible. The standard $k-\epsilon$ model is therefore valid only for fully turbulent flows.

The classical $k-\epsilon$ transport equations for the turbulence kinetic energy and its rate of dissipation (neglecting the effects of volume forces and compressibility) are [61]:

$$\frac{\partial}{\partial t}(\rho k) + \frac{\partial}{\partial x_i}(\rho k \overline{u}_i) = \frac{\partial}{\partial x_j}\Big[(\mu + \frac{\mu_t}{\sigma_k})\frac{\partial k}{\partial x_j}\Big] + P_k - \rho\epsilon \tag{3.12}$$

and

$$\frac{\partial}{\partial t}(\rho \epsilon) + \frac{\partial}{\partial x_i}(\rho \epsilon u_i) = \frac{\partial}{\partial x_j}\Big[(\mu + \frac{\mu_t}{\sigma_\epsilon})\frac{\partial \epsilon}{\partial x_j}\Big] + C_{1\epsilon}\frac{\epsilon}{k}(G_k) - C_{2\epsilon}\rho\frac{\epsilon^2}{k} \tag{3.13}$$

in which P_k represents the production of turbulence kinetic energy due to the mean velocity gradients, $C_{1\epsilon}$ and $C_{2\epsilon}$ are constants, σ_k and σ_ϵ are the turbulent Prandtl numbers for k and ϵ, respectively.

The turbulence (or eddy) viscosity, μ_t is computed by combining k and ϵ as follows:

$$\mu_t = \rho C_\mu \frac{k^2}{\epsilon} \tag{3.14}$$

The values of the constants have been determined by experiments, and have been found to work fairly well for a wide range of flows. More sophisticated $k-\epsilon$ model i.e. RNG $k-\epsilon$ model, realizable $k-\epsilon$ were later made available.

The standard $k-\omega$ model is an empirical model based on model transport equations for the turbulent kinetic energy k and the specific dissipation rate ω, which can be seen as the ratio of ϵ and k. The transport equations of the Standard $k-\omega$ model are:

$$\frac{\partial}{\partial t}(\rho k)+\frac{\partial}{\partial x_i}(\rho k\overline{u}_i)=\frac{\partial}{\partial x_j}\Big[(\mu+\frac{\mu_t}{\sigma_k^*})\frac{\partial k}{\partial x_j}\Big]+P_k-\rho\beta^* k\omega \tag{3.15}$$

and

$$\frac{\partial}{\partial t}(\rho\omega)+\frac{\partial}{\partial x_i}(\rho\omega\overline{u}_i)=\frac{\partial}{\partial x_j}\Big[(\mu+\frac{\mu_t}{\sigma_\omega^*})\frac{\partial \omega}{\partial x_j}\Big]+\alpha\frac{\omega}{k}P_k-\rho\beta\omega^2 \tag{3.16}$$

in which the eddy viscosity is given by:

$$\mu_t=\rho\frac{k}{\omega} \tag{3.17}$$

and α, β and β^* are constants.

It is generally noticed that the $k-\omega$ model is capable of superior performance near wall boundaries, due to the more natural boundary conditions on the turbulence frequency. However, the model transport equation used for ω is less complete than the transport equation used for ϵ in regions away from the wall. The shear-stress transport (SST) $k-\omega$ model is an attempt to combine the two models discussed, and is currently widely used in many engineering applications.

III. Near-wall treatment

In confined flows, a boundary layer adjacent to a solid surface is formed, whose computation is a historical challenge for CFD codes. The wall layer can be seen as divided into two regions. The inner region, generally occupying 10-20% of the total thickness of the wall layer, is composed of three sub-layers, usually discerned based on the dimensionless velocity $u^+=\overline{u}/u_\tau$, with $u_\tau=\sqrt{\tau_w/\rho}$, and dimensionless wall distance $y^+=u_\tau y/\nu$, where y is the distance from the wall, τ_w is the wall shear stress and ν is the fluid kinematic viscosity (Figure 3.1) [60]. In this inner region, the shear stress in the flow can be assumed constant and equal to the wall shear stress τ_w. A first sub-layer ($y^+<5$) dominated by viscous effects exists, in which a linear relation $u^+=y^+$ between velocity and wall distance is established. In a second sub-layer, the so-called buffer layer, viscous and turbulent stresses are of similar magnitude. Outside

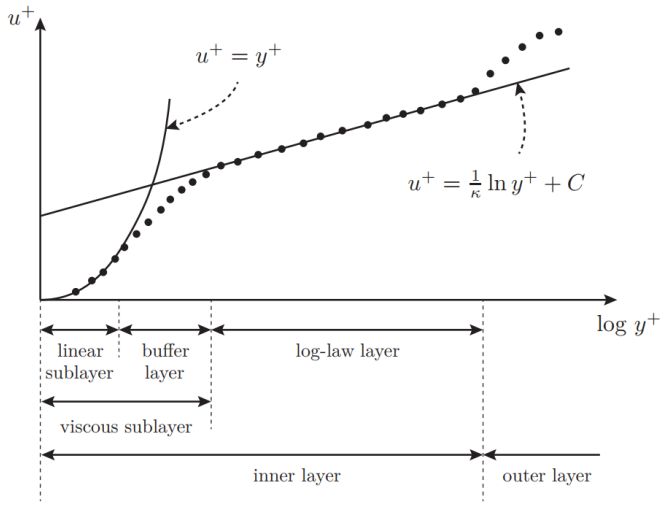

Figure 3.1: Structure of the wall boundary layer as a function of the dimensionless quantities u^+ and y^+.

the viscous sub-layer ($30 < y^+ < 500$), a logarithmic relation (log-law) between velocity and distance exists:

$$u^+ = \frac{1}{K} ln\ y^+ + C \tag{3.18}$$

with K and C being constants whose values were retrieved from experiments and are generally valid for all turbulent flows. The outer region of the boundary layer (law-of-the-wake layer) is inertia-dominated and viscous effects become less important.

To model the wall boundary layer, two approaches are possible i.e. near-wall models and wall functions. In the first approach, the near-wall grid is sufficiently fine ($y^+ \approx 1$) to resolve the different layers, yielding accurate results for the near-wall flow. However, for the applications treated in this work, prohibitive computational costs would be required, especially if the Reynolds number is high hence the viscous layer very thin. Using wall functions, the first grid point is typically located in the range of applicability for the log-law, leading to the possibility of using coarser grids. The standard wall functions [62] are widely used in industrial applications and implemented in FLUENT. More advanced near-wall treatment functions are also available [63].

IV. Solver theory

The CFD code FLUENT solves the flow governing equations using a finite volume discretization. The domain is divided into discrete control volumes, on which the governing equations are integrated to construct algebraic equations for the dependent variables.

As known, a difficulty in solving the CFD governing equations is the pressure-velocity coupling, and the absence in incompressible flows of an explicit equation for the pressure. In the pressure-based segregated methods (SIMPLE, SIMPEC, PISO) used in this work, the velocity field is obtained from the momentum equation. The pressure field is solved through a pressure or a pressure correction equation obtained by manipulating the mass continuity and momentum equation [61].

More information on the FLUENT code structure, methods and models can be found in the theory manual [63].

V. Additional CFD models

In addition to what is described above, some of the simulations discussed in this dissertation (chapter 5, chapter 6) make use of addition CFD models, specifically porous media [64] and multi-phase Volume Of Fluid (VOF) models [65].

3.1.2 RELAP5-3D

RELAP5-3D is the system thermal-hydraulic code developed at the Idaho National Engineering and Environmental Laboratory (INEEL) for the U.S. Nuclear Regulatory Commission (NRC). It is a best-estimate code originally developed for the analysis of accidents and operational transients in LWRs to support the design, licensing and operation. The code is able to represent and simulate the behavior of a complete plant through the use of:

- 1-D or 3-D hydrodynamic volumes and junctions (domain for the mass, momentum and energy balance equations);
- 2-D heat structures (simulating the solid structures of the system where heat generations and/or exchanges take place);
- A point neutron kinetics module to take into account for reactivity feedbacks.

For the solution of the hydrodynamic problem, the code uses two-fluid model formulated in terms of volume and time-averaged parameters. Additionally, a large number of empirical models for specific components are implemented. Phenomena that depend upon transverse gradients, such as friction and heat transfer, are formulated in terms of the bulk properties by using empirical transfer coefficient correlations. Compared to previous versions of the code (RELAP5/MOD3), RELAP5-3D is based on a multi-dimensional formulation that allows to certain extent for a more detailed representation of three-dimensional flows. However, given the nature of this work, in none of the computational models presented in this dissertation has the multi-dimensional (MULTID) component been used. In recent years, the properties of additional working fluids were implemented allowing for the use of the tool not only for the analyses of LWRs but also, for instance, of liquid metals- and gas-cooled systems.

The RELAP5-3D code is currently adopted at SCK•CEN as the reference tool for the thermal-hydraulic and safety analyses of the MYRRHA reactor, fact that motivated its use in this work.

I. Hydrodynamic models

Governing equations The RELAP5-3D hydrodynamic model solves eight field equations for eight primary dependent variables [66]. The primary dependent variables are pressure p, phasic specific internal energies U_f, U_g, vapor volume fraction α_g, phasic velocities u_f, u_g, noncondensable quality X_n, and boron density ρ_b. The independent variables are time t and space coordinate x. The derivation of the governing equations is based on the fundamental principles of conservation of mass, momentum and energy.

The continuity equation for liquid and gas phases is reported below:

$$\frac{\partial \alpha_f \rho_f}{\partial t} + \frac{1}{A}\frac{\partial (\alpha_f \rho_f u_f A)}{\partial x} = \Gamma_f \tag{3.19}$$

$$\frac{\partial \alpha_g \rho_g}{\partial t} + \frac{1}{A}\frac{\partial (\alpha_g \rho_g u_g A)}{\partial x} = \Gamma_g \tag{3.20}$$

These equations come from the one-dimensional phasic mass conservation equations [67]. Generally, the flow does not include mass sources or sinks, and overall continuity consideration yields the requirement that the liquid generation term be the negative of the vapor generation, that is:

$$\Gamma_f = -\Gamma_g \tag{3.21}$$

The interfacial mass transfer model assumes that total mass transfer can be partitioned into mass transfer at the vapor/liquid interface in the bulk fluid (Γ_{ig}) and mass transfer at the vapor/liquid interface in the thermal boundary layer near the walls (Γ_w), that is:

$$\Gamma_g = \Gamma_{ig} + \Gamma_w \tag{3.22}$$

The phasic conservation of momentum equations are:

$$\begin{gathered}\alpha_f\rho_f A\frac{\partial u_f}{\partial t} + \frac{1}{2}\alpha_f\rho_f A\frac{\partial u_f^2}{\partial x} = -\alpha_f A\frac{\partial p}{\partial x} + \alpha_f\rho_f f_x A - \\ (\alpha_f\rho_f A)FWF(u_f) - \Gamma_g A(u_{fI} - u_f) - \\ (\alpha_f\rho_f A)FIF(u_f - u_g) - C\alpha_f\alpha_g\rho_m A\left[\frac{\partial(u_f - u_g)}{\partial t} + u_g\frac{\partial u_f}{\partial x} - u_f\frac{\partial u_g}{\partial x}\right]\end{gathered} \tag{3.23}$$

$$\begin{gathered}\alpha_g\rho_g A\frac{\partial u_g}{\partial t} + \frac{1}{2}\alpha_g\rho_g A\frac{\partial u_g^2}{\partial x} = -\alpha_g A\frac{\partial p}{\partial x} + \alpha_g\rho_g f_x A - \\ (\alpha_g\rho_g A)FWG(u_g) + \Gamma_g A(u_{gI} - u_g) - \\ (\alpha_g\rho_g A)FIG(u_g - u_f) - C\alpha_g\alpha_f\rho_m A\left[\frac{\partial(u_g - u_f)}{\partial t} + u_f\frac{\partial u_g}{\partial x} - u_g\frac{\partial u_f}{\partial x}\right]\end{gathered} \tag{3.24}$$

in which FWF, FWG are the wall drag coefficients and FIF, FIG are the interphase drag coefficients for the liquid and vapor phases. The terms FWG and FWF are the products of interface friction coefficient, frictional reference area per unit of volume, and the fluid bulk velocity. The coefficients FIG and FIF are part of the interface frictional drag. In the development of the above equations, the Reynolds stresses are neglected, the phasic pressures are assumed equal, the interfacial pressure is assumed equal to the phasic pressures (except for stratified flow), the covariance terms are universally neglected, interfacial momentum storage is neglected, phasic viscous stresses are neglected, the interface force terms consist of both pressure and viscous stresses, and the normal wall forces are assumed adequately modeled by the variable area momentum flux formulation. The force terms on the right side of Equation 3.23 and Equation 3.24 are, respectively, the pressure gradient, the body force, wall friction, momentum transfer due to interface mass transfer, interface frictional drag, and force due to virtual mass.

It is useful to see how the above equation simplifies in the case of single-phase liquid flow, considering that the application of the RELAP5-3D code in this work is limited to single-phase flows. In such a case, $\alpha_f = 1$,

$\alpha_g = 0$, $u_f = u$ and $\rho_f = \rho$, resulting in the classical one-dimensional momentum equation for pipe flows:

$$\rho A\frac{\partial u}{\partial t} + \frac{1}{2}\rho A\frac{\partial u^2}{\partial x} = -A\frac{\partial p}{\partial x} + \rho f_x A - (\rho A)FWF(u) \tag{3.25}$$

The phasic thermal energy equations are:

$$\frac{\partial}{\partial t}(\alpha_f \rho_f U_f) + \frac{1}{A}\frac{\partial}{\partial x}(\alpha_f \rho_f U_f u_f A) = -P(\frac{\partial \alpha_f}{\partial t}) - \frac{p}{A}\frac{\partial}{\partial x}(\alpha_f u_f A) + Q_{wf} + Q_{if} - \Gamma_{ig}h_f^* - \Gamma_w h_f^{'} + DISS_f \tag{3.26}$$

$$\frac{\partial}{\partial t}(\alpha_g \rho_g U_g) + \frac{1}{A}\frac{\partial}{\partial x}(\alpha_g \rho_g U_g u_g A) = -P(\frac{\partial \alpha_g}{\partial t}) - \frac{p}{A}\frac{\partial}{\partial x}(\alpha_g u_g A) + Q_{wg} + Q_{ig} + \Gamma_{ig}h_g^* + \Gamma_w h_g^{'} + DISS_g \tag{3.27}$$

The Reynolds heat flux is neglected, the covariance terms are universally neglected, interfacial energy storage is neglected, and internal phasic heat transfer is neglected. In the phasic energy equations, Q_{wg} and Q_{wf} are the phasic wall heat transfer rates per unit volume. These phasic wall heat transfer rates satisfy the equation

$$Q = Q_{wg} + Q_{wf} \tag{3.28}$$

where Q is the total wall heat transfer rate to the fluid per unit of volume. The phasic energy dissipation terms, $DISS_g$ and $DISS_f$, are the sums of wall friction, pump, and turbine effects.

$$DISS_g = \alpha_g \rho_g FWG u_g^2 \tag{3.29}$$

and

$$DISS_f = \alpha_f \rho_f FWG u_f^2 \tag{3.30}$$

The phasic energy dissipation terms satisfy the relation:

$$DISS = DISS_g + DISS_f \tag{3.31}$$

The dissipation effects due to interface mass transfer, interface friction, and virtual mass are neglected.

Wall friction Due to the lumped parameters formulation, RELAP5-3D requires models to compute the effect of the forces exerted on the fluid due to wall friction. Being conceived for two-phase computations, in RELAP5-3D the wall friction is determined based on the volume flow regime map, and makes use of a two-phase multiplier approach. As this work does not deal with two-phase flow analyses, only the evaluation of friction-induced pressure drops in single-phase flows is discussed below. The force term due to wall friction in the right side of Equation 3.23 can be expressed in terms of wall shear stresses:

$$(\alpha_f \rho_f A) FWF(u_f) = \tau_f P_f = A\Big(\frac{\partial p}{\partial x}\Big)_{fr} \tag{3.32}$$

where P_f is the liquid wetted perimeter. The liquid wall shear stress is classically determined using the liquid Darcy-Weisbach friction factor:

$$\tau = \frac{\lambda(Re)}{4}\frac{\rho u^2}{2} \tag{3.33}$$

leading to the following:

$$\Big(\frac{\partial p}{\partial x}\Big)_{fr} = \frac{\lambda \rho u^2}{2D_h} \tag{3.34}$$

The Darcy-Weisbach friction factor is computed from correlations for laminar and turbulent flows with interpolation in the transition regime. The laminar friction factor is calculated as:

$$\lambda = \frac{64}{Re\Phi_s} \tag{3.35}$$

where Φ_s is a shape factor, which differs from unity in non-circular channels. The turbulent friction factor is calculated through the following correlation:

$$\frac{1}{\sqrt{\lambda}} = -2log_{10}\Big\{\frac{\epsilon}{3.7D} + \frac{2.51}{Re}\Big[1.14 - 2log_{10}\Big(\frac{\epsilon}{D} + \frac{21.25}{Re^{0.9}}\Big)\Big]\Big\} \tag{3.36}$$

where ϵ is the surface roughness. Losses due to abrupt area change are calculated using mechanistic form-loss models. Other losses due to complicated flow passage geometry are modeled using energy-loss coefficients input by the user.

Semi-implicit scheme difference equations In the RELAP5/RELAP5-3D code, a more convenient set of differential equations upon which to base the numerical scheme is obtained by

combining the previously discussed conservation equations into a sum and difference form, for which the interested reader can find detailed information in the code manuals [66]. The semi-implicit numerical solution scheme implemented in the code is based on replacing the system of differential equations with a system of finite difference equations partially implicit in time. The implicit terms are formulated to be linear in the dependent variables at new time, so that a linear time advancement-matrix is obtained.

The difference equations are based on control volumes (or mesh cell) in which mass and energy are conserved. This model results in defining mass and energy volume average properties and requiring knowledge of velocities at the volume boundaries. The velocities at boundaries are most conveniently defined through use of momentum control volumes (cells) centered on the mass and energy cell boundaries. This approach results in a numerical scheme having a staggered spatial mesh. The scalar properties (pressure, specific internal energies, and void fraction) of the flow are defined at cell centers, and vector quantities (velocities) are defined on the cell boundaries, as shown in Figure 3.2.

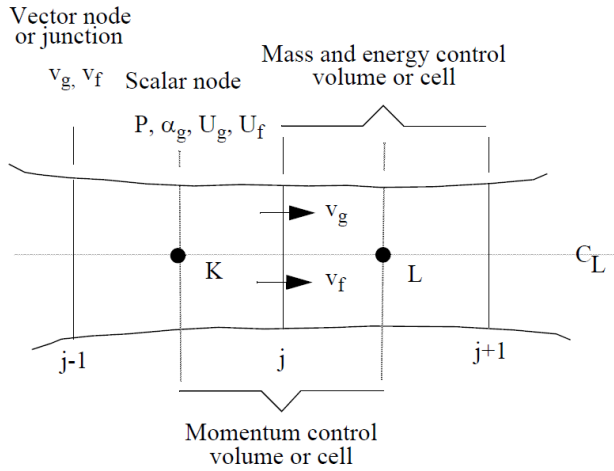

Figure 3.2: RELAP5/RELAP5-3D difference equation nodalization schematic [66].

The discretised equations for each cell are obtained by integrating the mass and energy equations with respect to the spatial variable, x, from the junction at x_j to x_{j+1}. The momentum equations are integrated with respect to the spatial variable from cell center to adjoining cell center (x_K to x_L, Figure 3.2) The nearly-implicit scheme is also available, and

is usually used for problems where the flow is expected to change very slowly with time, so that it is possible to use a large time step.

II. Heat structure models

In RELAP5-3D, the heat transfer is modeled using the heat structure components: solid structures that could be coupled with the hydrodynamics volumes. Temperatures and heat fluxes are computed from the one-dimensional heat conduction equation based on heat conduction code HEAT-1, developed at the INL [68]. The following is the equation of the one-dimensional heat conduction in the integral form that is resolved by RELAP5-3D in a heat structure:

$$\iiint_V \rho C_p(T,\overline{x})\frac{\partial T}{\partial t}(\overline{x},t)dV = \iint_S k(T,\overline{x})\overline{\nabla}T(\overline{x},t)\cdot ds + \iiint_V S(\overline{x},t)dV \tag{3.37}$$

in which C_p is the specific heat, T the temperature, $\overline{x}$ the space coordinate, t the time, S the surface, k the thermal conductivity and S the heat source.

3.2 STH-CFD coupling method development

In chapter 2, the literature on multi-scale fluid flow simulations was reviewed, and the possible modeling approaches have been outlined. The work presented in this dissertation follows a partitioning approach, considering that the use of proprietary codes does not allow for modification of the sources, thus making a monolithic implementation practically unfeasible. For what concerns the coupling in space, the domain decomposition technique was selected. Both explicit and implicit schemes have been implemented and tested; as it will be discussed in the next paragraphs, an extensive investigation of coupling numerical schemes has been carried out.

3.2.1 Hydrodynamic coupling

I. Problem formulation

In the developed domain decomposition technique, the original domain Ω is divided into two (or more) non-overlapping sub-domains Ω_{STH} and Ω_{CFD}. The coupling is executed through a dynamic exchange of BC at coupling interfaces, each of them characterized by a defined set of

thermal-hydraulic variables exchanged by the solvers, as conceptually shown in Figure 3.3.

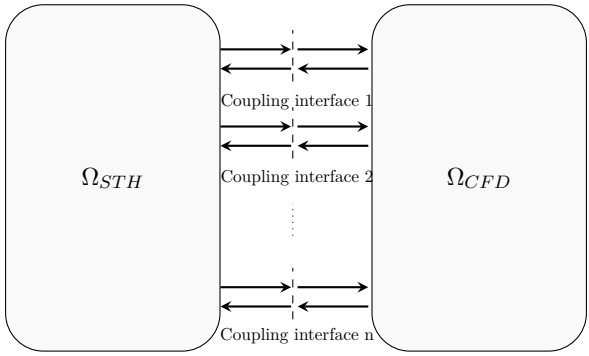

Figure 3.3: Conceptual scheme of a partitioned non-overlapping coupling method.

In the discussion that follows, a unique input vector $\mathbf{U}_{CFD}$ and $\mathbf{U}_{STH}$ is introduced for each of the coupled solvers, considered as black-boxes represented by the following input-output relations:

$$\mathbf{Y}_{CFD} = \phi_{CFD}(\mathbf{U}_{CFD}) \tag{3.38}$$

$$\mathbf{Y}_{STH} = \phi_{STH}(\mathbf{U}_{STH}) \tag{3.39}$$

The operators ϕ_{CFD} and ϕ_{STH} are a synthesis of a number of operations in the solution process, and generally require additional internal boundary condition input data. By definition, the variables stored in the input and output vectors are the thermal-hydraulic variables exchanged by the coupled codes. The condition on these vectors to be fulfilled is:

$$\mathbf{Y}_{CFD} = \mathbf{U}_{STH} \tag{3.40}$$

$$\mathbf{Y}_{STH} = \mathbf{U}_{CFD} \tag{3.41}$$

Equation 3.38 to Equation 3.41 yield the STH-CFD hydrodynamic coupled problem which can be expressed, in its fixed-point formulation, as:

$$\mathbf{U}_{CFD} = \phi_{STH}(\mathbf{U}_{STH}) = \phi_{STH}(\phi_{CFD}(\mathbf{U}_{CFD})) \tag{3.42}$$

As already mentioned, in partitioned coupling methods two numerical schemes can be used, namely the explicit and implicit methods, which are reviewed in subsection 3.2.2.

II. Hydraulic coupling interfaces

The data exchange at the hydraulic coupling interfaces has to be such to guarantee that the main transported quantities, mainly mass and energy, are conserved. Different schemes are possible for the choice of data to be shared between the codes. A typical one, which has been implemented in this in-house tool, is transferring velocity (or mass flow rate) information in one direction and pressure information in the opposite one. Energy terms e.g. temperature, are passed dynamically in both directions, and used in the solution process according to the direction of the flow. This data transfer option, shown in Figure 3.4, is conceived to enable the simulation of transients with inversions of the flow.

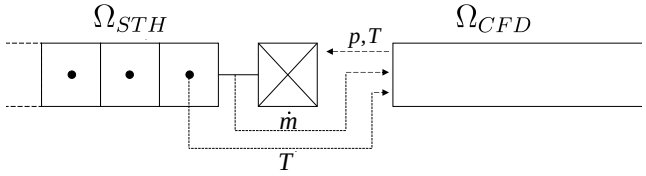

Figure 3.4: Boundary condition data transfer at a typical hydraulic coupling interface.

When passing pressure and temperature boundary conditions data from the 3D solver to the 1D code at a given hydraulic interface Γ_{hyd} of surface $A_{\Gamma_{hyd}}$, surface-averaged pressure and mass flow rate-weighted temperature values are computed:

$$p_{\Gamma_{hyd}} = \frac{1}{A_{\Gamma_{hyd}}} \int p dA_{\Gamma_{hyd}} = \frac{\sum_{i=1}^{n_{\Gamma_{hyd}}} p_i \ A_i}{\sum_{i=1}^{n_{\Gamma_{hyd}}} A_i} \tag{3.43}$$

$$T_{\Gamma_{hyd}} = \frac{1}{\dot{m}_{\Gamma_{hyd}}} \int T \rho v \cdot dA_{\Gamma_{hyd}} = \frac{\sum_{i=1}^{n_{\Gamma_{hyd}}} T_i \ \dot{m}_i}{\sum_{i=1}^{n_{\Gamma_{hyd}}} \dot{m}_i} \tag{3.44}$$

where $n_{\Gamma_{hyd}}$ is the number of cell facets in the CFD grid corresponding to the interface Γ_{hyd}. This necessary implies a loss of information on the 3D profiles, reason why in coupling implementation the ideal locations of the interfaces are regions of the system where no relevant gradients are present. For what concerns data that is passed from the 1D to the 3D solver, a number of up-scaling assumptions may be taken into account if velocity or mass flow rate is transferred, given the fact that the latter requires cell-wise BCs. In this regard, velocity profiles can be reconstructed on the basis of the average values provided by the STH

code. Also, if required, inlet turbulence parameters can be retrieved from 1D BC values through the use of empirical correlations. In this respect, it is however rather challenging to develop general methodologies which are valid for a wide range of flow patterns and geometries. In the current implementation, no particular data up-scaling is done, and flat velocity profiles are imposed in the CFD code. The source of error introduced by this assumption is deemed not relevant in the applications discussed in this dissertation. On the other hand, if pressure is passed from the STH to the CFD code, extrapolation of the interface value is performed based on the volume-centered pressures in two nearest volumes of the STH nodalization.

3.2.2 Numerical schemes

I. Explicit scheme

In the explicit scheme, the coupled domains are resolved only once every coupling time step. In the developed tool, a sequential communication pattern has been implemented, which is schematically represented in Figure 3.5.

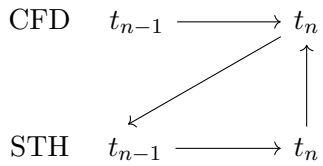

Figure 3.5: STH-CFD sequential data communication pattern.

This scheme for data exchange implies that the CFD code advances first its time level using BCs calculated by the STH code in the previous time step. The computed updated BCs are then sent to the STH code, which generally uses its own internal time stepping scheme (sub-cycling), to advance to the same time level. This coupling method is formally expressed by the equations below, which show how the input vector for the nth coupling time step is computed through a single coupling iteration.

$$ {}^{n}\mathbf{Y}_{CFD} = \phi_{CFD}({}^{n}\mathbf{U}_{CFD} = {}^{n-1}\mathbf{Y}_{STH}) \tag{3.45} $$

$$ {}^{n+1}\mathbf{U}_{CFD} = {}^{n}\mathbf{Y}_{STH} = \phi_{STH}({}^{n}\mathbf{U}_{STH} = {}^{n}\mathbf{Y}_{CFD}) = \phi_{STH}(\phi_{CFD}({}^{n}\mathbf{U}_{CFD})) \tag{3.46} $$

The same numerical scheme is represented in the flowchart in Figure 3.6.

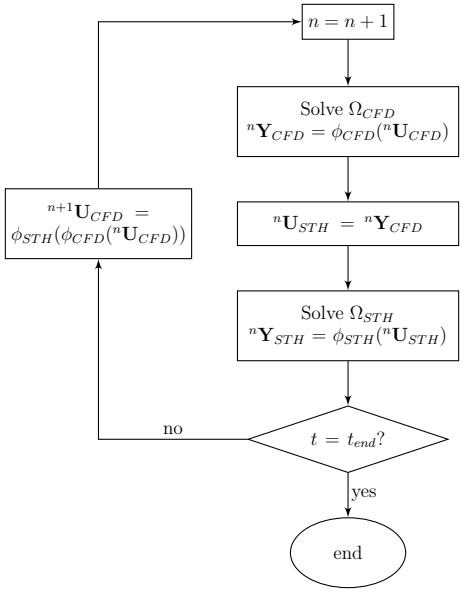

Figure 3.6: Flowchart of the generic sequential explicit coupling numerical algorithm.

Using the explicit scheme, Equation 3.42 is generally not solved at each coupling time step, eventually leading to pressure-velocity imbalance at the coupling interfaces. Particularly when simulating fast transients in incompressible fluid systems, this fact can lead to numerical stability issues, and introduces severe restrictions in the size of the coupling time step [47, 58].

II. Implicit scheme

In order to reach equilibrium of the momentum terms at the coupling boundary interfaces, an implicit scheme that approximates the solution of Equation 3.42 through an iterative procedure can be implemented. In implicit methods, the exchange of data between the codes is thus repeated within a coupling time step until a defined convergence criterion is met. In this way, global conservation of transported quantities should be assured, leading to numerical stability and improved accuracy of the results.

Fixed-point iteration Using the serial communication pattern previously introduced, the Gauss-Seidel fixed-point iteration scheme is:

$$ {}^{n}\mathbf{Y}^{k}_{CFD} = \phi_{CFD}({}^{n}\mathbf{U}^{k}_{CFD} = {}^{n}\mathbf{Y}^{k-1}_{STH}) \tag{3.47} $$

$$ {}^{n}\mathbf{U}^{k+1}_{CFD} = {}^{n}\mathbf{Y}^{k}_{STH} = \phi_{STH}({}^{n}\mathbf{U}^{k}_{STH} = {}^{n}\mathbf{Y}^{k}_{CFD}) = \phi_{STH}(\phi_{CFD}({}^{n}\mathbf{U}^{k}_{CFD})) \tag{3.48} $$

where, in this case, the index k refers to the coupling iteration at the time level n. In order to define the convergence criterion for the coupling iterations, the residual vector is introduced:

$$ {}^{n}\mathbf{R}^{k} = {}^{n}\mathbf{Y}^{k}_{STH} - {}^{n}\mathbf{U}^{k}_{CFD} \tag{3.49} $$

A schematic flowchart of the generic implicit coupling algorithm is represented in Figure 3.7.

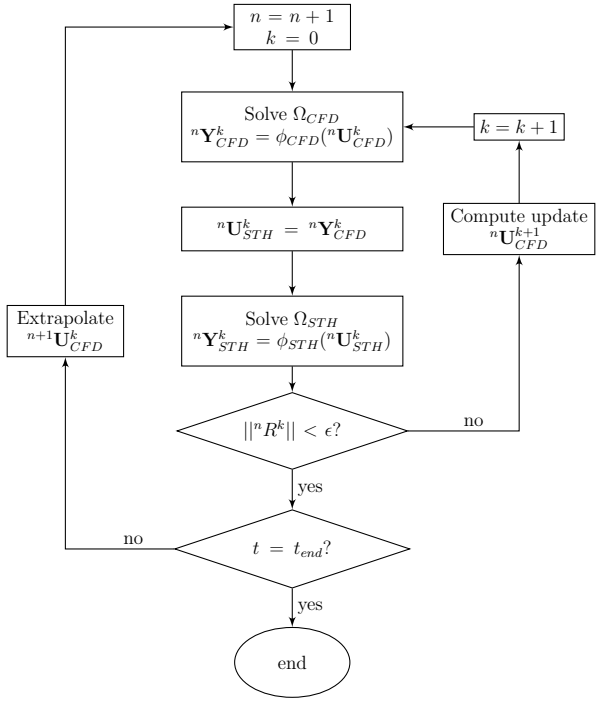

Figure 3.7: Flowchart of the generic implicit coupling numerical algorithm.

Scalar relaxation methods Constant or adaptive scalar relaxation can be adopted to improve stability and accelerate solution convergence.

At each coupling iteration, the updated CFD input vector can be evaluated as a linear combination between the previous input vector and the last STH output vector:

$$\begin{aligned} {}^{n}\mathbf{U}_{CFD}^{k+1} = {}^{n}\mathbf{U}_{CFD}^{k}(1 - {}^{n}\omega^{k}) + {}^{n}\mathbf{Y}_{STH}^{k}\,{}^{n}\omega^{k} = \\ = {}^{n}\mathbf{U}_{CFD}^{k} + {}^{n}\omega^{k}\ {}^{n}\mathbf{R}^{k} \end{aligned} \tag{3.50}$$

If a fixed relaxation is used, ${}^{n}\omega^{k} = \omega = const.$ for the whole simulation. This scheme is clearly of simple implementation, but its main disadvantage consists in the lack of physical information carried by the relaxation factor, whose value is often evaluated through trial-and-error procedures. A more efficient relaxation method can be obtained by using the Aitken Δ^2 method, in which the relaxation parameter is evaluated from two previous coupling iterations through a step of the secant method [69]:

$${}^{n}\mathbf{U}_{CFD}^{k+1} = \frac{{}^{n}\mathbf{Y}_{STH}^{k}\,{}^{n}\mathbf{U}_{CFD}^{k-1} - {}^{n}\mathbf{U}_{CFD}^{k}\,{}^{n}\mathbf{Y}_{STH}^{k-1}}{{}^{n}\mathbf{Y}_{STH}^{k} - {}^{n}\mathbf{U}_{CFD}^{k} - {}^{n}\mathbf{Y}_{STH}^{k-1} + {}^{n}\mathbf{U}_{CFD}^{k-1}} \tag{3.51}$$

Recalling that ${}^{n}\mathbf{U}_{CFD}^{k+1} = {}^{n}\mathbf{U}_{CFD}^{k} + {}^{n}\omega^{k}\ {}^{n}\mathbf{R}^{k}$, the Aitken relaxation factor can be obtained as:

$${}^{n}\omega^{k} = -{}^{n}\omega^{k-1}\frac{{}^{n}\mathbf{R}^{k-1}}{{}^{n}\mathbf{R}^{k} - {}^{n}\mathbf{R}^{k-1}} \tag{3.52}$$

In case of vectors, the under-relaxation factor is evaluated as:

$${}^{n}\omega^{k} = -{}^{n}\omega^{k-1}\frac{\left({}^{n}\mathbf{R}^{k-1}\right)^{T}\left({}^{n}\mathbf{R}^{k} - {}^{n}\mathbf{R}^{k-1}\right)}{|{}^{n}\mathbf{R}^{k} - {}^{n}\mathbf{R}^{k-1}|^{2}} \tag{3.53}$$

Two coupling iterations are needed to compute the first value of the relaxation factor; in the first iteration of a time step, its value can be set equal to the last relaxation parameter computed in the previous time step, as expressed by Equation 3.54.

$${}^{n}\omega^{0} = {}^{n-1}\omega^{k_{end}} \tag{3.54}$$

Moreover, if necessary for stability reasons, the relaxation factor can be forced to remain within a certain range by imposing a lower and upper limit. It is worth remarking that the Aitken scheme is proven to work well if the residual vector holds same physical variables, which might be not the case in fluid-fluid coupled domains. For instance, in case of a CFD domain with inlet and outlet coupling interfaces, the residual vector may hold mass flow rate and pressure differences. In order to implement the Aitken algorithm in an effective manner, dimensionless residuals are evaluated by means of a residual vector computed through a reference coupling iteration.

Quasi-Newton (QN) method An effective dynamic relaxation scheme can be achieved through the application of the Quasi-Newton method, which is essentially based on the linearization of the residual function around the current solution at each coupling iteration, and approximation of the terms of the Jacobian matrix. Recalling Equation 3.42, it is convenient here to formulate the coupled problem in the form of a root-finding problem:

$$\mathbf{R}(\mathbf{U}_{CFD}) = \phi_{STH}(\phi_{CFD}(\mathbf{U}_{CFD})) - \mathbf{U}_{CFD} = 0 \tag{3.55}$$

The solution of the previous equation can be approximated by using a first order Taylor expansion around the current solution:

$${}^{n}\mathbf{R}^{k+1} = {}^{n}\mathbf{R}^{k} + {}^{n}\mathbf{J}^{k}({}^{n}\Delta\mathbf{U}^{k}_{CFD}) = 0 \tag{3.56}$$

where the Jacobian matrix ${}^{n}\mathbf{J}^{k}$ contains the partial derivatives of the residual vector terms $\mathbf{R} = [r_1, r_2, .., r_n]$ with respect to the terms of the CFD input vector $\mathbf{U}_{CFD} = [u_1, u_2, .., u_n]$:

$${}^{n}\mathbf{J}^{k} = \begin{bmatrix} {}^{n}\dfrac{\partial r_1}{\partial u_1}^{k} & {}^{n}\dfrac{\partial r_1}{\partial u_2}^{k} & \cdots & {}^{n}\dfrac{\partial r_1}{\partial u_n}^{k} \\ {}^{n}\dfrac{\partial r_2}{\partial u_1}^{k} & {}^{n}\dfrac{\partial r_2}{\partial u_2}^{k} & \cdots & {}^{n}\dfrac{\partial r_2}{\partial u_n}^{k} \\ \vdots & \vdots & \ddots & \vdots \\ {}^{n}\dfrac{\partial r_n}{\partial u_1}^{k} & {}^{n}\dfrac{\partial r_n}{\partial u_2}^{k} & \cdots & {}^{n}\dfrac{\partial r_n}{\partial u_n}^{k} \end{bmatrix} \tag{3.57}$$

When coupling black-box solvers, the terms of the Jacobian matrix are in general unknown and hardly accessible; nevertheless, they can be approximated with finite differences:

$${}^{n}\frac{\partial r_i}{\partial u_j}^{k} \simeq \frac{{}^{n}r_i^{k} - {}^{n}r_i^{k-1}}{{}^{n}u_j^{k} - {}^{n}u_j^{k-1}} \tag{3.58}$$

Once the approximated Jacobian matrix is known, Equation 3.56 allows for the computation of the update ${}^{n}\Delta\mathbf{U}^{k}_{CFD}$ to be applied to the CFD input vector at the next coupling iteration $k+1$:

$${}^{n}\mathbf{U}^{k+1}_{CFD} = {}^{n}\mathbf{U}^{k}_{CFD} + {}^{n}\Delta\mathbf{U}^{k}_{CFD} \tag{3.59}$$

The method developed in this work to approximate the Jabobian matrix will be presented in detail in subsection 3.2.6, in which the implementation tests are discussed. It is straightforward to notice that the Quasi-Newton method is also a relaxation method, with a matrix relaxation factor instead of a scalar value; if the inverse of the Jacobian ${}^{n}(\mathbf{J}^{-1})^{k}$ is approximated by $-{}^{n}\omega^{k}\mathbf{I}$, the scalar relaxation and the Quasi-Newton method are identical.

QN method extension for multi-domain problems Coupled models of full reactor systems may require a large number of hydraulic interfaces, resulting in a large number of degrees of freedom which can be costly from the computational point of view. A novel technique to reduce the degree-of-freedom of the problem, specifically conceived for pool-type systems analyses, has been developed and is here presented.

The method consists in considering as terms of the input vectors the sum (in case of mass flow rates) or average (in case of pressure) of BC values of a number of coupling interfaces. In a pool-type reactor calculation, a typical case where this assumption is particularly valid is the case of hydraulic interfaces connecting the outlet of the core, often modeled using a large number of parallel channels in the STH code, to a CFD model of the hot plenum of the reactor vessel. In such a case, this assumption is consistent not only from the numerical point of view, but also physically considering that the distribution of the flow in the single interfaces can often be considered as a local phenomenon, with the overall pressure-velocity fields balance being dependent only on net flows. Such a situation can be schematically represented as in Figure 3.8, which shows two coupled domains connected by a number of hydraulic interfaces n_i, where the index i refers to the corresponding term ${}^n u_i^k$ of the reduced input vector considered in the Quasi-Newton algorithm.

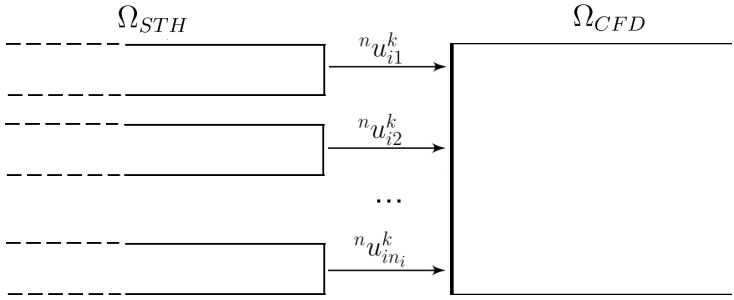

Figure 3.8: Two coupled domains connected by multiple hydraulic interfaces, grouped to reduce the number of degrees of freedom of the Quasi-Newton scheme.

Adopting this strategy, the term ${}^n u_i^k$ of the CFD input vector is therefore expressed as the sum of the BC values e.g. mass flow rates, at a number

of interfaces n_i associated with it:

$$ {}^{n}u_i^k = \sum_{j=1}^{n_i} {}^{n}u_{ij}^k \tag{3.60} $$

As it will be explained in subsection 3.2.6, to approximate the Jacobian matrix a small perturbation is applied to a single term of the CFD input vector, while maintaining the others unchanged. Once the Jacobian is computed, the new CFD input vector ${}^{n}\mathbf{U}_{CFD}^{k+1}$, holding only total mass flow rates, is computed. However, single BC values for each interface need to be calculated to proceed to the next coupling iteration. The requirements for these BC interface values are i) to satisfy the new computed update ${}^{n}\mathbf{U}_{CFD}^{k+1}$ and ii) to take into account updated single BC values computed by the STH code. One way to meet both the two requirements is based on the evaluation of the vector ${}^{n}\Delta\mathbf{U}^{k+1}$ [1], difference between the new CFD input ${}^{n}\mathbf{U}_{CFD}^{k+1}$ and the old STH output vector ${}^{n}\mathbf{Y}_{STH}^{k}$;

$$ {}^{n}\Delta\mathbf{U}^{k+1} = {}^{n}\mathbf{U}_{CFD}^{k+1} - {}^{n}\mathbf{Y}_{STH}^{k} \tag{3.61} $$

Recalling the definition of the generic term i of the BC input vector in Equation 3.60, it is straightforward to define the corresponding term of this vector:

$$ {}^{n}\Delta u_i^{k+1} = \sum_{j=1}^{n_i} {}^{n}u_{ij}^{k+1} - \sum_{j=1}^{n_i} {}^{n}\widetilde{u}_{ij}^{k} \tag{3.62} $$

where the terms with the tilde symbol refer as usual to values computed by the STH code. In Equation 3.62, the single interface BC values ${}^{n}u_{ij}^{k+1}$ are unknown, since only new total mass flow rates are computed by the Quasi-Newton algorithm. These n_i BC values are computed by equally distributing to the interested interfaces the quantity ${}^{n}\Delta u_i^{k+1}$, which can be expressed as follows:

$$ {}^{n}\Delta u_i^{k+1} = \sum_{j=1}^{n_i} {}^{n}\delta u_i^{k+1} = n_i({}^{n}\delta u_i^{k+1}) \tag{3.63} $$

The same adjustment ${}^{n}\delta u_i^{k+1}$ is thus applied to the BC values computed by the STH code to evaluate new values to be imposed in the CFD code:

$$ {}^{n}u_{ij}^{k+1} = {}^{n}\widetilde{u}_{ij}^{k} + {}^{n}\delta u_i^{k+1} \tag{3.64} $$

The application of this methodology will be presented in chapter 5 and chapter 6.

1. This vector and its terms do not have to be confused with the vector ${}^{n}\Delta\mathbf{U}_{CFD}^{k}$ computed by the Quasi-Newton algorithm

3.2.3 Thermal coupling

Coupled models may require an additional type of interface when conjugate heat transfer across boundary walls separating different subdomains is to be computed. The requirement for these interfaces is the sole conservation of energy, as there is no mass transfer across them. A possible choice for the BC exchange is shown in Figure 3.9.

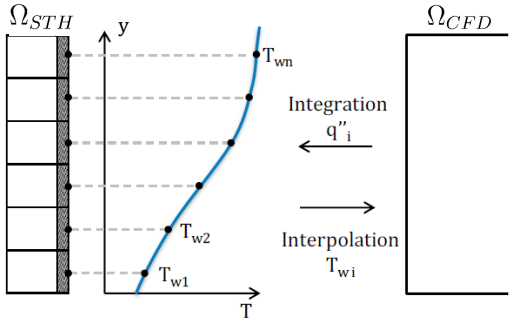

Figure 3.9: Data mapping and BC exchange at thermal coupling interfaces.

The data mapping for a generic thermal interface Γ_{th} is based on the discretization of the interface surface into a number of nodes $N_{\Gamma_{th}}$, corresponding to the number of nodes of the interested volume in the STH nodalization. Each node i, which identifies a portion of the boundary wall of surface A_i, corresponds in the CFD grid to a number n_i of cell wall facets, each of face area A_{f_j}. The total surface of the thermal coupling interface $A_{\Gamma_{th}}$ is thus given by:

$$A_{\Gamma_{th}} = \sum_{i=1}^{N_{\Gamma_{th}}} A_i = \sum_{i=1}^{N_{\Gamma_{th}}} \sum_{j=1}^{n_i} A_{f_j} \tag{3.65}$$

In the coupled solution process, the STH codes computes for each node i the wall temperatures T_i^w, which are the interface BC input for the CFD code. The CFD solver requires however cell-wise data, which are obtained through interpolation of the aforementioned wall temperature T_i provided by the STH code; for each wall cell facet whose y_{f_j} coordinate (the axial direction in the STH nodalization) is in the range (y_{i-1}, y_i), the wall temperature is evaluated as:

$$T^w(y_{f_j}) = T_i^w + \frac{T_i^w - T_{i-1}^w}{y_i - y_{i-1}}(y_{f_j} - y_i) \tag{3.66}$$

In turn, for each interface node i the CFD code computes the average heat flux q_i'', imposed in the STH code at each node as fixed wall heat flux BC.

$$q_i'' = \frac{1}{A_i} \int_{A_i} q'' dA_i = \frac{\sum_{j=1}^{n_i} q_{f_j}}{\sum_{j=1}^{n_i} A_{f_j}} \tag{3.67}$$

This scheme for the data exchange assures that, at the end of each coupling iteration, the heat flux in the coupled codes is equal.

3.2.4 Programming architecture

In the first implementation of the tool, which included only the explicit scheme, the coupling algorithm was executed within the FLUENT code, which acted as master process in charge of driving the exchange of information between the codes. In such a configuration, the coupling instructions are executed within a User Defined Function (UDF), which includes an *EXECUTE_AT_END* macro used to call the RELAP5-3D code, and a *DEFINE_PROFILE* macro to update interface BC. To implement the implicit scheme, which requires the execution of coupling instructions and numerical algorithms without advancing time level, a more sophisticated and versatile software architecture was required. In the new implementation, the coupling method is executed via an external supervisor code, written in Python language. The code FLUENT runs in parallel to the supervisor through a dedicated input file; it receives from the supervisor updated BC input vector and sends back BC data after the computation of a time step (explicit scheme) or a coupling iteration (implicit scheme). A diagram illustrating this new programming architecture is shown in Figure 3.10.

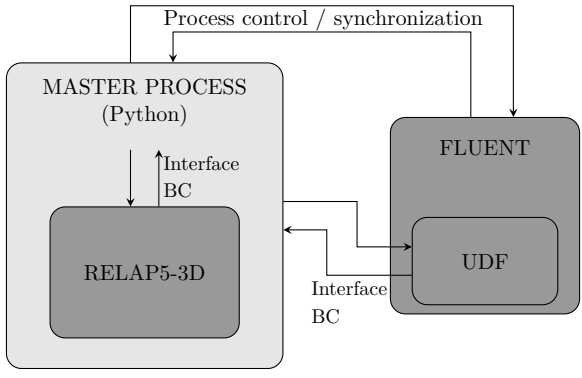

Figure 3.10: Coupling programming architecture.

Within the FLUENT process a UDF, developed for parallel computations, is compiled to allow receiving and sending interface BCs. Its source code, written in C language, makes use of `struct` variables to guarantee flexibility and re-usability of the UDF for different applications. The UDF includes a *DEFINE_ON_DEMAND* macro executed at the beginning of a coupled calculation to initialize interface data and BCs values. A further *DEFINE_ON_DEMAND* macro is used to read, at the beginning of each coupling iteration/time step, interface BCs. A third *DEFINE_ON_DEMAND* macro computes interface BCs to be sent to the master process via text files. Additional UDF macros can be added depending of the specific calculation requirements. A technique has been developed to assure the synchronization of the codes, which have to remain in idle mode while other processes are executed. As for the STH code RELAP5-3D, at present there is no possibility to implement user defined routines or to modify the source code, therefore the only way to implement the coupling is to execute the STH code block as a sub-routine of the supervisor, which is responsible of preparing the input file and extracting the time step results. Although this procedure for running the STH code might be inefficient, the computational costs associated with the execution of the STH code remain almost negligible compared to the CFD code, which takes up most of the simulation runtime. In order to avoid excessive growth of the RELAP5-3D restart and plot files, a routine has been developed to save the intermediate results of interest and reset those files. A detailed block diagram of the coupling mechanism is shown in Figure 3.11.

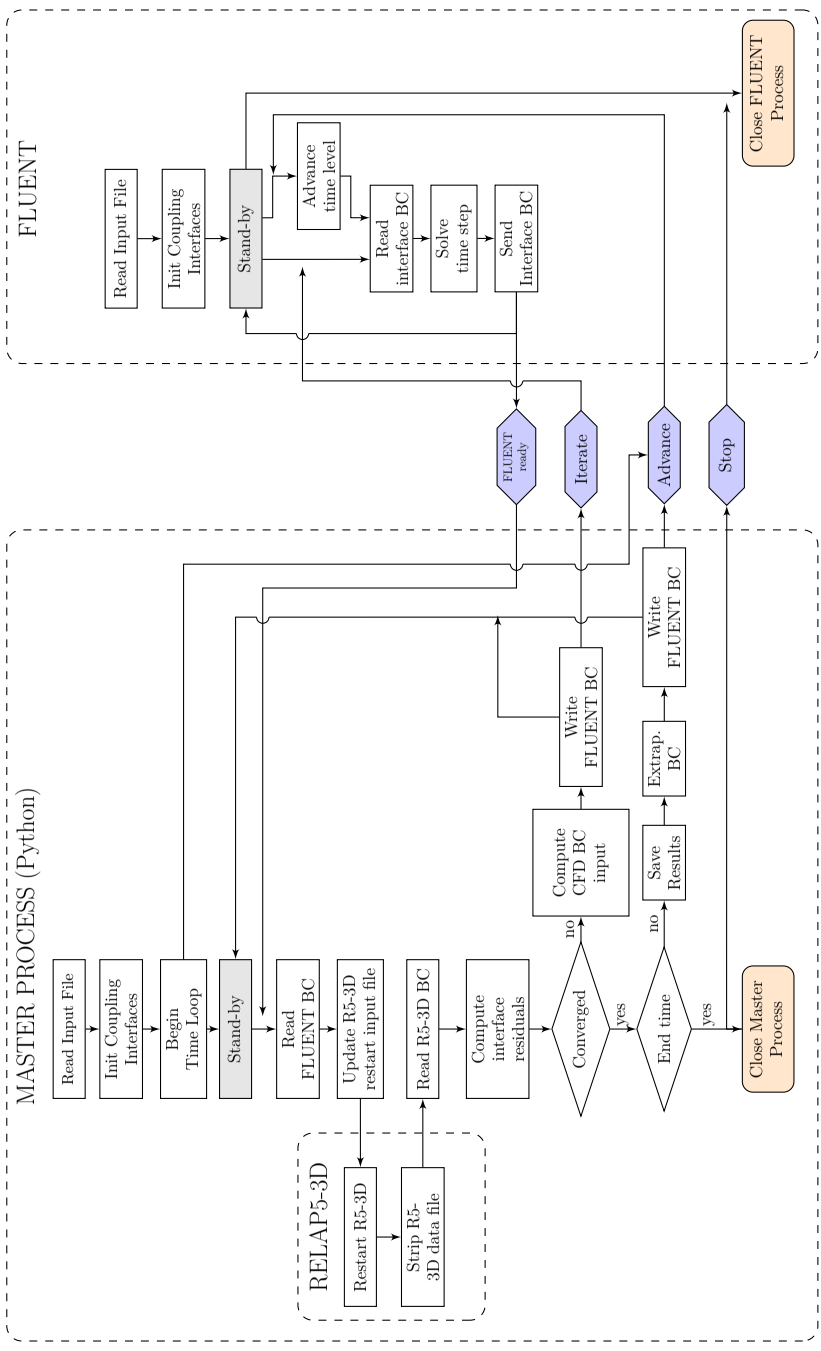

Figure 3.11: Outline of the coupling execution.

3.2.5 V&V approach

A V&V plan for the computational method is going to be established with the aim of verifying that methods and numerical schemes are correctly implemented (verification), and that the coupling methodology provides accurate results according to reference experimental data (validation) [70, 71].

In coupled thermal-hydraulic codes, an additional level of solution is introduced on top of the stand-alone codes; therefore, the use of well validated STH and CFD models is an essential pre-requisite for the validation of coupling methods. The V&V of the stand-alone STH and CFD codes is, however, not exhaustive as the coupling algorithm introduces, depending on the coupling approach, some additional approximations that need appropriate validation. To this purpose, integral experiments which feature two-way feedback between the regions modeled by the coupled codes are needed [72].

Preliminary verification of the developed computational method has been performed against analytical solutions and through code-to-code comparisons on simple flow problems, for which no relevant 3D phenomena are present. This allows adopting well validated and congruent full stand-alone STH and CFD models, thus directly assessing the impact of the implemented coupling algorithm on the solution. Some of the verification tests are discussed in subsection 3.2.6.

The validation of STH, CFD and coupled codes for liquid metal-cooled systems is currently based on a large number of separate-effect experiments, component-scale experiments and scaled integral experiments, performed at national level and within the EC-funded projects SESAME and MYRTE [17]. As introduced in chapter 1, these projects will also provide the basis for the establishment of BPGs, V&V methodologies and UQ methods.

At present, the validation of the developed multi-scale tool against experiments is planned to be performed on the basis of small- and large-scale test facilities, specifically:

- The TALL-3D LBE loop [73],
- The water scale model MYRRHABELLE [74],
- The E-SCAPE pool-type facility.

A first validation against an integral loss of flow test in the TALL-3D loop is discussed in chapter 4. As for the E-SCAPE experimental

programme, first measured data on forced circulation isothermal operating conditions are going to be used for input models calibration, with particular focus on operating parameters (total LBE mass, Ar cover gas pressure, electric power input, secondary system operation), hydraulic losses etc. The planned tests, performed within the MYRTE WP3, will provide data-sets for the validation of the stand-alone models in relation to the regions and phenomena relevant to them, and successively for the validation of the coupling tool on integral transient test data.

It is worth remarking that the computational method is still in an early stage of development; therefore, a complete validation matrix, the specification and use of validation metrics and acceptance criteria are still under assessment and development.

3.2.6 Verification analyses

I. Open pipe flow test

Case set up A simple coupled problem consisting of single-phase isothermal water flow in an open pipe has been addressed for a first testing of the developed tool. The analyzed pipe is of length L=8.5 m and internal diameter D=0.1 m. In the developed coupled model, the original pipe is divided into a CFD domain simulating a middle part of length L_{CFD}=0.5 m, and a STH domain resolving the remaining initial and ending portions. The verification of the coupling methodology was carried out by comparing the simulation results of the coupled model against a full RELAP5-3D model. Given the fact that in this configuration there are no relevant three-dimensional phenomena that may affect the solution, agreement between the results is to be expected. The computational models are shown in Figure 3.12. At the top the full STH model is depicted, while the coupled STH-CFD model is shown at the bottom. The CFD portion of the pipe is computed using a full 3D model. The computational grid, shown in Figure 3.13, is generated using a surface mesh sweeping method and counts about $145 \cdot 10^3$ cells, with a minimum orthogonal quality of 0.76. The standard $k - \epsilon$ turbulence model is used in these tests.

In these preliminary analyses, we neglect the energy terms (isothermal conditions) and focus on the hydraulic coupling, mainly related to numerical stability aspects. In this way, it is possible to recognize that the terms of the CFD input vector are the mass flow rate at the inlet interface Γ_1 and pressure at the outlet interface Γ_2. In the implicit scheme, at each coupling iteration, the CFD code calculates inlet pressure and

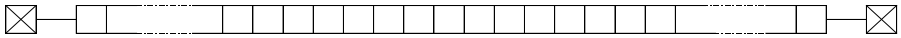

(a) Full STH model

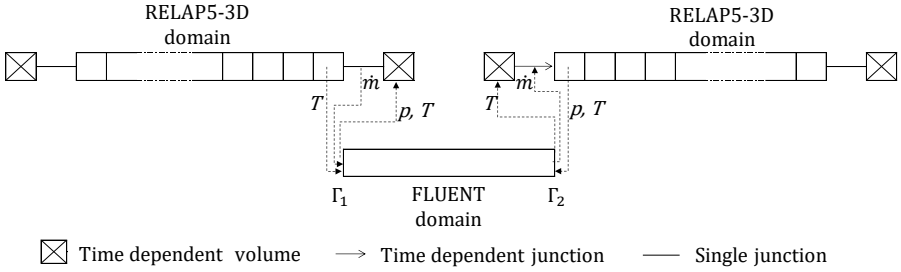

(b) STH-CFD coupled model

Figure 3.12: Domain decomposition and data exchange at the interfaces for a single-phase open pipe flow coupled problem.

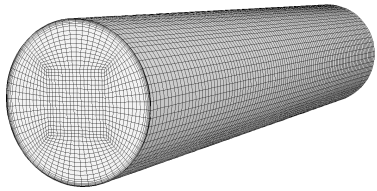

Figure 3.13: Computational grid for the portion of the pipe computed by FLUENT.

outlet mass flow rate, which are the terms of the input vector for the STH solver. The STH code calculates then new mass flow rate at the interface Γ_1 and pressure at the interface Γ_2, which represent the terms of the STH output vector and are indicated with the tilde symbol.

$$ {}^{n}\mathbf{U}^{k}_{CFD} = \begin{bmatrix} {}^{n}\dot{m}^{k}_{\Gamma_1} \\ {}^{n}p^{k}_{\Gamma_2} \end{bmatrix}, \quad {}^{n}\mathbf{Y}^{k}_{STH} = \begin{bmatrix} {}^{n}\widetilde{\dot{m}}^{k}_{\Gamma_1} \\ {}^{n}\widetilde{p}^{k}_{\Gamma_2} \end{bmatrix} \tag{3.68} $$

On the basis of the above definitions, the interface residual vector, evaluated according to Equation 3.49, assumes for this test case the following form:

$$ {}^{n}\mathbf{R}^{k} = \begin{bmatrix} {}^{n}r^{k}_{\Gamma_1} \\ {}^{n}r^{k}_{\Gamma_2} \end{bmatrix} = \begin{bmatrix} {}^{n}\widetilde{\dot{m}}^{k}_{\Gamma_1} - {}^{n}\dot{m}^{k}_{\Gamma_1} \\ {}^{n}\widetilde{p}^{k}_{\Gamma_2} - {}^{n}p^{k}_{\Gamma_2} \end{bmatrix} \tag{3.69} $$

Considering that the residual vector holds different physical quantities, namely mass flow rate and pressure values, the residual vector is evaluated in dimensionless terms, as explained in section II.:

$$ {}^{n}\mathbf{R}^{k} = \begin{bmatrix} ({}^{n}\tilde{\dot{m}}^{k}_{\Gamma_1} - {}^{n}\dot{m}^{k}_{\Gamma_1})/\Delta\dot{m}_{ref} \\ ({}^{n}\tilde{p}^{k}_{\Gamma_2} - {}^{n}p^{k}_{\Gamma_2})/\Delta p_{ref} \end{bmatrix} \tag{3.70} $$

The linearization of the residual function at the k iteration of the time level n is therefore expressed as follows:

$$ \begin{bmatrix} {}^{n}r^{k+1}_{\Gamma_1} \\ {}^{n}r^{k+1}_{\Gamma_2} \end{bmatrix} = \begin{bmatrix} {}^{n}r^{k}_{\Gamma_1} \\ {}^{n}r^{k}_{\Gamma_2} \end{bmatrix} + \begin{bmatrix} {}^{n}\left(\frac{\partial r_{\Gamma_1}}{\partial \dot{m}_{\Gamma_1}}\right)^{k} & {}^{n}\left(\frac{\partial r_{\Gamma_1}}{\partial p_{\Gamma_2}}\right)^{k} \\ {}^{n}\left(\frac{\partial r_{\Gamma_2}}{\partial \dot{m}_{\Gamma_1}}\right)^{k} & {}^{n}\left(\frac{\partial r_{\Gamma_2}}{\partial p_{\Gamma_2}}\right)^{k} \end{bmatrix} \begin{bmatrix} {}^{n}\Delta\dot{m}^{k}_{\Gamma_1} \\ {}^{n}\Delta p^{k}_{\Gamma_2} \end{bmatrix} = 0 \tag{3.71} $$

which allows for the evaluation of the CFD input update to be used for the iteration $k+1$:

$$ {}^{n}\mathbf{U}^{k+1}_{CFD} = \begin{bmatrix} {}^{n}\dot{m}^{k+1}_{\Gamma_1} \\ {}^{n}p^{k+1}_{\Gamma_2} \end{bmatrix} = \begin{bmatrix} {}^{n}\dot{m}^{k}_{\Gamma_1} + {}^{n}\Delta\dot{m}^{k}_{\Gamma_1} \\ {}^{n}p^{k}_{\Gamma_2} + {}^{n}\Delta p^{k}_{\Gamma_2} \end{bmatrix} \tag{3.72} $$

This test case consists of a 2-degree of freedom coupled problem, thus two consecutive coupling iterations are used to evaluate the approximated Jacobian. Given two sequential coupling iterations a and b, the following system of 4 equations can be built, in which the unknowns are the approximated terms of the Jacobian, $\frac{\Delta r_{\Gamma_1}}{\Delta \dot{m}_{\Gamma_1}}$, $\frac{\Delta r_{\Gamma_1}}{\Delta p_{\Gamma_2}}$, $\frac{\Delta r_{\Gamma_2}}{\Delta \dot{m}_{\Gamma_1}}$ and $\frac{\Delta r_{\Gamma_2}}{\Delta p_{\Gamma_2}}$.

$$ \begin{cases} \Delta r^{a}_{\Gamma_1} = \dfrac{\Delta r_{\Gamma_1}}{\Delta \dot{m}_{\Gamma_1}} \Delta \dot{m}^{a}_{\Gamma_1} + \dfrac{\Delta r_{\Gamma_1}}{\Delta p_{\Gamma_2}} \Delta p^{a}_{\Gamma_2} \\ \Delta r^{a}_{\Gamma_2} = \dfrac{\Delta r_{\Gamma_2}}{\Delta \dot{m}_{\Gamma_1}} \Delta \dot{m}^{a}_{\Gamma_1} + \dfrac{\Delta r_{\Gamma_2}}{\Delta p_{\Gamma_2}} \Delta p^{a}_{\Gamma_2} \\ \Delta r^{b}_{\Gamma_1} = \dfrac{\Delta r_{1}}{\Delta \dot{m}_{\Gamma_1}} \Delta \dot{m}^{b}_{\Gamma_1} + \dfrac{\Delta r_{\Gamma_1}}{\Delta p_{\Gamma_2}} \Delta p^{b}_{\Gamma_2} \\ \Delta r^{b}_{\Gamma_2} = \dfrac{\Delta r_{\Gamma_2}}{\Delta \dot{m}_{\Gamma_1}} \Delta \dot{m}^{b}_{\Gamma_1} + \dfrac{\Delta r_{\Gamma_2}}{\Delta p_{\Gamma_2}} \Delta p^{b}_{\Gamma_2} \end{cases} \tag{3.73} $$

In order to be sure that the two input vectors used in the two coupling iterations are orthogonal, independent perturbations of the single terms of the CFD input vector are applied. Supposing that at a certain iteration ($k = k^*$) the Jacobian has to be computed, in the first coupling

iteration a small perturbation is thus applied to the inlet mass flow rate while keeping constant the outlet pressure:

$$ {}^{n}\mathbf{U}_{CFD}^{k^*+1} = \begin{bmatrix} {}^{n}\dot{m}_{\Gamma_1}^{k^*+1} \\ {}^{n}p_{\Gamma_2}^{k^*+1} \end{bmatrix} = \begin{bmatrix} {}^{n}\dot{m}_{\Gamma_1}^{k^*} + \delta m \\ {}^{n}p_{\Gamma_2}^{k^*} \end{bmatrix} \tag{3.74} $$

while in the second iteration the inlet mass flow rate is kept unchanged and a small perturbation is applied to the outlet pressure.

$$ {}^{n}\mathbf{U}_{CFD}^{k^*+2} = \begin{bmatrix} {}^{n}\dot{m}_{\Gamma_1}^{k^*+2} \\ {}^{n}p_{\Gamma_2}^{k^*+2} \end{bmatrix} = \begin{bmatrix} {}^{n}\dot{m}_{\Gamma_1}^{k^*+1} \\ {}^{n}p_{\Gamma_2}^{k^*+1} + \delta p \end{bmatrix} \tag{3.75} $$

The two coupling iterations result in the following data:

$$ \begin{cases} \Delta\dot{m}_{\Gamma_1}^{a} = \delta m \\ \Delta p_{\Gamma_2}^{a} = 0 \end{cases} \tag{3.76} $$

$$ \begin{cases} \Delta\dot{m}_{\Gamma_1}^{b} = 0 \\ \Delta p_{\Gamma_2}^{b} = \delta p \end{cases} \tag{3.77} $$

as well as:

$$ \begin{cases} \Delta r_{\Gamma_1}^{a} = r_{\Gamma_1}^{k^*+1} - r_{\Gamma_1}^{k^*} \\ \Delta r_{\Gamma_2}^{a} = r_{\Gamma_2}^{k^*+1} - r_{\Gamma_2}^{k^*} \end{cases} \tag{3.78} $$

$$ \begin{cases} \Delta r_{\Gamma_1}^{b} = r_{\Gamma_1}^{k^*+2} - r_{\Gamma_1}^{k^*+1} \\ \Delta r_{\Gamma_2}^{b} = r_{\Gamma_2}^{k^*+2} - r_{\Gamma_2}^{k^*+1} \end{cases} \tag{3.79} $$

which allow for the evaluation of the components of the approximated Jacobian, according to Equation 3.73:

$$ {}^{n}\mathbf{J}^{k} = \begin{bmatrix} \left(\dfrac{\Delta r_{\Gamma_1}^{a}}{\Delta\dot{m}_{\Gamma_1}^{a}}\right) & \left(\dfrac{\Delta r_{\Gamma_1}^{b}}{\Delta p_{\Gamma_2}^{b}}\right) \\ \left(\dfrac{\Delta r_{\Gamma_2}^{a}}{\Delta\dot{m}_{\Gamma_1}^{a}}\right) & \left(\dfrac{\Delta r_{\Gamma_2}^{b}}{\Delta p_{\Gamma_2}^{b}}\right) \end{bmatrix} \tag{3.80} $$

When the calculation advances to a new time step, the Jacobian computed in the previous step is used after the first iteration (in which the input vector is extrapolated from previous time steps) to compute the update of the CFD input vector for the second iteration. After its first use, the quality of the Jacobian is checked, in order to determine whether the code will use it for the entire time step. In this test case, the quality of the Jacobian is considered acceptable if the residuals drop at least one order of magnitude after its first use:

$$ {}^{n}R^{1} < \frac{{}^{n}R^{0}}{10} \tag{3.81} $$

If the above is not satisfied, the Jacobian is re-updated through the same procedure involving two coupling iterations. A simplified flowchart of this implicit scheme with the Quasi-Newton algorithm is shown in Figure 3.14. Similar methods have been successfully implemented for fluid-structure interaction simulations, as presented for instance in [75].

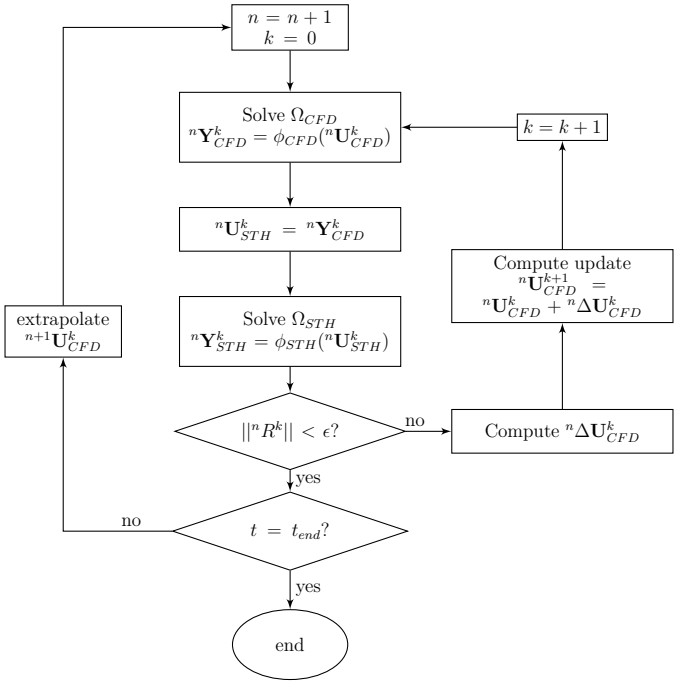

Figure 3.14: Simplified flowchart of the implicit coupling scheme with the interface Quasi-Newton algorithm.

A detailed flowchart of the QN algorithm, executed at each coupling iteration k to compute the new CFD input vector ${}^{n}\mathbf{U}^{k+1}_{CFD}$, is shown in Figure 3.15. The inputs of this algorithm are the iteration counter k, the old CFD input vector ${}^{n}\mathbf{U}^{k}_{CFD}$, the index i which counts the iterations during the update of the Jacobian, and the old and new residuals vectors. The flag j is used to keep track of the status of the Jacobian matrix, which can be available ($j = 1$) or unavailable ($j = 0$), for instance during the coupling iterations required for its approximation.

Results The first transient simulation performed consists of a mass flow ramp, from fluid initially at rest, driven by an abrupt pressure difference applied at the pipe boundaries. The transient evolution of

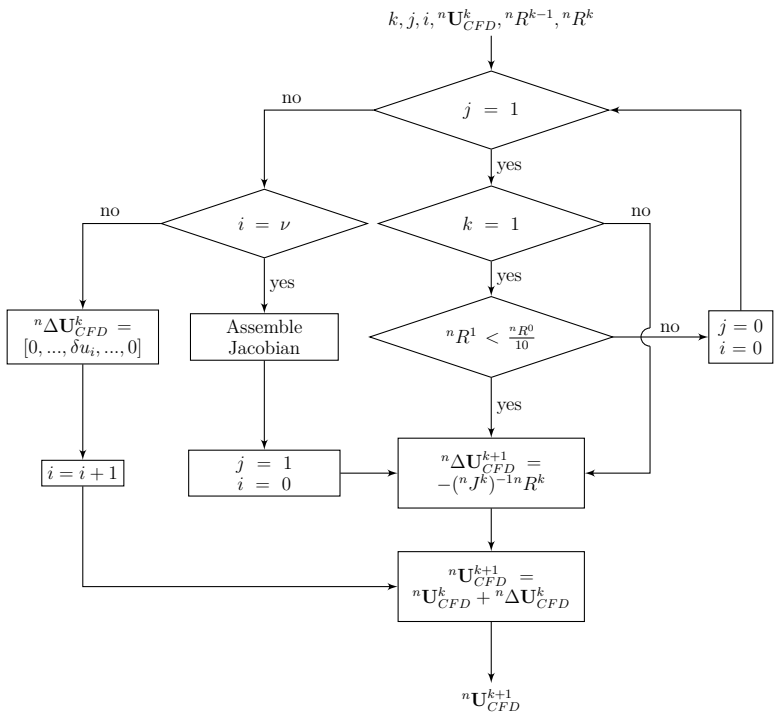

Figure 3.15: Detailed flowchart of the Quasi-Newton algorithm.

the mass flow rate through the pipe is shown in Figure 3.16, in which it is possible to appreciate the overall agreement between the stand-alone STH calculation and the coupled simulations. The pressure evolution at a coupling interface is shown in Figure 3.17. As expected, the explicit scheme shows significant numerical fluctuations in the first part of the transient, for all sizes of the coupling time steps considered. It can also be noticed that the maximum pressure oscillation amplitude is independent from the time step, which only affects how rapidly the numerical oscillations are damped. As pointed out by previous works on domain decomposition methods, the onset of such instabilities is caused by overshooting of the mass flow rate in the first portion of the STH domain (L_{STH-1}) when computing the first time steps. Due the incompressibility of the fluid and the initial stagnant conditions, the outlet pressure information travels backward through the downstream portion of the STH and the CFD domains, until the upstream portion of the STH domain sees applied at its boundaries the whole Δp that is, in reality, imposed at the boundaries of the whole pipe. This leads to an overestimation of the mass flow rate, which consequently causes the establishment of the observed oscillating behavior. The overshot mass

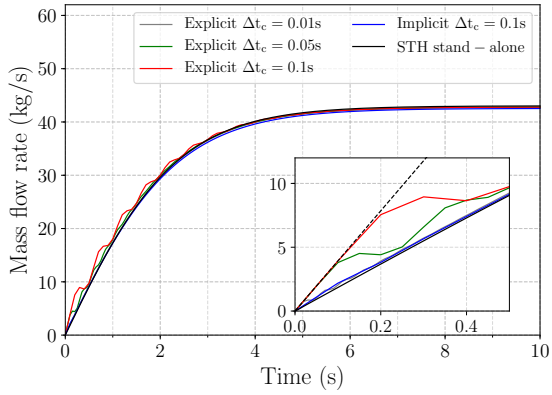

Figure 3.16: Time evolution of the mass flow rate through the pipe in the abrupt pressure difference transient ($\Delta p = 0.2 \cdot 10^5 Pa$).

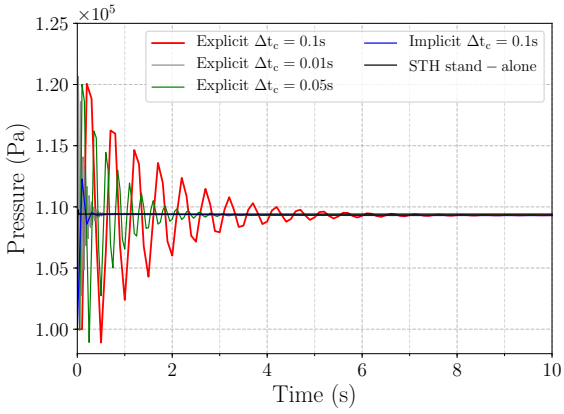

Figure 3.17: Time evolution of the pressure at a coupling interface in the abrupt pressure different transient ($\Delta p = 0.2 \cdot 10^5 Pa$).

flow rates lay on the same curve for all the time steps, considering that in the first part of the transient the pressure drop is dominated by the inertial term, so that the initial mass flow variation can be estimated according to the following (dotted line in Figure 3.16):

$$\frac{\partial \dot{m}}{\partial t} = A_p \frac{\Delta p}{L_{STH-1}} \tag{3.82}$$

where A_p is the pipe cross section. From these considerations, it is possible to conclude that the instabilities related to the explicit schemes are strongly sensitive to the characteristic dimensions of the coupled domains. It is also confirmed that, based on Equation 3.82, the numerical instabilities of explicit schemes reduce with the reduction of the size of the coupling time step. With the use of the implicit scheme, as it can be observed in Figure 3.16, numerical oscillations are not observed thanks to the convergence of the pressure-velocity fields.

To give an idea of the performance of the different implicit algorithms implemented, Figure 3.18 shows the convergence history for the first three coupling time steps. The plots in the same row show the convergence history of the same variable, specifically the two terms of the CFD input vector and the interface residual norm, while the plots in the same column are related to the same time step. It can be observed that the computational gain provided by the Aitken relaxation scheme is limited, while the Quasi-Newton method leads to a significant reduction of the coupling iterations requirement. In the first iteration of the first time step, the Jacobian is not available, therefore two consecutive iterations are performed to compute it. During these two iterations,

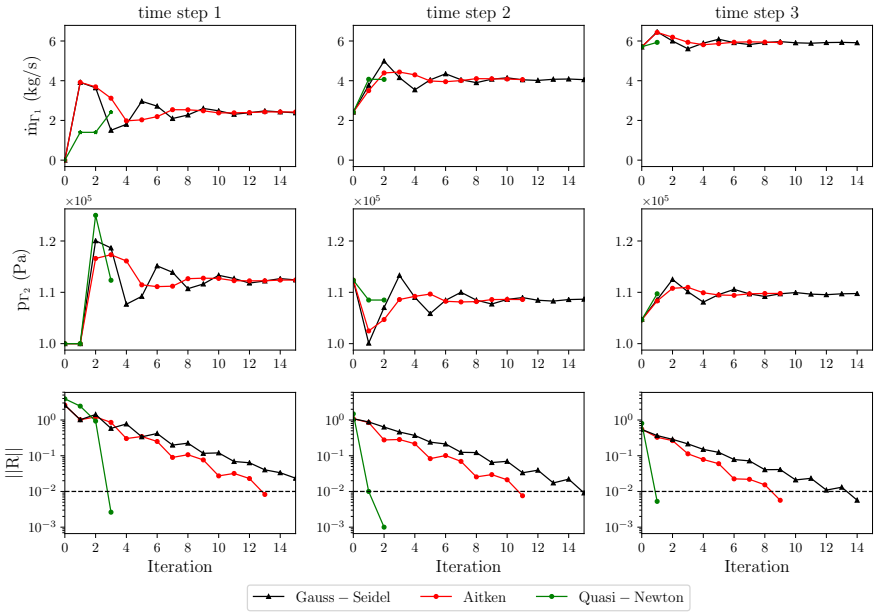

Figure 3.18: Interface convergence history for the first three time steps of the abrupt pressure difference transient.

the interface residuals do not significantly drop because of the arbitrary choice of the perturbations applied to the terms of input vector. After the Jacobian is computed, a single iteration leads to residual values below the defined tolerance. In the following coupling time step, the Jacobian computed in the first time step is used in the first iteration; the condition of Equation 3.81 is satisfied after the second iteration, therefore the Jacobian is kept for the same time step and leads to satisfying the convergence criterion with only one additional iteration. In the third step, a single use of the same Jacobian is enough to compute the time step. Overall, it is evident the significant gain in terms of coupling iterations offered by the algorithm.

II. Open pipe flow reversal test

The computational method must be able to compute transients with sudden inversion of the flow direction. To investigate this aspect, the same open pipe model has been tested on a transient involving an abrupt inversion of the pressure boundary conditions to force the flow to quickly reverse. The results of such test, shown in Figure 3.19 and Figure 3.20, were found satisfactory and in line with previous findings for what concerns numerical stability.

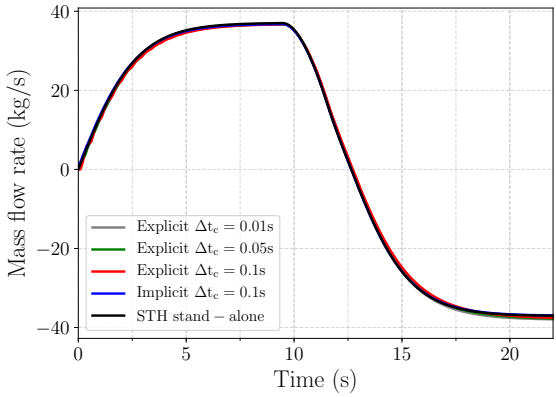

Figure 3.19: Time evolution of the mass flow rate through the pipe in the abrupt forward and reverse pressure different transient.

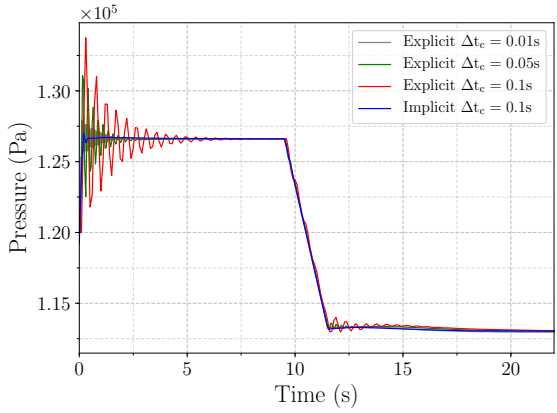

Figure 3.20: Time evolution of the pressure at a coupling interface in the abrupt forward and reverse pressure different transient.

III. Open pipe non-isothermal flow test

A further verification test on the open pipe flow configuration has been performed to verify the correct implementation of thermal boundary conditions exchange. The simulation of a temperature step propagation through the pipe has been carried out to this purpose. The results, shown in Figure 3.21, were found satisfactory.

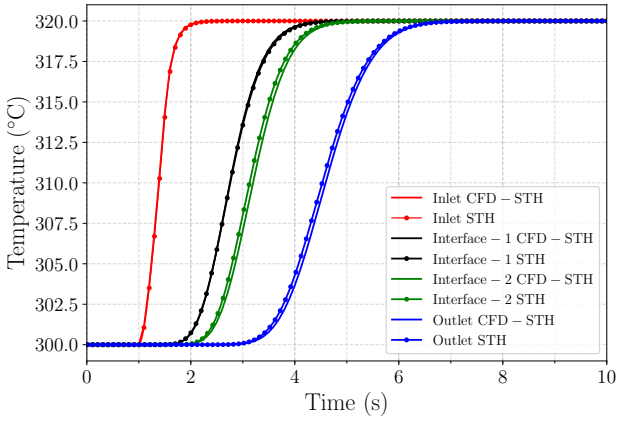

Figure 3.21: Temperature step propagation through the open pipe.

IV. Closed pipe flow problem

A verification case has been set up also on a closed loop, derived from the open pipe model by closing the STH pipe and adding a circulation pump and an expansion tank. The two horizontal pipes are 8.5 m long as in the open pipe test case, while the two vertical legs are 1.6 m long. The derivation of the coupled model from the full STH nodalization and the interface exchange of BC data, shown in Figure 3.22, follow the same logic previously discussed.

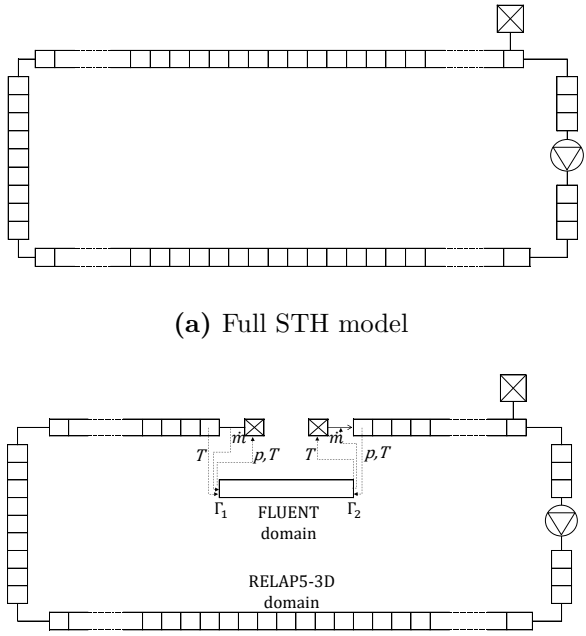

(a) Full STH model

(b) STH-CFD coupled model

Figure 3.22: Domain decomposition and exchange of data at the interfaces for a single-phase closed pipe flow coupled problem.

The tested numerical schemes are also the same of the open loop case. The analyzed transient consists again of a mass flow ramp, this time driven by the rotating pump, from fluid at rest. The mass flow rate in the loop is plotted in Figure 3.23, in which it is possible to observe even for this test the consistency between the coupled and stand-alone STH simulations. The interface pressure evolution is shown in Figure 3.24.

The simulation confirmed also the advantages, in terms of numerical stability and reduced computational costs, of the Quasi-Newton scheme

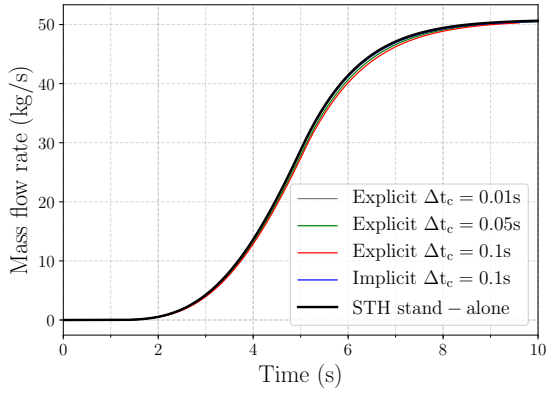

Figure 3.23: Time evolution of the mass flow rate in the closed pipe test.

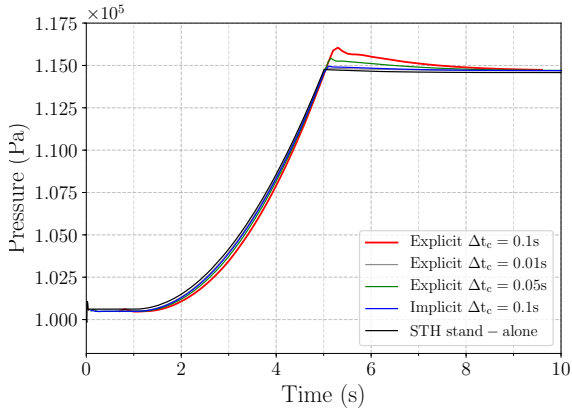

Figure 3.24: Time evolution of the pressure at a coupling interface in the closed pipe test.

compared to the other methods. This can be observed in Figure 3.25, which shows the convergence history of a typical coupling time step. It is noticed that the closed loop is less prone to numerical instabilities, and that the convergence rate is generally higher compared to the open loop case. The reason can be attributed to the absence of interruptions in the STH domain; in the open pipe, the upstream and downstream STH portions of the pipe are hydraulically decoupled, and a perturbation in one of the two would require several coupling iterations to reach the other one. In the case of a closed loop, such perturbation is immediately transported throughout the whole STH domain within a single coupling

iteration, which tends to improve the convergence rate.

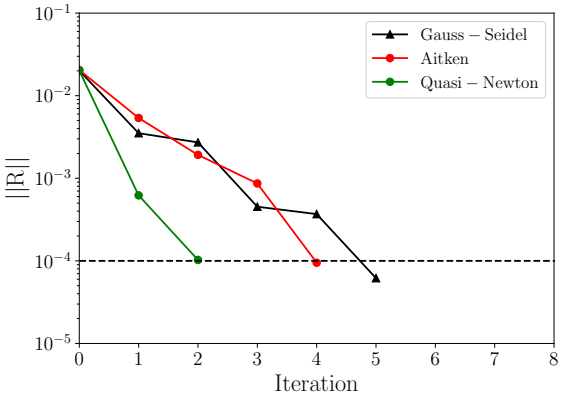

Figure 3.25: Interface convergence history of a typical time step of the closed loop test case.

3.3 Conclusions

The best-estimate system thermal–hydraulic code RELAP5-3D has been coupled with the CFD code Ansys FLUENT to perform high-fidelity transient simulations of pool-type systems, with particular focus on the MYRRHA reactor. The computational methodology is based on domain decomposition technique and exchange of interface boundary conditions, and is realized through a supervisor code written in Python that communicates with the FLUENT code and executes RELAP5-3D as a sub-routine.

Several numerical schemes have been investigated and tested on proof-of-principle calculations of single-phase water flow problems, and assessed against full STH models. The use of a pure explicit time stepping scheme led, as expected, to numerical stability issues caused by the imbalance of the momentum terms at the interfaces. Implicit schemes, which require coupling iterations within every time step to be performed until convergence of the momentum terms is reached, led to significant improvement of the results and the possibility to adopt relatively larger sizes of the coupling time step. These schemes theoretically lead to the same solution that would be obtained with a fully implicit monolithic implementation.

To accelerate convergence rates and reduce computational costs, dynamic relaxation algorithms have been implemented and tested. The development of a Quasi-Newton method, based on the linearization of the residual function and the approximation of the Jacobian through finite differences, has shown significant improvements of the performance of the tool. The methodology has been extended for its application on multi-domain coupled problems, as it will be presented later on in the dissertation. A further extension of the coupled modeling capabilities has been achieved through the implementation of thermal interfaces, which allow for the computation of conjugate heat transfer across boundary walls separating domains.

Chapter 4

Coupling method validation: the TALL-3D experiment

A first validation of the developed computational method against experimental data has been performed on the basis of the experiments performed at the TALL-3D facility, operated by the Royal Institute of Technology (KTH) in Stockholm, Sweden. This choice was motivated by the analysis of the main achievements of the completed EC-funded project THINS (Thermal-Hydraulics of Innovative Nuclear Systems), launched in the 7th Framework Programme FP7 of the European Union, which included a dedicated work package on coupled codes development and validation [76]. Within the project, a benchmark was performed on the TALL-3D loop, allowing for the comparison between different coupling techniques [54]. In this context, the application of the developed tool on this experiment provided a valuable occasion to perform comparison against a high-quality set of experimental data, as well as to assess its performance in relation to different modeling approaches. The content of the chapter is based on the second part of a paper published in a peer-reviewed scientific journal [59].

4.1 TALL-3D test facility

The TALL-3D facility is an experimental loop operated with LBE, used to investigate a number of scientific and technical aspects related to the thermal-hydraulics of heavy liquid metals. The technical objectives of

the facility design are to provide (i) mutual feedback between natural circulation in the loop and 3D mixing and stratification phenomena in the pool-type test section, (ii) a possibility to validate stand-alone STH and CFD codes for each subsection of the facility, and (iii) sufficient number of experimental data to separate the process of input model calibration and code validation [73].

The schematic of the installation is shown in Figure 4.1. The system includes a main LBE loop, the secondary cooling loop operated with oil and differential pressure measurement system. The total height of the installation is about 6.5 m.

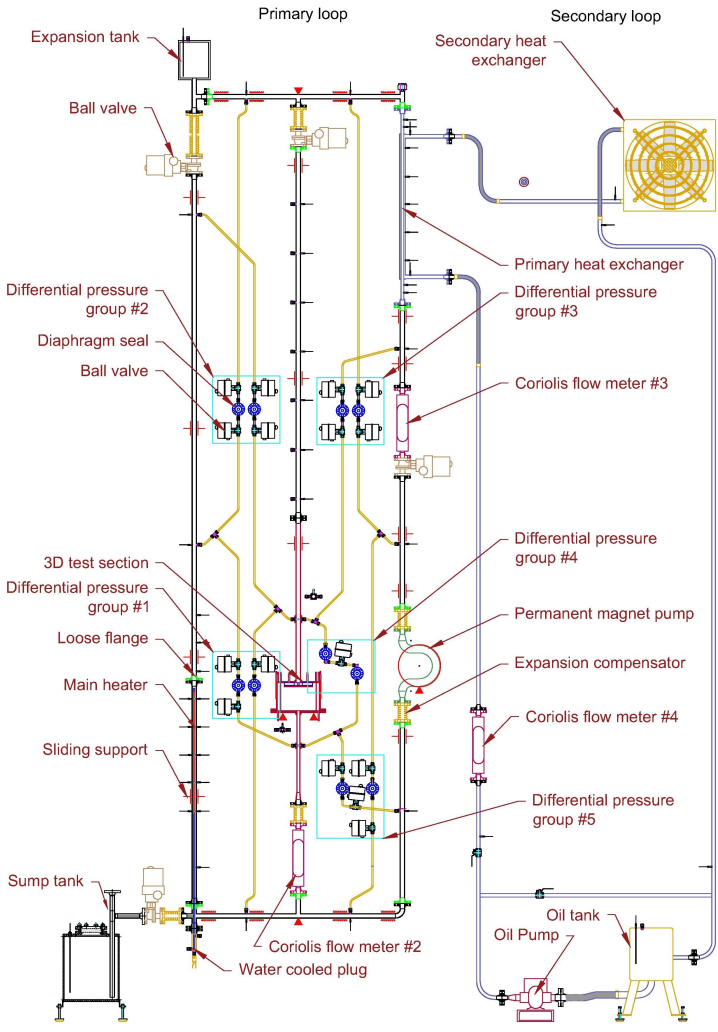

Figure 4.1: Schematic of the LBE facility TALL-3D [73].

The main LBE loop consists of the sump tank (on the left) used to store, melt and supply LBE into the main loop, 3 vertical legs and 2 connecting horizontal sections each combining 2 elbows and a T-junction. The distance between adjacent vertical legs axes is 0.74 m and the length of every leg is 5.83 m (internal diameter of 27.86 mm). The main heater (MH) leg (left) accommodates a rod-type 27 kW electric heater (outer diameter 8.2 mm, heated length of 870 mm) inserted in the lower part (Figure 4.2a) and an expansion tank at the top. The expansion tank is used to maintain the loop pressure during temperature-induced deformation of the components and LBE volumetric expansion/contraction, as well as to to monitor the level of LBE. The heat exchanger (HX) leg (right) includes (i) a counter-current double-pipe heat exchanger (Figure 4.2b) placed at the top and (ii) an electric permanent magnet (EPM) pump at the bottom (Figure 4.2c).

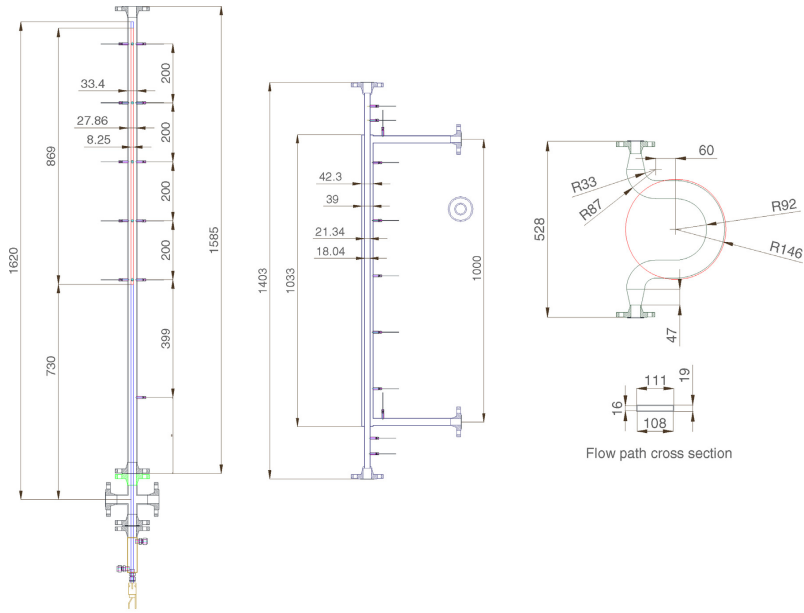

Figure 4.2: Main heater (a), heat exchanger (b) and EM pump (c) of the TALL3D facility.

The 3D leg (middle) connects a pool-type 3D test section to the loop. Depending on instantaneous flow characteristics, the LBE in the test section can undergo thermal mixing or stratification. The test section, shown in Figure 4.3, is a cylindrical stainless steel vessel with an inlet at the bottom and an outlet at the top. The upper part (two-thirds) of

the section is equipped with a 15 kW band heater installed around the circumference, which promotes the development of thermal stratification at low flow conditions. Inside the test section, a circular plate is placed orthogonal to the flow path in order to enhance pool mixing by deflecting the inlet flow to the periphery. The plate is attached to the ceiling of the pool with 4 fin-shape separators, which are designed to minimize the disturbance on the flow.

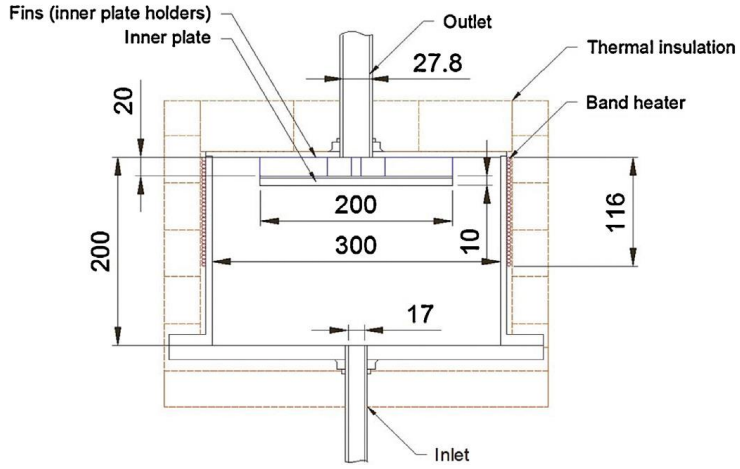

Figure 4.3: TALL3D test section.

Temperature measurements in the main heater provide data on the radial temperature profile in the annulus between the main heater and the pipe. The TCs are arranged into 5 groups located at different elevation with 200 mm pitch. Every group comprises three single level TCs and one multilevel thermocouple. The locations of TCs in the TS is indicated in Figure 4.4. In total 154 temperature measurements are provided including 114 in the LBE pool. All thermocouples are Ø1 mm and provided through special feeds making the implementation less intrusive for the flow.

Two types of thermal insulation are used around the test section: *ISOVER TapeLock*7300 and *NanoTUltra*. They are labeled and color-marked in the left side of Figure 4.5.

During normal operation, the flow in the loop is directed downwards in the HX leg, upwards in the MH leg and in the 3D leg. However, during transients the flow can be reversed in all legs depending on the power of the heaters and on the initial conditions. Flow resistance in the MH and 3D legs is adjusted to provide as close as possible mass flow

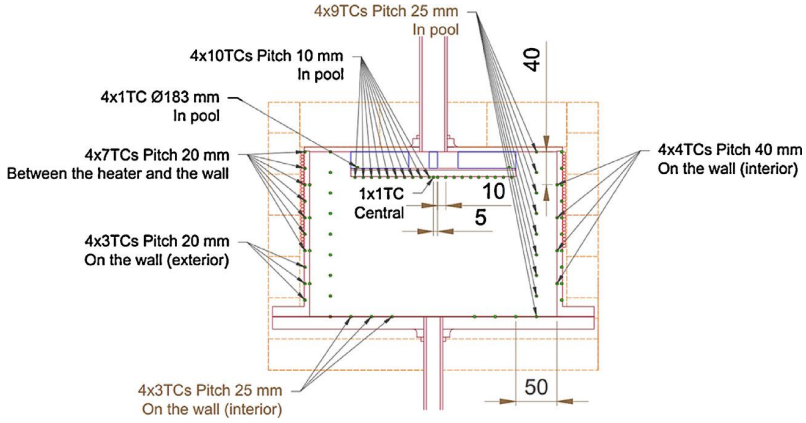

Figure 4.4: TCs location in the TALL3D test section.

rates with equal heater powers in natural circulation conditions. There is also a possibility for fine tuning of the hydraulic resistances in the legs by adjusting the flow control ball valves. Competing nature of the buoyancy forces in natural circulation flow regimes in the MH and 3D legs is expected to result in development of transient flow oscillations. The aim of the 3D test section design was to allow alternations of pool conditions between mixing and stratification in natural circulation flow regimes. Scaling analysis and detailed CFD simulations, carried out to determine pool sizes, heater power and inlet jet diameter, can be found in [72].

During the operation of the loop, temperatures up to 500 °C, pressures up to 0.7 MPa and flow rates up to about 5 kg/s (corresponding flow velocity of approx. 1.7 m/s) can be achieved in the HX leg. All parts of the installation in direct contact with LBE are manufactured with SS-316L to ensure its corrosion and erosion resistance. Oxygen control system is implemented to monitor chemical potential of the LBE dissolved oxygen.

The secondary side of the facility is a closed loop operated with Dowtherm RP fluid. With reference to Figure 4.1, the direction of the flow is clockwise: the fluid is supplied from the oil tank, through the rotary pump, to the main loop heat exchanger, it flows through the secondary side of the heat exchanger, designed to remove up to 40 kW, and is returned back to the oil tank. The oil tank is equipped with a 2 kW band heater to provide nominal operational temperature for the Dowtherm fluid.

More information on the facility, including all details of instrumentation, can be found in [73].

4.2 Computational models

The first step for developing a coupled STH-CFD model of the TALL-3D loop was building a full RELAP5-3D nodalization. The developed nodalization for the facility is shown in Figure 4.7a. Piping is modeled through the use of pipe components, and branches are used to simulate tees. The expansion tank is modeled by a time dependent volume, and the electromagnetic pump by a time dependent junction. The power generated by the two heaters and transferred to the secondary system through the HX is computed by using heat structures components. A simplified model for the secondary system was developed, consisting of an inlet time dependent volume and time dependent junction, a pipe simulating the HX secondary side and an outlet time dependent volume. Default Dowtherm oil properties implemented in RELAP5-3D are adopted [77]. As confirmed by the THINS benchmark, an accurate simulation of the TALL-3D system requires the computation of conjugate heat transfer and the thermal inertia of the solid structures. Therefore, piping structures and insulation layers have been included in all the developed models.

In the TALL3D-loop, the region of interest for the CFD simulation is clearly the pool test section, designed to induce a 3D flow field with potential influence on the integral transient behavior. The remaining portion of the loop, composed of piping, heat exchanger and circulating pump, can be represented with sufficient accuracy using the STH code. In the first model developed, a 2D axial-symmetric CFD model of the TS was adopted, which includes both fluid domain and solid structures i.e. the internal plate, steel walls and the different insulation layers (left side of Figure 4.5). The computational grid, shown in the right side of Figure 4.5, counts $68.9 \cdot 10^3$ rectangular cells, characterized by an orthogonal quality of 8.15e-01 and maximum aspect ratio of 1.1225e+01. The simulations discussed in this chapter make use of the realizable $k-\epsilon$ turbulence model.

As for the implementation of physical properties, it was important to assure that congruent data is used in the coupled codes. In RELAP5-3D, at present there is no straight forward method to implement user-defined property data. Therefore, default properties for LBE have been extracted and implemented in FLUENT using interpolating polynomial

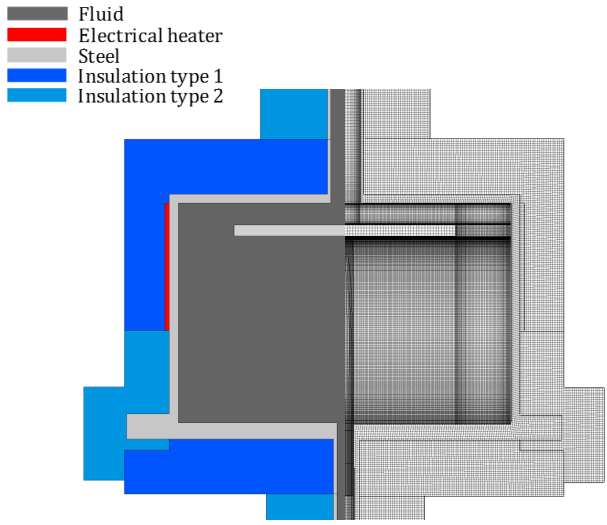

Figure 4.5: CFD model of the TALL-3D test section.

functions. It is worth remarking that some differences were found between RELAP5-3D data and reference properties [78]. The polynomials generated for LBE density, specific heat and thermal conductivity are reported below:

$$\rho(T) = 11058 - 1.2575T + 8 \cdot 10^{-5}T^2 \tag{4.1}$$

$$C_p(T) = 175.89 - 0.0548T + 2 \cdot 10^{-5}T^2 \tag{4.2}$$

$$k(T) = 3.9245 + 0.0118T + 10^{-6}T^2 - 4 \cdot 10^{-5}T^3 \tag{4.3}$$

As for LBE viscosity, the polynomial function interpolating data from Kutateladze, taken from [79], has been found in good agreement with RELAP5-3D data, thus it has been implemented in the CFD model.

$$\begin{aligned}\mu(T) = (2.077 - 8.983 \cdot 10^{-6}T + 1.629 \cdot 10^{-5}T^2 \\ -1.352 \cdot 10^{-8}T^3 \cdot 10^{-12}T^4) \cdot 10^{-2}\end{aligned} \tag{4.4}$$

The comparison between the RELAP5-3D LBE data and the above functions used in FLUENT is shown in Figure 4.6

The coupled model is implemented by eliminating the test section model from the full STH nodalization, and by replacing it with appropriate boundary condition components required for the execution of the coupling scheme. These components are a time-dependent volume and

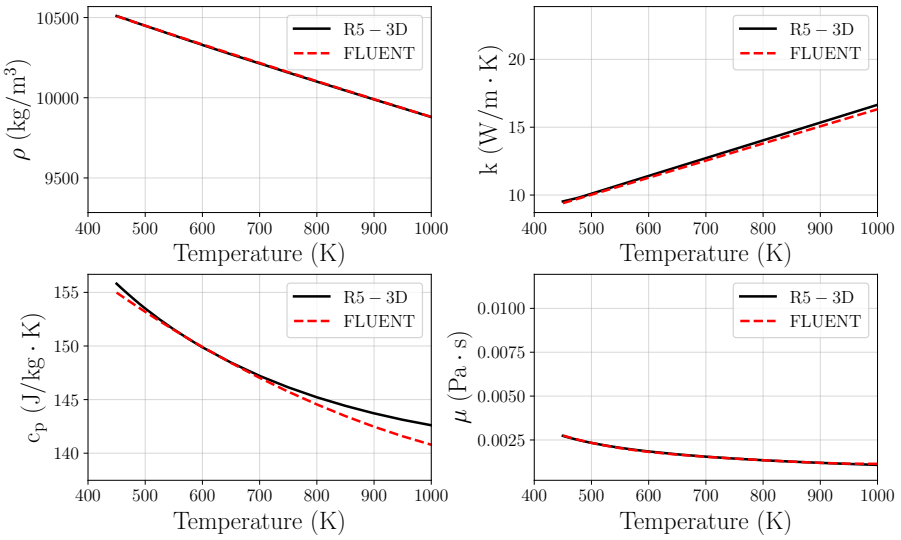

Figure 4.6: LBE physical properties extracted by RELAP5-3D code and interpolating polynomials implemented in the CFD code FLUENT.

single junction at the TS inlet, to receive pressure and back-flow temperature from FLUENT, and a time-dependent volume and time-dependent junction at the TS outlet to receive mass flow rate and temperature. The model is shown in Figure 4.7b, whose coupling settings are identical to the pipe flow coupled calculations discussed in chapter 3. Moreover, on the basis of those analyses, the implicit numerical scheme based on the Quasi-Newton algorithm is used.

4.3 Simulation results

4.3.1 Forced circulation regime

A steady-state stand-alone CFD simulation of the test section in forced circulation was first performed. Few remarks are needed here: first, it is known that an impinging jet has intrinsic unsteady physics, which cannot be fully represented by a 2D discretization even with unsteady simulation. Furthermore, it is known that RANS models, depending also on the particular turbulence model adopted, might be not appropriate for an accurate computation of such flows. Nevertheless, a 2D model was deemed appropriate for this preliminary analysis, as it allows for

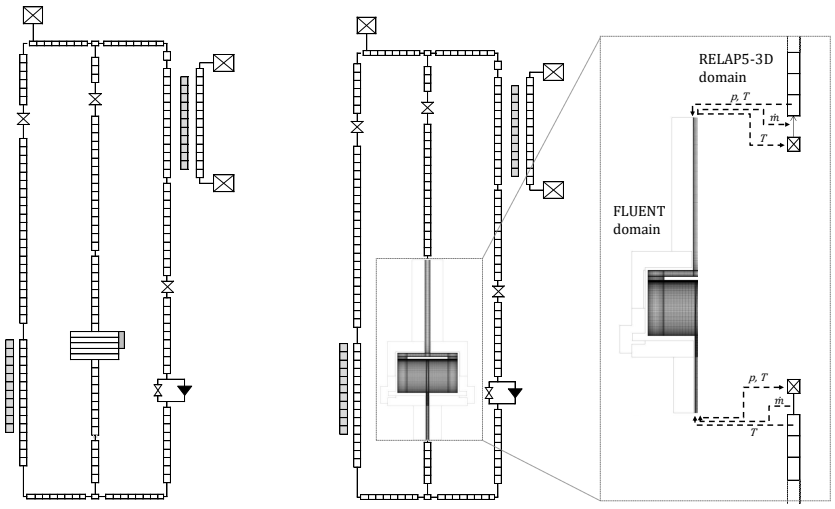

(a) *Full RELAP5−3D model* **(b)** *Coupled RELAP5−3D/FLUENT model*

Figure 4.7: Full RELAP5-3D and RELAP5-3D/FLUENT coupled model of the TALL-3D facility. The test section is modeled by the CFD code, while the rest of the primary loop and the secondary oil system are computed by the STH code.

fast calculations and for the identification of eventual numerical issues related to the coupling methodology.

The operating conditions considered for the simulation are reported in Table 4.1:

Table 4.1: Adopted boundary conditions data for the simulation of forced circulation conditions

Parameter (unit)	Value
TS power (kW)	4.81
Inlet mass flow rate (kg/s)	1.649
Inlet temperature (°C)	240.0
External air temperature (°C)	25.0
External air heat transfer coefficient (W/m^{2}K)	10.0

The predicted flow and temperature fields in the test section are shown in Figure 4.8. It can be noticed that the calculation predicts, as a consequence of the presence of the internal plate, a large vortex in the

center of the TS volume, and two smaller ones at the bottom and top of the pool. These results were found in line with similar investigations carried out with the CFD code Star-CCM+ [80].

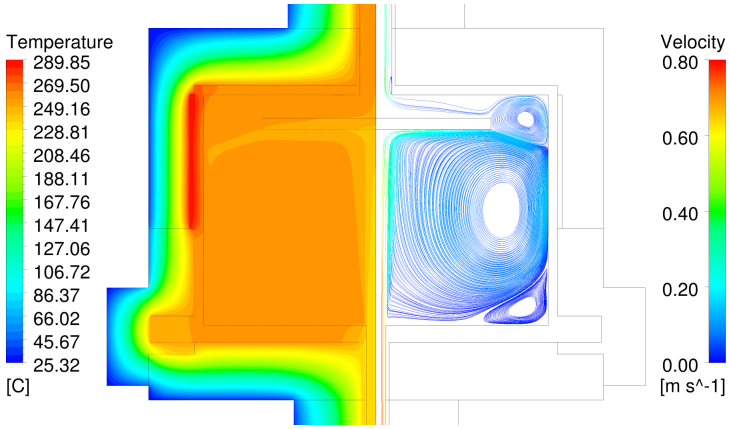

Figure 4.8: Flow pathlines and temperature field in the TALL-3D test section in forced circulation operating condition.

4.3.2 Transient T01.09 - Loss of forced circulation

The validation analysis discussed in this section focuses on the computation of the T01.09 experimental test, a loss of forced circulation transient with transition to natural circulation. As it was mentioned, code-to-code comparisons and assessment against experimental data for this test were object of a specific benchmark within the project THINS, whose results are extensively presented in [54]. These computational analyses provided a valuable additional data set to further verify and assess the performances of the developed tool.

I. Initial conditions

The T01.09 transient experiment was carried out starting from initial forced circulation condition, characterized by a total LBE mass flow driven by the EM pump of about 4.27 kg/s. The MH provides a power of 2.58 kW, while the TS heater provides a power of 4.81 kW. In such conditions, as described in section 4.1, high degree of mixing is induced in the pool test section due to presence of the internal plate. The value of the main operational parameters in these initial conditions are summarized in Table 4.2.

Table 4.2: Initial conditions for the T01.09 transient test simulations

Parameter (unit)	Value
TS power (kW)	4.81
MH power (kW)	2.58
Pump mass flow rate (kg/s)	4.27
TS leg mass flow rate (kg/s)	1.64
Secondary mass flow rate (kg/s)	0.15
LBE temperature at the TS inlet (°C)	240
LBE temperature at the TS outlet (°C)	261
Secondary oil temperature at HX inlet (°C)	61

II. Transient results

From initial conditions, at the time t_0 the EM pump is switched off with a linear cost-down Δt_{pp}=7 s, while the power provided by both the heaters is kept at the nominal value. The imposed linear mass flow rate ramp in the EM pump is shown in Figure 4.9.

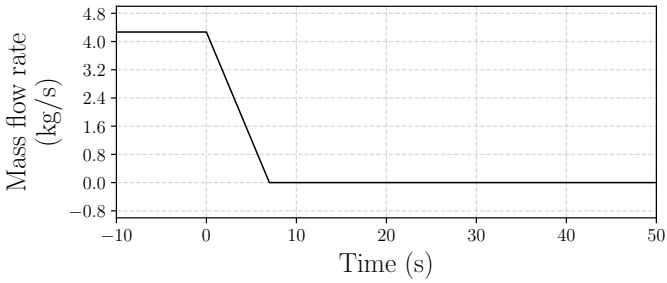

Figure 4.9: EM pump coast down for the T01.09 transient test simulation.

An oscillating plant dynamic response was obtained by the experimentalists, which terminated in new steady-state conditions in natural circulation and thermally stratified flow in the TS. Figure 4.10 shows the evolution over time of the mass flow rate measured in the HX, MH and TS legs, compared with the values predicted by the STH and coupled STH-CFD simulations. Due to the pump trip, the mass flow rate in all the legs of the loop drops abruptly; given the smaller volume of LBE in the MH, the establishment of natural circulation in this leg is faster, as confirmed by the mass flow rate peak occurring at about t=150 s, which induces for a short time window reversal of LBE flow in the TS. The

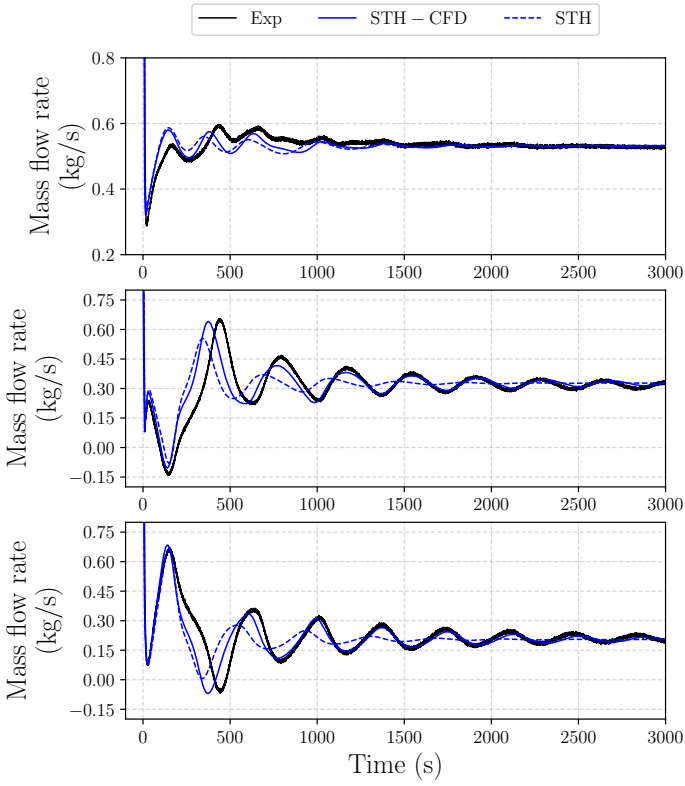

Figure 4.10: Time evolution of the mass flow rate in the HX (top), TS (middle) and MH (bottom) legs during the T01.09 transient test.

LBE in the TS successively heats up due to the continued power provided by the heater, and the consequent buoyancy induces upward LBE flow which reaches its peak at about t=440 s, coinciding with nearly stagnant flow in the MH leg. Both the STH and coupled STH-CFD calculations predict this first peak to occur earlier, due to discrepancies in the thermal inertia and heat losses computed in the loop by the STH code. Apart from that, for the whole evolution of the transient it is evident that the coupled code is able to predict more accurately the plant dynamic behavior and the characteristic frequency of the oscillations, while the stand-alone STH code results in a faster damping.

Figure 4.11 shows the temperature evolution over time in key locations of the facility, namely, from the top to the bottom, the TS inlet, the TS outlet, the MH outlet and the HX inlet sections. It is possible to

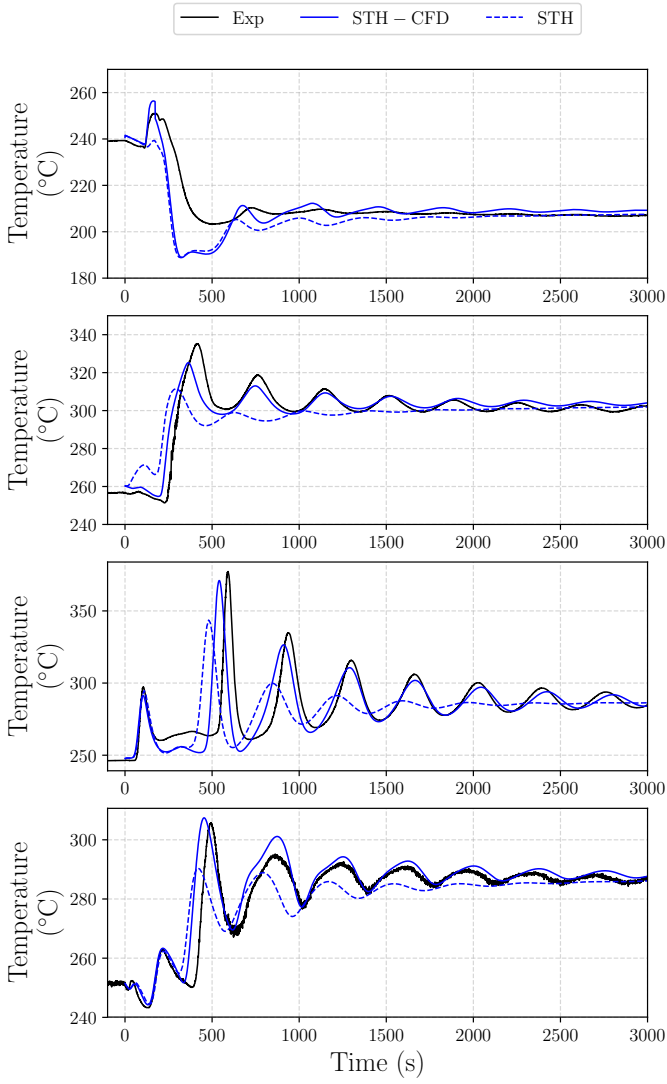

Figure 4.11: Time evolution of the temperature at the TS inlet and outlet, MH outlet and HX inlet sections during the T01.09 transient test.

notice that, except for the already discussed shifting in time in the first part of the transient, the coupled code correctly captures the oscillating behavior experimentally observed. It is interesting to focus on the temperature at the inlet of the TS; at about t=150 s, a sudden temperature increase is predicted by the coupled simulation in correspondence of the flow inversion, as can be observed in Figure 4.10, and confirmed

by the experiment. This temperature peak is related to the initial flow path in the TS, shown in Figure 4.8, and in particular to the LBE vortices which, in forced circulation conditions, carry high temperature fluid from the top to the bottom of the pool. When flow reversal occurs, this high temperature is immediately transported to the inlet section, explaining the observed sudden increase. Given its 1D simplification, this behavior is clearly not predictable by the stand-alone STH code, in which an artificial thermal stratification is calculated due to the location of the heater only in the upper part of the pool; the short time window of flow reversal impedes the heated LBE, located in the upper part of the TS volume, to reach the inlet section, therefore this temperature increase is not observed. In both the simulations, the deviation from the experimental data, in particular the overcooling of LBE at the TS inlet in the first part of the transient, is mostly caused by an inaccurate simulation of the HX behavior. It is however difficult to correct such discrepancy as the precise operating parameters of the secondary side were not initially known during the experiments. A good agreement is observed on the temperature at the MH outlet and HX inlet sections. Even for these parameters, the most appreciable deviation for the coupled calculation is the shifting in time of the first temperature peaks.

An important characteristic of STH-CFD coupling techniques is the possibility to monitor local parameters in the region computed by the CFD code, the pool test section in this application. Therefore, an extensive comparison between experimental data and calculations was performed on local temperature measurements in the TS (see Figure 4.4 for detailed location of TCs); the measured and calculated values of a selected set of temperatures are shown in Figure 4.12. The CIP0 TC is located at the center of the internal plate, therefore its measurements directly reflect the temperature variations caused by the LBE jet oscillations. The coupled simulation is able to predict the first peak, slightly shifted in time, but is not capable to capture the following ones. The single peak measured by the CIP5 TC is not captured either. The discrepancy can be explained, on one side, by deviations in the prediction of the inlet mass flow rate that influences the jet penetration length, and on the other side by the use of RANS models. To better evaluate which effect is predominant, a stand-alone CFD simulation has been performed using experimental data for inlet boundary conditions. Figure 4.13 shows the comparison between the experimental data, the stand-alone CFD simulation and the STH-CFD coupled simulation.

It can be noticed that the stand-alone CFD calculation is, obviously,

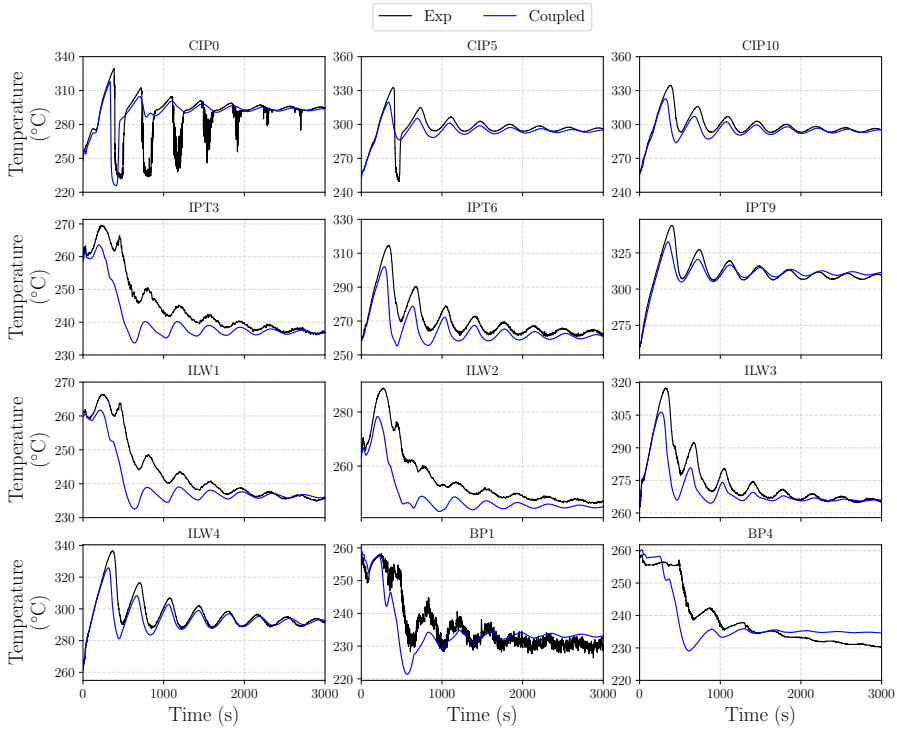

Figure 4.12: Local temperature measurements in the TS. Comparison between coupled simulation and experimental data.

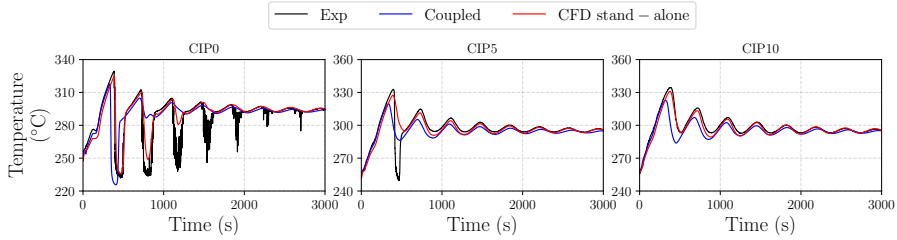

Figure 4.13: CIP TCs group measurements. Comparison between experimental data, coupled simulation and stand-alone CFD simulation with experimental data imposed as boundary conditions.

closer to the measured values, but it still presents certain deviations; the first two peaks measured by the CIP0 TC are captured quite well, but not the following ones, and the only peak measured by CIP5 TC is not predicted by the CFD stand-alone simulation. This result reveals

that the shape of the LBE jet might be not correctly represented by the particular turbulence model adopted in the simulation and the 2D axial-symmetric modeling choice. A full 3D model and more advanced turbulence modeling might be able to improve these results. The comparison on the ILW and IPT TCs shows in general a good agreement between measured and calculated temperatures. Except for the shifting in time at the beginning of the transient that characterizes the whole simulation, the overall behavior is well captured. The under-prediction observed, especially in the TCs located in the lower part of the pool, are mostly explained by the deviation on the temperature at the inlet of the pool. It is important to remark that the above discussed causes of discrepancies between the simulation and experimental data are attributed to single model deficiencies. For what concerns the multi-scale approach and the coupling implementation, it is evident that an improvement in the solution accuracy can be achieved, whose demonstration was the main goal of this analysis.

Finally, the evolution of the temperature field in the TS during the loss of flow transient is shown in Figure 4.14. It is possible to distinguish the transition from the mixing regime at the beginning of the transient, characterized by nearly uniform temperature in the TS, to the thermal stratification in the final state of the transient, in natural circulation regime. It is also worth noticing the flow field corresponding to the first and second mass flow peaks, occurring at about t=370 s and t=770 s (see Figure 4.10 and Figure 4.11); it can be observed that at the first peak, the cold jet visibly reaches the internal plate, and indeed the first low temperature peak measured by the CIP0 TC is captured. At the following peak, the jet does not have enough momentum to reach the internal plate, because the coupled calculation predicts a slightly lower mass flow rate peak compared to the experimental data. This is confirmed by the CFD stand-alone simulation which, with the correct mass flow rate, is able to capture the second cold peak.

4.4 Conclusions

Before the application on more complex pool-type systems, first validation studies on the developed coupling method were performed on the TALL-3D experimental campaign. The experimental installation, operated by the KTH in Sweden, is a LBE loop composed of the three parallel vertical legs, with a pool-type test section included in the central leg to promote 3D effects.

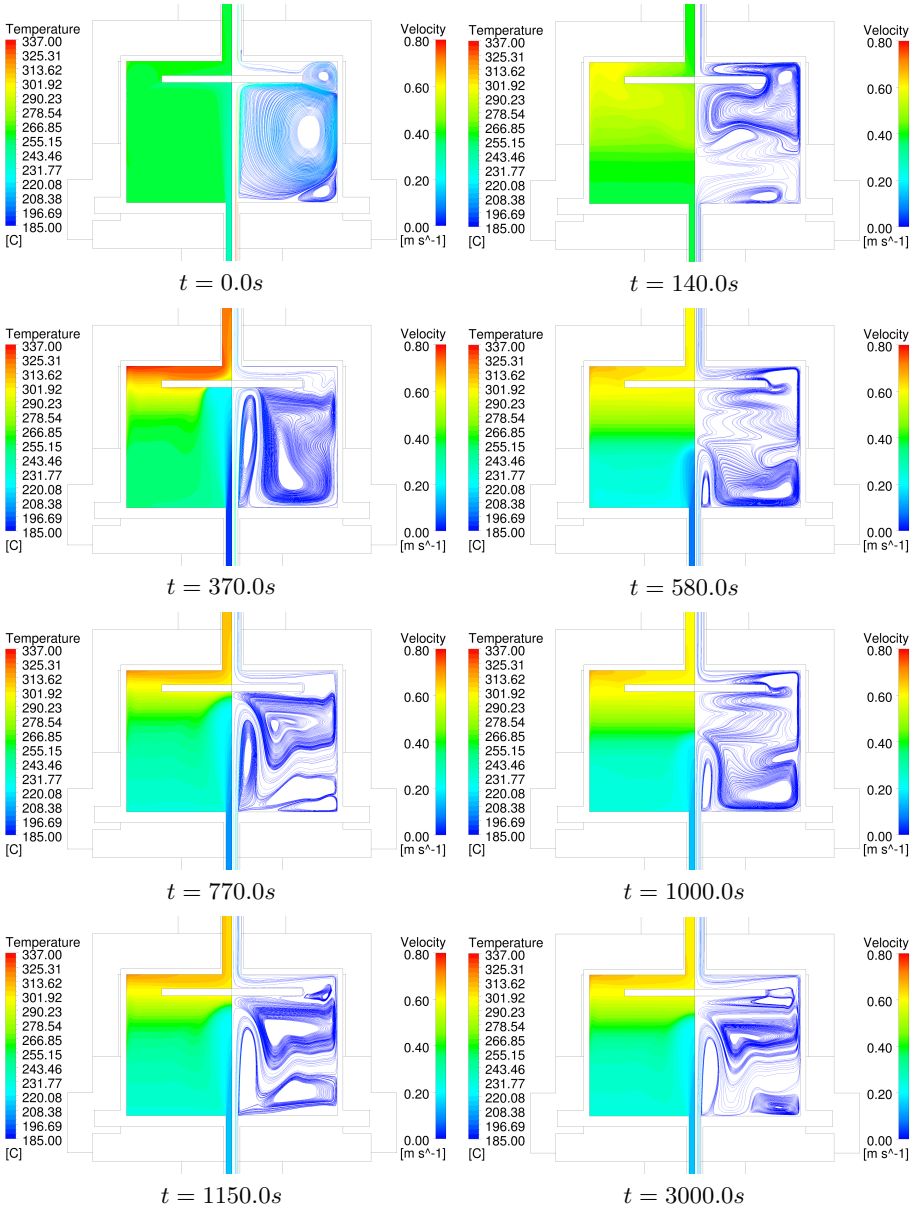

Figure 4.14: Temperature contour and flow pathlines in the TS at different times of the transient T01.09.

Both full STH and coupled STH-CFD models of the facility were developed and assessed against the available experimental data. The developed coupled model of the facility includes a CFD model of the 3D test section and a 1D model of the remaining portion of the loop.

A 2D axial-symmetric model has been preliminary considered, in order to speed up the calculation and perform more efficiently preliminary assessments of the performances of the coupling tool. A main challenge for the CFD simulation of the TALL-3D test section is the complex physics related to a LBE impinging jet, which would require in the future a full 3D computational grid and more advanced turbulence modeling.

The analysis presented in this chapter was centered on the simulation of a loss of forced circulation transient (test T01.09) with transition to natural circulation, for which both coupled and full 1D simulations were compared against measurements. Overall agreement was observed, although the coupled simulation showed a more accurate prediction of the dynamic behavior of the system, in terms of characteristic frequency and amplitude of the mass flow and temperature oscillations observed during the transient. The comparisons between coupled simulation and experimental data on local temperature measurements inside the test section showed some differences, mainly due to discrepancies in the mass flow rate in the section and the use of a 2D axial-symmetric model. The relative importance of these two factors, in relation to the adopted turbulence model, has been better assessed through a stand-alone CFD calculation using experimental conditions, which confirmed that the adopted turbulence model does not correctly predict the shape of the LBE jet. It was however highlighted that all the observed discrepancies are related to inaccuracy of the single codes, while the implementation of the coupling scheme clearly led to an improvement of the stand-alone STH results. This confirms that a fundamental pre-requisite for future detailed V&V analyses of coupled codes is having well validated STH and CFD models.

The overall results of these simulations are in line with the main findings of the benchmark performed within the THINS project [54], and are a further demonstration of the improvement that can be achieved, over full STH models, in the simulation of transients affected by 3D effects.

Chapter 5

Analysis of the E-SCAPE pool-type test facility

This chapter describes the development of a STH-CFD coupled model for the analysis of the pool-type test facility E-SCAPE (European SCAled Pool Experiment), built at SCK•CEN and currently under commissioning tests. The experimental installation is a thermal-hydraulic scaled model of the MYRRHA reactor, with an electrical core simulator, cooled by LBE. In addition to providing feedback to the designers on the thermal-hydraulic characteristics of a pool-type cooling system operated with LBE, the installation represents a major framework for the validation of thermal-hydraulic codes used in the design and safety analyses, including STH, CFD and coupled codes. This chapter details on the developed computational methods, and discusses the results of a number of pre-test simulations of planned transient tests, which represent the content of a paper published in a peer-reviewed journal [81] and of a contribution to an international conference [82].

5.1 E-SCAPE facility

5.1.1 Layout description

The design of the E-SCAPE facility is based on the MYRRHA design version 1.2 [83]. The installation represents a thermal-hydraulic 1/6-scale model of the primary system, and it aims at investigating on the feasibility of the passive decay heat removal after reactor shut-down and

providing experimental feedback to the designers on the flow patterns in pool-type reactors. Moreover, the experimental campaign enables to benchmark and validate the computational methods for their use with LBE, including STH codes, CFD and coupling methodologies. The layout of the facility is shown in Figure 5.1 and Figure 5.2.

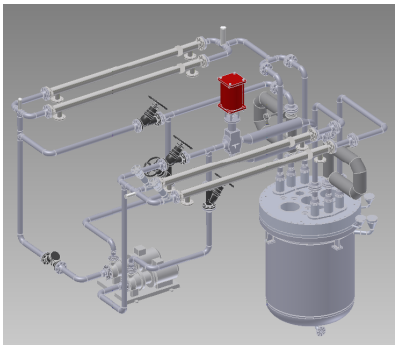

(a) E-SCAPE facility schematic

(b) Photo of the experimental installation

Figure 5.1: E-SCAPE facility.

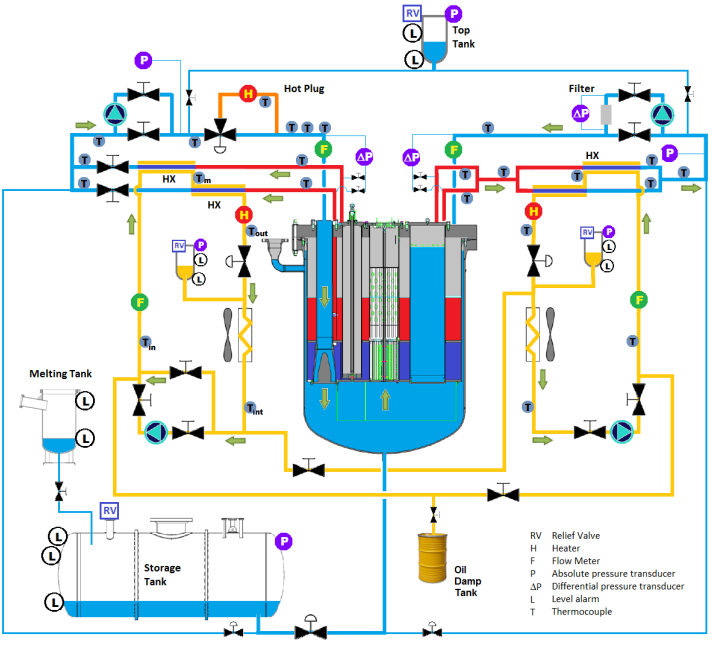

Figure 5.2: E-SCAPE facility simplified layout.

Unlike MYRRHA's full pool-type primary system configuration, E-SCAPE is equipped with external primary cooling circuits, due to the technical difficulties related to the accommodation of pumps and heat exchangers in the scaled vessel [84]. Apart from those, a replica of all main components is placed in the main vessel in order to maintain a geometric similarity. A melting tank and a storage tank handle the filling and draining of the facility. The facility is heavily instrumented with thermocouples, pressure transducers, velocity probes and flow meters, to have a good characterization of the thermal-hydraulic phenomena in view of the validation of simulation tools.

The main characteristics of the E-SCAPE facility and the reference MYRRHA values are listed in Table 5.1. The dimensions have been derived from the scaling based on non-dimensional analysis and CFD simulations, which are discussed in [84].

The main vessel of E-SCAPE, shown in Figure 5.3, maintains all the most relevant features of MYRRHA, including the lower plenum (LP) and baffle, core, core barrel and above-core structure (ACS), upper plenum (UP), the Silicon Doping (SDs) and In-Vessel Fuel Handling Machines (IVFHMs) mock-ups and the annular region between diaphragm and the external vessel (Annulus).

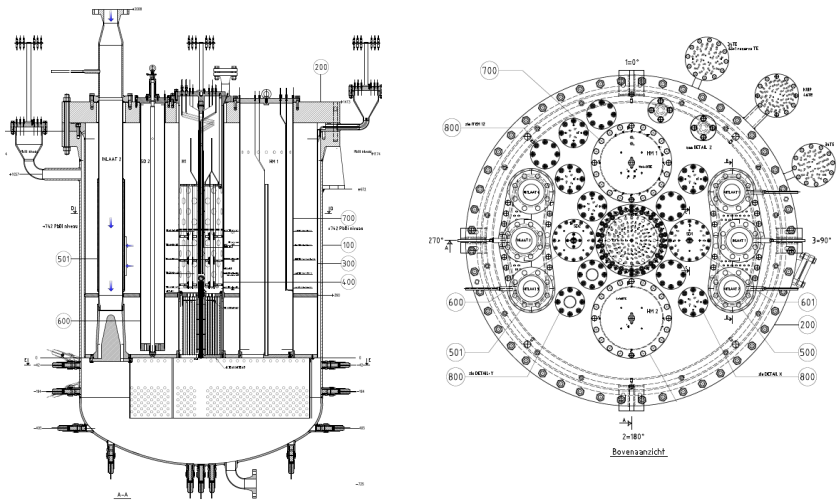

Figure 5.3: E-SCAPE main vessel details.

Table 5.1: E-SCAPE main parameters compared to MYRRHA reactor

	Parameter (unit)	E-SCAPE	MYRRHA
Main Vessel	Outside diameter (mm)	1400	8140
	Wall thickness (mm)	10	
	Height (mm) (from bottom to top flange)	2100	12000
	Material	AISI316L	AISI316L
	LBE inventory (l)	2500	500000
	Core heat source (kW)	100	110000
	Temperature range (°C)	200-340	270-410
System	Ar cover gas pressure (bar)	4	
	Total mass flow rate (kg/s)	2.4-120	650-9560
LBE circuits	Pumps number	2	2
	Heat exchanger number	4	4
	Heat exchanger maximum power (kW)	30	27500
Cooling circuits	Secondary coolant	Oil	Water-steam
	Operating pressure (bar)	2	16
	Flow rate (l/s)	10	
	Temperature range (°C)	135-200	
Air cooling	Air-cooler, number	2	
	Flow rate (m^3/h)	11142	
	Air cooler maximum power (kW)	60	

The nominal temperature of the lower plenum is 200 °C and the upper plenum temperature is expected to vary between 206 °C for a total flow rate of 120 kg/s (forced circulation) and 315 °C for a total flow rate of 2.4 kg/s (natural circulation). The pressure in the vessel is set by an Argon blanket at 4 bar, necessary to fill the external circuits and to prevent oxygen ingress limiting the formation of lead-oxides.

The LBE flows from the lower plenum upwards through the core generating 100 kW power by means of 11 electric heated wires. An upper grid simulates the core support plate, and a lower grid allows respecting the scaled pressure losses in the core. Leaving the core, the coolant enters the ACS and flows through the barrel holes to the upper plenum. In the upper plenum, mock-ups of SDs and IVFHMs are installed. The latter are hydraulically connected to the lower plenum, as foreseen in the MYRRHA reactor. From the upper plenum, the coolant flows in four vertical channels, named HX channels hereafter, which convey the fluid to the external cooling circuits, where the LBE is cooled down by four LBE-oil tube-in-shell counter flow heat exchangers, each capable of removing 30 kW. Two centrifugal pumps, capable of providing a head of 5 bar at a flow rate of 20 m^3/h, pump back the LBE to the main vessel, where it flows downward to the lower plenum through two vertical channels, named pump channels hereafter, whose ending part reproduces the primary pumps-induced jet flow. In both the A- and B-loops a "natural circulation branch" is placed in parallel to the “forced circulation branch” (LBE flowing through the pumps). The selection is made by actuating two different manual globe valves as soon as the coast-down of the pumps is finished. When the pumps are not running, the LBE flows in the "natural circulation branch" in order to reduce the pressure drops over the loops. In the A-loop the hot plug can be simulated: in normal condition the valve in the upper branch is open while the valve in the lower branch is closed. In the lower branch, LBE is kept at 300 °C; in order to push this hotter LBE volume in the vessel, the valves switch automatically from open to close and vice versa in 3 seconds, reproducing the behavior of the pneumatic 3-way valve. In the lower plenum, a small amount of LBE fills the annular gap between the diaphragm and the vessel, in which free surface is established. As mentioned, numerous instrumentation devices are installed, for control and experimental purposes. The main measurement systems are discussed in [84].

Two external oil circuits and air coolers remove the power generated by the electrical core simulator. The layout of these systems is shown in Figure 5.4.

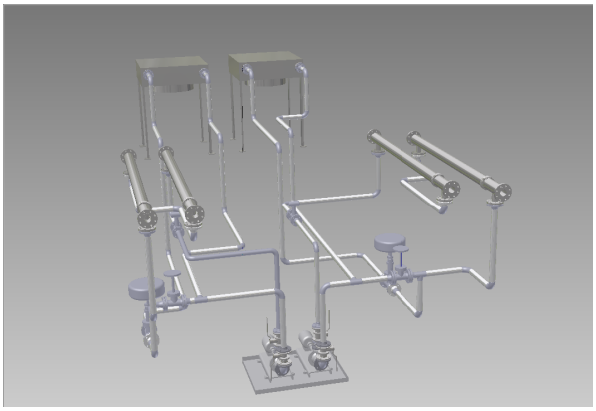

Figure 5.4: E-SCAPE secondary oil system layout.

5.1.2 Design scaling analysis

The design of the E-SCAPE vessel was based on a non-dimensional scaling analysis aimed at preserving the main features of the MYRRHA primary system coolant flow field. This analysis is detailed in [84] and summarized here. The study was focused on steady state operating conditions, and no transient events were considered.

The followed scaling approach was based on the preservation of the Richardson (Ri), the Heat Source and Euler (Eu) numbers as primary objective. Deviations in the Reynolds (Re) and Péclet (Pe) numbers were accepted as long as the flow remains in the correct regime. The Reynolds number was already defined in chapter 3. The definition of the other non-dimensional numbers introduced above is given below:

$$Ri = \frac{g\beta\Delta H\Delta T}{u^2} \tag{5.1}$$

$$Eu = \frac{\Delta p}{\rho u^2} \tag{5.2}$$

$$HS = \frac{Q}{\rho u A C_p \Delta T} \tag{5.3}$$

$$Pe = \frac{C_p \rho u D_h}{k} \tag{5.4}$$

where:

ΔT is the temperature difference between the core inlet and outlet,
u is the average velocity at the core outlet,
ΔH is the height difference between the thermal centers of the core and HXs,
Δp is the total pressure drop in the system,
g is the gravitational acceleration,
β is the thermal expansion coefficient,
ρ is the density,
A is the core area,
C_p is the specific heat,
D_h is hydraulic diameter in the core,
k is the thermal conductivity,
μ is the dynamic viscosity.

For the mixing and stratification phenomena in the three-dimensional upper plenum, Ri, Re and Pe numbers govern the flow pattern in natural convection. Ri is most relevant if temperature differences lead to a significant contribution of buoyancy. If the contribution of buoyancy is not important, as in the case of forced convection, Ri loses importance. Other non-dimensional numbers or dimensional characteristic variables can become important in particular flow configurations or when addressing specific phenomena e.g. flow patterns near free surfaces, residence time of the fluid particles, jet flows. In particular, when flow patterns near the free surface are addressed, the Froude (Fr) number should be preserved:

$$Fr = \frac{u^2}{gL} \tag{5.5}$$

where L is a characteristic length. The residence time of fluid particles in plena is related to the Time (Ti) number (dimensional), defined as:

$$Ti = \frac{\Delta H}{u} \tag{5.6}$$

Together with the scaling requirements, the following constraints were set:

- LBE has been selected to be the working fluid, so that experience with LBE technology will be gained in similar temperature and pressure ranges as in MYRRHA;
- An isotropic geometrical scaling factor was used;
- The core and heat exchangers were assumed as “black boxes” in which the fluid flow is unidirectional and subject to uniform volumetric heating or cooling.

The analysis led to the geometrical scaling factor of 6, the 100 kW core simulator and the pump mass flow rate of 60 kg/s per pump. Such a scaling factor implies that with a power of 100 kW, the same ΔT of MYRRHA in natural circulation (considering 7% of the nominal power of MYRRHA) is obtained. Operating at maximal core power allows reaching the highest values of Re and Pe. Operating at slightly lower power allows for the preservation of Fr or Ti but leads to lower values of Re and Pe.

In forced convection, Eu is preserved. Operating at maximal core power and maximal flow rate, the highest values of Re and Pe are reached. However, the core ΔT is not representative for MYRRHA, because of the lower power density in the core. Changing the flow rate, preservation of Fr, Ti or Ri can be achieved but leads to lower values of Re and Pe. Operating at higher flow rates is not realistic from a technical point of view and would lead to strong deformation of the free surfaces as can be derived from the values of Fr.

As mentioned earlier, it was technically difficult to accommodate pumps and heat exchangers in the scaled vessel, therefore external circuits were designed. However, these are considered as "black boxes" that reproduce the correct boundary conditions at the vessel inlets. This can influence the behavior of the system especially in natural circulation. For this reason, pressure drops controlled by valves are used to equal the system behavior with external circuits to that of a vessel with only internal components such as MYRRHA.

A number of system thermal-hydraulic and CFD simulations of E-SCAPE were performed in support of the scaling analysis and the facility design, which are detailed in [85].

5.2 Phenomena investigation and experimental program

The E-SCAPE facility allows for the investigation of a series of thermal-hydraulic phenomena, characteristic of the MYRRHA reactor. An overview of such phenomena is given in Table 5.2. Moreover, the facility allows testing the behavior of different components in LBE and gaining technological and operational experience [84].

The tests foreseen in E-SCAPE, listed in Table 5.3, are representative of some of the most relevant corresponding scenarios in MYRRHA. In particular, they are significant for the normal operation and the expected

Table 5.2: Main phenomena of investigation for the E-SCAPE facility

Upper plenum	Mixing of non-isothermal jets (e.g. Core outlet)
	Thermal stratification
	Flow distribution at the HXs
	Free surface oscillations
Lower plenum	Flow distribution
	Primary pump jet behavior
Integral	Natural convection DHR
system	Velocity and temperature fields in non-symmetrical conditions
behavior	Residence times of fluid particles
	Particle and/or bubble transport

design basis accidents. However, it is worth remarking that transient scenarios cannot be fully representative of the MYRRHA behavior, due to the external circuits and because E-SCAPE is not meant to scale dynamic events. However, these experiments will be carried out to support codes V&V.

Table 5.3: E-SCAPE test matrix

ID	Case	Regime	Power	Pumps	HX
0	Calibration	Steady State (SS)	N/A	2	4
1	Isothermal	SS	N-A	2	0
2	hot Plug	Transient (T)	N-A	2	0
3	Forced Circulation	SS	Reduced	2	4
4	Natural Circulation	SS	Peak decay, Long term decay	0	4
5	Loss of Flow	T	Peak decay	C	4
6	Pump failure	SS, T	Peak decay, Long term decay	1	4
7	HX failure	SS, T	Peak decay	2	2

5.3 STH model

A full STH model of the E-SCAPE facility was first developed, upon which the coupled model has been successively built. The nodalization is shown in Figure 5.7. The core is modeled using two pipe channels, representing respectively the core simulator active region and the bypass region. All the volumes with a free surface i.e. above-core structure, upper plenum, cold annulus and the IVFHMs, are connected to a gas branch, which in turn is connected to a time-dependent volume used to set the pressure level in the system at 4 bar. The barrel holes are modeled using cross junctions hydraulically connecting above-core structure and upper plenum.

The secondary oil system is composed of two distinct oil circuits, one per LBE external loop. Each simplified oil circuit is modeled by an inlet time-dependent volume and time-dependent junction, two pipes in series which simulate the secondary sides of the heat exchangers, and outlet single-junction and time-dependent volume. Heat structures are implemented to simulate the power generated by the heater and the LBE-oil heat exchangers, as well as to compute heat transfer between hot plenum and cold annulus and IVFHMs.

5.4 Coupled model - Hot Plenum

In a pool-type system, the main regions generally of interest for 3D CFD computations are the lower and upper plena, usually characterized by 3D coolant flow fields. In the upper plenum, the degree of mixing of non-isothermal coolant streams and thermal stratification are effects of particular relevance. For this reason, a first coupled computational model of the E-SCAPE facility has been developed focusing only on this region.

5.4.1 Domain decomposition

The domain of the whole system has been divided into a CFD model of the upper plenum, coupled with the STH model of the remaining portion of the installation, whose code input is the same as in the full STH model. A full 3D CFD model is developed, shown in Figure 5.5, including the above-core structure region, upper plenum and a portion of the vertical HX channels that connect the vessel to the external loops.

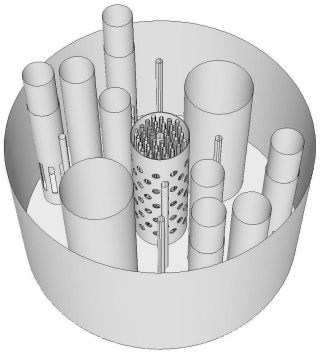

Figure 5.5: FLUENT model of the E-SCAPE upper plenum.

The computational grid, shown in Figure 5.6, is composed of about $3 \cdot 10^6$ cells, generated through a Cartesian grid generation method. The $SST\ k-\omega$ turbulence model is adopted, and the Volume Of Fluid (VOF) multi-phase model is used to be able to compute free surface level variations during transients.

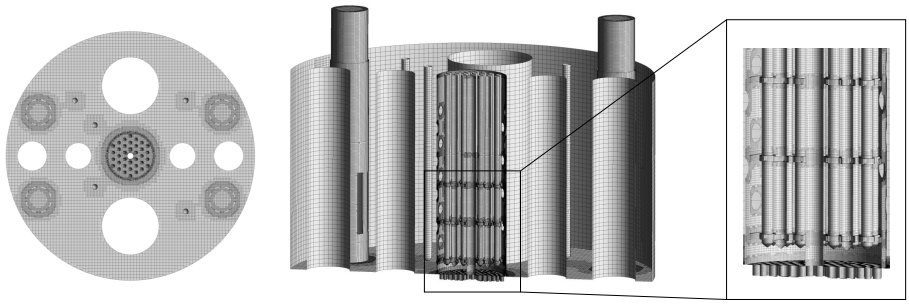

Figure 5.6: Details of the computational grid of the Upper Plenum.

The coupled model, derived from the full STH nodalization by removing the CFD domain and replacing it with appropriate BC components (time-dependent volumes and single-junctions), is shown in Figure 5.8.

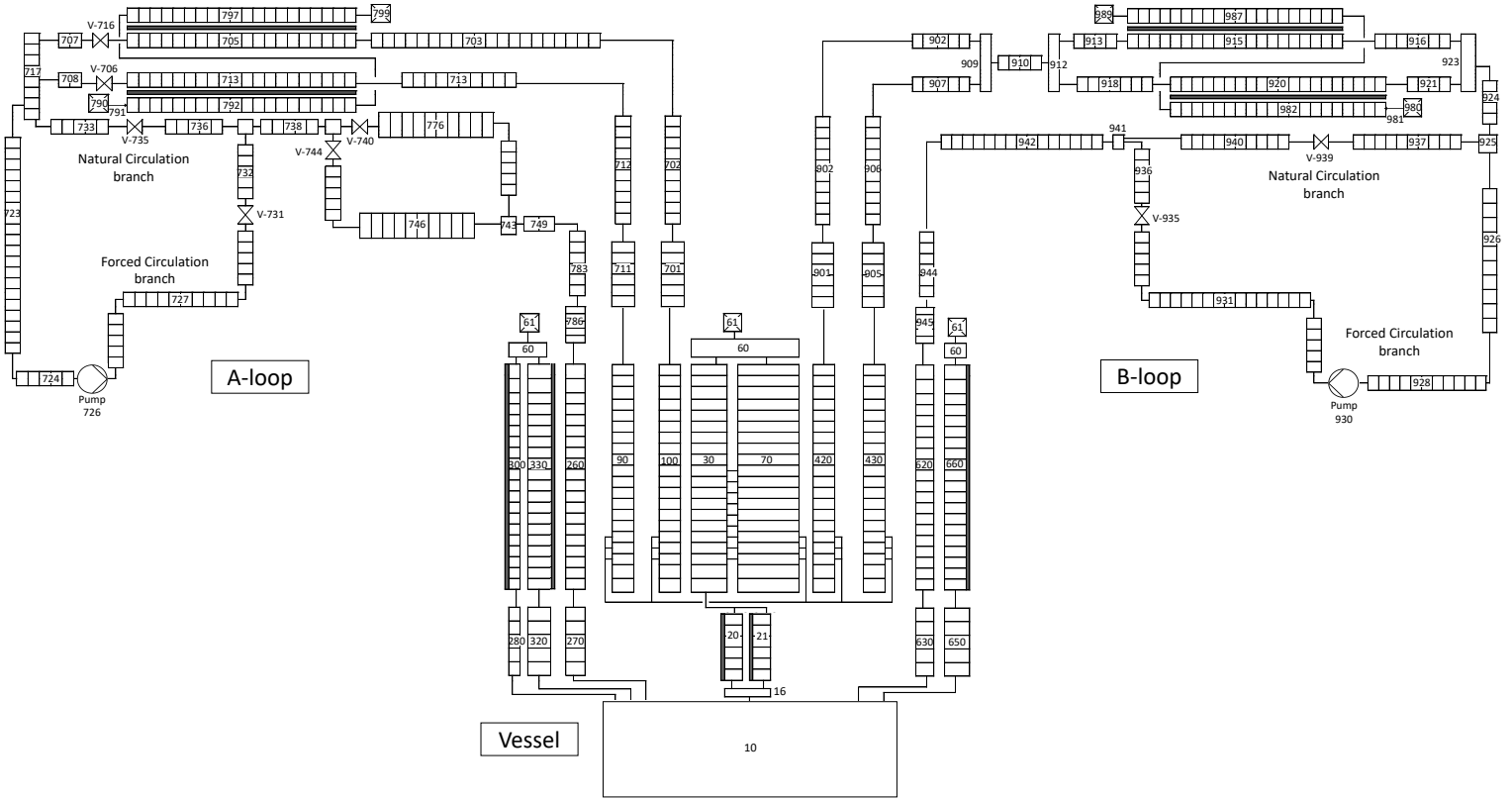

Figure 5.7: Full STH model of the E-SCAPE facility.

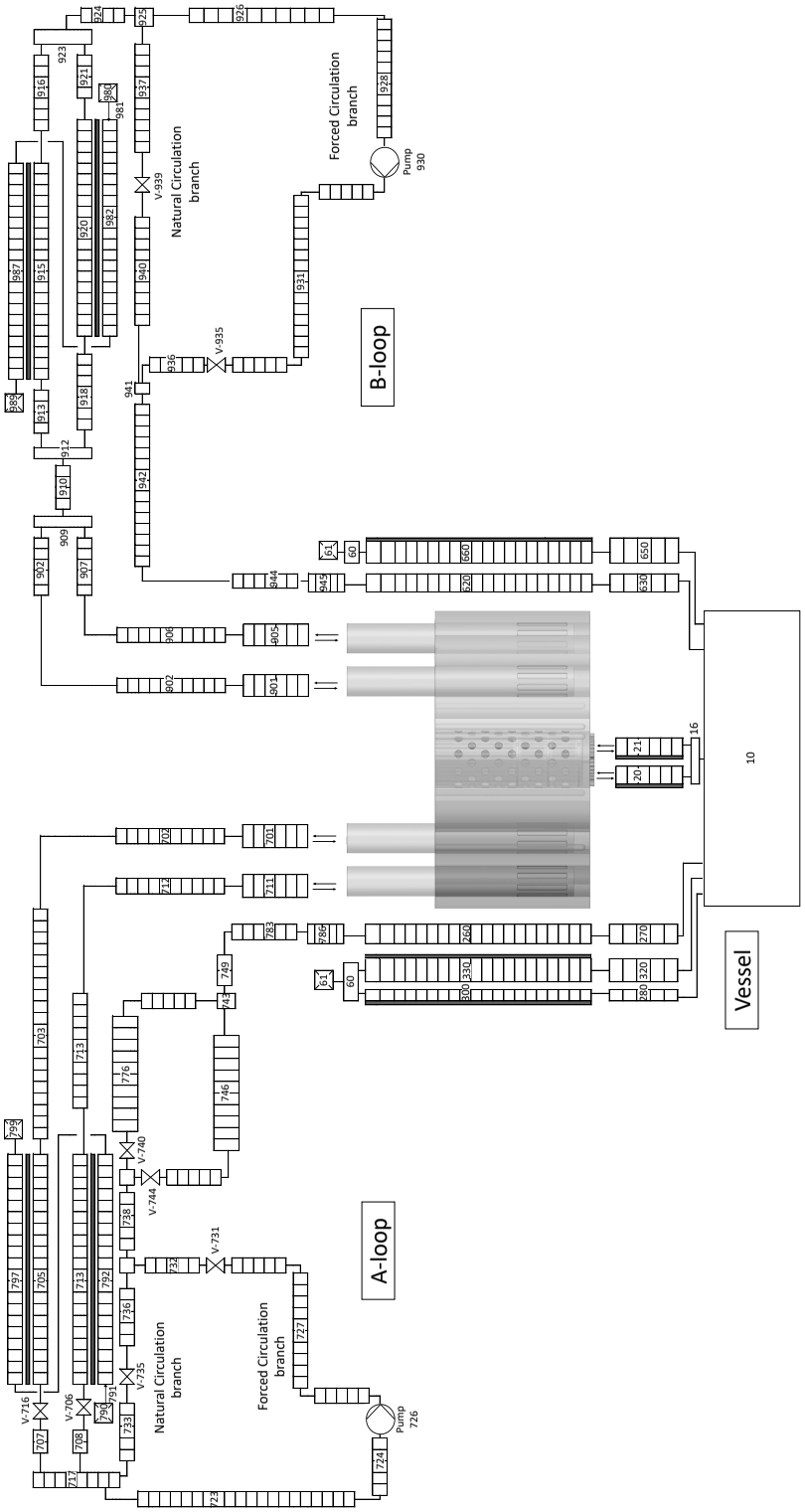

Figure 5.8: Coupled model of the E-SCAPE facility.

In the CFD region, the same pressure BC of 4 bar is set in the gas region above the LBE. The CFD domain and the detailed location of the coupling interfaces are shown in Figure 5.9.

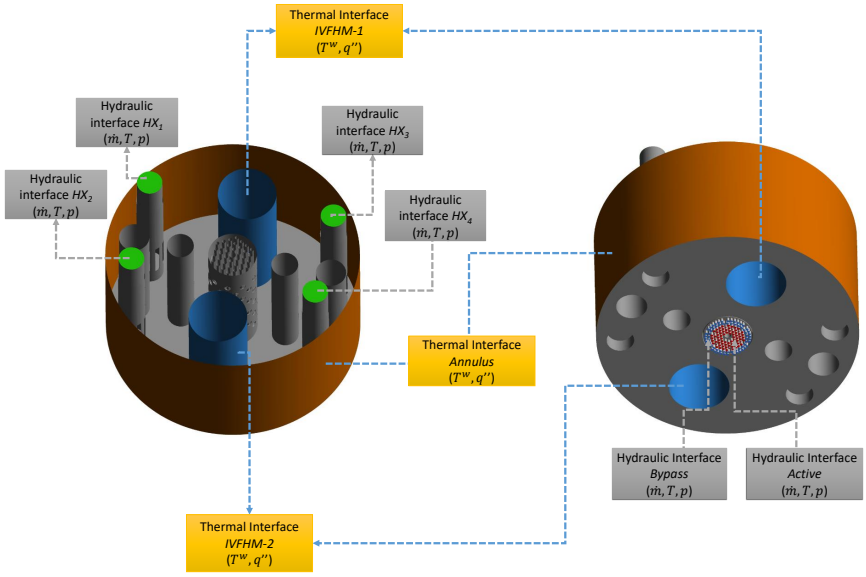

Figure 5.9: Location of the hydraulic and thermal coupling interfaces in the STH-CFD coupled model of the E-SCAPE facility.

Six hydraulic interfaces are implemented, located at the core active region outlet, bypass outlet and at intermediate heights of the HX channels. At all these interfaces, mass flow rate is imposed to the CFD code, and pressure is transferred to the STH solver, as shown in Figure 5.10. This modeling choice is allowed by the presence of a compressible phase in the CFD domain introduced by the use of the VOF model. The equilibrium between the pressure fields in the coupled domains is achieved by imposing the same pressure in the cover gas region, present in both the models. In this regard, as absolute static pressures are used, including therefore the hydrostatic component, it is fundamental for a correct implementation of this scheme to have very accurate and congruent elevation changes in the coupled domains.

Thermal coupling interfaces are represented by the boundary walls separating upper plenum from the cold annulus and from the two IVFHM mock-ups.

Based on the defined number and location of hydraulic interfaces, the Quasi-Newton algorithm would result in a degree-of-freedom $\nu = 6$,

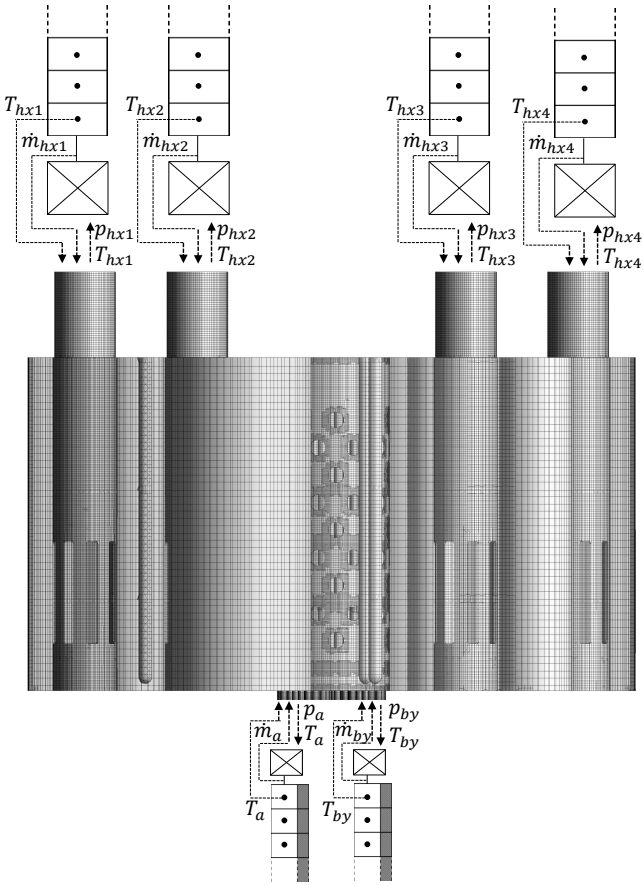

Figure 5.10: Exchange of BC at the hydraulic coupling interfaces

with a $\nu x \nu$ Jacobian matrix that requires ν coupling iterations to be approximated. To reduce overall computational costs, the methodology to reduce the number of degrees of freedom of the problem discussed in chapter 3 is adopted, thus only the total mass flow rate $\dot{m}_c$ at the inlet of the upper plenum (core outlet) and the mass flow rate $\dot{m}_{hx}$ at the outlet (HX channels) are considered in the numerical algorithm, reducing the problem degree-of-freedom to $\nu = 2$. With this simplification, the input vector considered for the coupling numerical algorithm is:

$$ {}^{n}\mathbf{U}^{k}_{CFD} = \begin{bmatrix} {}^{n}\dot{m}^{k}_{c} \\ {}^{n}\dot{m}^{k}_{hx} \end{bmatrix} = \begin{bmatrix} {}^{n}\dot{m}^{k}_{a} + {}^{n}\dot{m}^{k}_{by} \\ {}^{n}\dot{m}^{k}_{hx_1} + {}^{n}\dot{m}^{k}_{hx_2} + {}^{n}\dot{m}^{k}_{hx_3} + {}^{n}\dot{m}^{k}_{hx_4} \end{bmatrix} \tag{5.7} $$

which results, at the end of each coupling iteration, in the following STH

output vector:

$$
\begin{gathered}
{}^{n}\mathbf{Y}_{STH}^{k} = \phi_{STH}(\phi_{CFD}({}^{n}\mathbf{U}_{CFD}^{k})) = \\
\begin{bmatrix} {}^{n}\widetilde{\dot{m}}_{c}^{k} \\ {}^{n}\widetilde{\dot{m}}_{hx}^{k} \end{bmatrix} = \begin{bmatrix} {}^{n}\widetilde{\dot{m}}_{a}^{k} + {}^{n}\widetilde{\dot{m}}_{by}^{k} \\ {}^{n}\widetilde{\dot{m}}_{hx1}^{k} + {}^{n}\widetilde{\dot{m}}_{hx2}^{k} + {}^{n}\widetilde{\dot{m}}_{hx3}^{k} + {}^{n}\widetilde{\dot{m}}_{hx4}^{k} \end{bmatrix}
\end{gathered}
\tag{5.8}
$$

as well as in the level of interface residuals:

$$
{}^{n}\mathbf{R}^{k} = \begin{bmatrix} {}^{n}r_{c}^{k} \\ {}^{n}r_{hx}^{k} \end{bmatrix} = \begin{bmatrix} {}^{n}\widetilde{\dot{m}}_{c}^{k} - {}^{n}\dot{m}_{c}^{k} \\ {}^{n}\widetilde{\dot{m}}_{hx}^{k} - {}^{n}\dot{m}_{hx}^{k} \end{bmatrix}
\tag{5.9}
$$

Having in this case only mass flow rate components in the residual vector, there is no need to use relative residual terms. The residual vector above is used for the Quasi-Newton numerical algorithm; nevertheless, a convergence criterion is set for each coupling interface.

The same methodology applied in the previous chapters to approximate the terms of the Jacobian matrix, based on the small perturbation of a term at the time of the CFD input vector, is adopted. Once the new CFD input vector ${}^{n}\mathbf{U}_{CFD}^{k+1}$ is computed at each iteration, which contains new total mass flow rates at the core outlet ${}^{n}\dot{m}_{c}^{k+1}$ and in the HX channels ${}^{n}\dot{m}_{hx}^{k+1}$, single boundary condition values for each hydraulic interface are to be calculated in order to proceed to the new coupling iteration. This is done by evaluating the vector difference between the new CFD input vector and the old STH output vector, and equally distributing its terms to the corresponding coupling interfaces, as expressed below:

$$
\begin{gathered}
{}^{n}\Delta\mathbf{U}^{k+1} = {}^{n}\mathbf{U}_{CFD}^{k+1} - {}^{n}\mathbf{Y}_{STH}^{k} = \\
\begin{bmatrix} {}^{n}\dot{m}_{c}^{k+1} - {}^{n}\widetilde{\dot{m}}_{c}^{k} \\ {}^{n}\dot{m}_{hx}^{k+1} - {}^{n}\widetilde{\dot{m}}_{hx}^{k} \end{bmatrix} = \begin{bmatrix} n_{c}\,{}^{n}\delta\dot{m}_{c}^{k+1} \\ n_{hx}\,{}^{n}\delta\dot{m}_{hx}^{k+1} \end{bmatrix}
\end{gathered}
\tag{5.10}
$$

where n_c and n_{hx} are respectively the number of interfaces at the core outlet section and at the heat exchanger channels. In the specific case discussed in this application, $n_{core} = 2$ and $n_{hx} = 4$. The adjustments of the interface quantities ${}^{n}\delta\dot{m}_{c}^{k+1}$ and ${}^{n}\delta\dot{m}_{hx}^{k+1}$ are evaluated from the equation above, and applied to the STH interface quantities in order to have BC data that form the required input vector ${}^{n}\mathbf{U}_{CFD}^{k+1}$:

$$
\begin{cases}
{}^{n}\dot{m}_{a}^{k+1} = {}^{n}\widetilde{\dot{m}}_{a}^{k} + {}^{n}\delta\dot{m}_{c}^{k+1} \\
{}^{n}\dot{m}_{by}^{k+1} = {}^{n}\widetilde{\dot{m}}_{by}^{k} + {}^{n}\delta\dot{m}_{c}^{k+1} \\
{}^{n}\dot{m}_{hx1}^{k+1} = {}^{n}\widetilde{\dot{m}}_{hx1}^{k} + {}^{n}\delta\dot{m}_{hx}^{k+1} \\
{}^{n}\dot{m}_{hx2}^{k+1} = {}^{n}\widetilde{\dot{m}}_{hx2}^{k} + {}^{n}\delta\dot{m}_{hx}^{k+1} \\
{}^{n}\dot{m}_{hx3}^{k+1} = {}^{n}\widetilde{\dot{m}}_{hx3}^{k} + {}^{n}\delta\dot{m}_{hx}^{k+1} \\
{}^{n}\dot{m}_{hx4}^{k+1} = {}^{n}\widetilde{\dot{m}}_{hx4}^{k} + {}^{n}\delta\dot{m}_{hx}^{k+1}
\end{cases}
\tag{5.11}
$$

It is worth noticing that the presented method, in the prospective of reactor-scale integral simulations, can be applied to an arbitrary number of coupling interfaces. In fact, the same approach will be used in chapter 6 for the case of multiple channels used to model the reactor core.

5.4.2 Simulation results

I. Forced circulation analysis

A coupled simulation of the forced circulation operating condition is first performed. The first step of the coupled calculation procedure is to run a full STH calculation to reach steady-state results. Interface BC values are extracted from the STH results data and used to perform a stand-alone simulation of the CFD domain. At this point, after having modified the STH nodalization by removing the region modeled by the CFD code and replacing it with appropriate components to receive interface boundary conditions, the coupled calculation can be launched, which leads to new steady-state results after a short transient of stabilization. The results of the forced circulation coupled simulation are summarized in Table 5.4.

Table 5.4: Forced circulation steady state results

Parameter (unit)	Value
Core power (kW)	91.2
Core active region mass flow rate (kg/s)	62.5
Core bypass mass flow rate (kg/s)	57.5
Average HX channel mass flow rate (kg/s)	30.0
Core inlet temperature (°C)	199
Core outlet temperature (°C)	204
Secondary oil temperature at HX inlet (°C)	162
Secondary oil mass flow rate per external loop (kg/s)	4.5

For what concerns the numerical aspects of the coupled simulation, no instabilities and oscillations of the solution parameters were observed thanks to the implemented Quasi-Newton under-relaxation algorithm. Figure 5.11 shows the typical convergence history of three consecutive representative coupling time steps, with the terms of the Jacobian matrix computed in the first of them. In the first time step, it can be

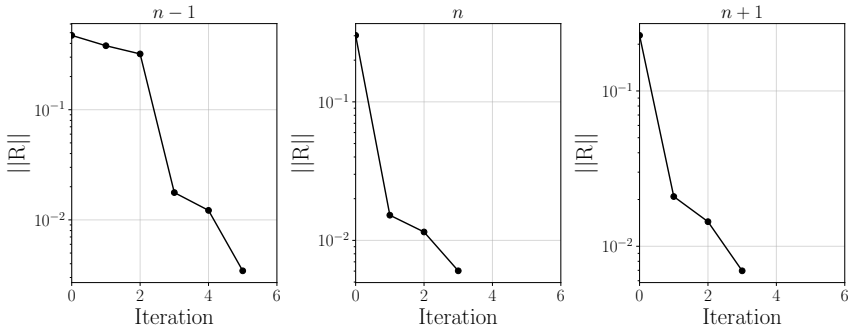

Figure 5.11: Interface convergence history for three coupling time steps.

observed that the residual norm does not drop significantly in the first two iterations, again because of the arbitrary perturbations applied to the two terms of the CFD input vector. Once the Jacobian matrix is approximated, the residual norm start decreasing significantly with the coupling iterations. In the following two coupling time steps, the quality of the Jacobian matrix is tested after its first use, as explained in subsection 3.2.2. The conditions expressed by Equation 3.81 is satisfied, thus the same matrix is used for the following coupling iterations.

Figure 5.12 and Figure 5.13 show the flow and temperature fields in the upper plenum, in forced circulation operating conditions, respectively on two orthogonal vertical cross sections and on four horizontal cross sections at different vertical positions of the domain. In Figure 5.12 it is possible to notice that the volume is only partially filled by LBE, the rest of it being filled by Argon cover gas. The level in the cold region interested by free surface, namely the cold annulus and IVFHM volumes included in the STH domain, is higher due to the higher pressure in the lower plenum. The difference in the hydrostatic heights between those volumes and the upper plenum (about 0.35 m) roughly corresponds to the pressure losses in the core (0.35 bar). The velocity contours show that higher fluid velocity is predicted in the ACS and in the barrel holes, while in the rest of the volume the LBE velocity is quite low. The temperature profiles show that hot LBE flowing from the core active region reaches the free surface and leaves the ACS volume mainly from the holes of the barrel located in the upper region of the plenum, while the holes at the bottom are crossed by cold LBE flowing through the core bypass.

In the horizontal cross sections shown in Figure 5.13, for the same reason

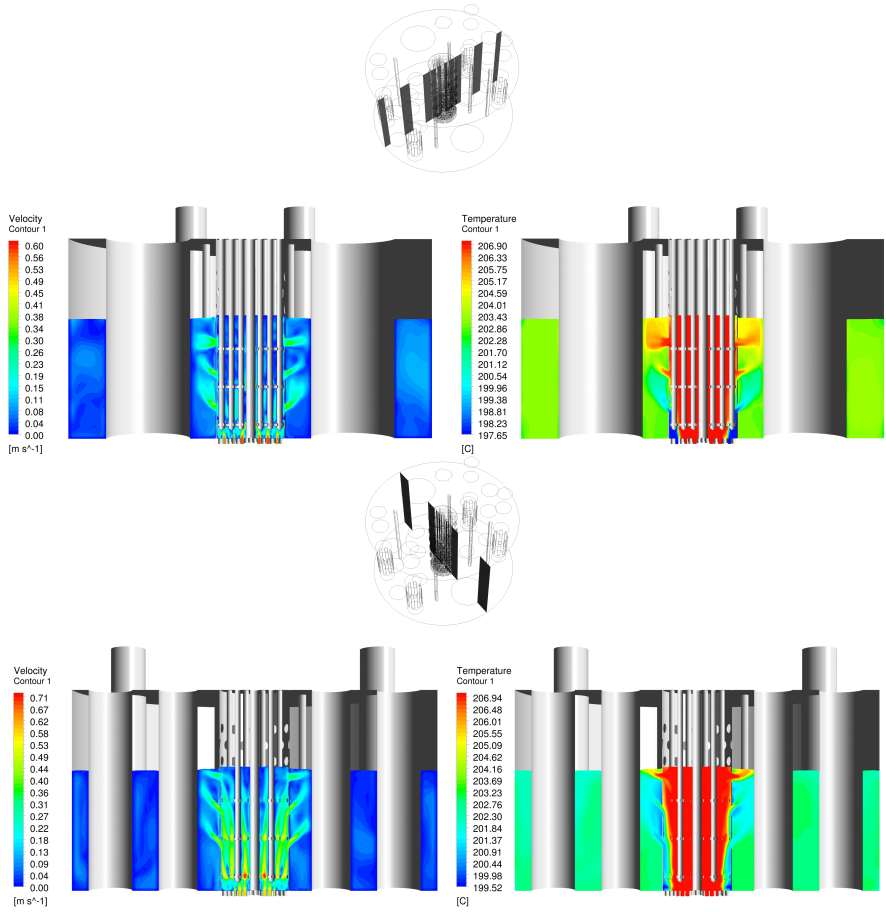

Figure 5.12: Velocity and temperature contour in the upper plenum in forced circulation operation.

it is possible to observe that higher LBE velocities are predicted in the upper part of the plenum, where the temperatures are also higher due to the hot plume of LBE reaching the free surface. These results are in line with previous analyses performed within the design of the facility [84].

II. Loss of flow transient analysis

A proof-of-principle loss of flow transient simulation was carried out. From steady state forced circulation conditions, the transient is initiated by tripping both the circulating pumps, placed in the external loops, at the time t_0. The power provided by the core is kept at the nominal

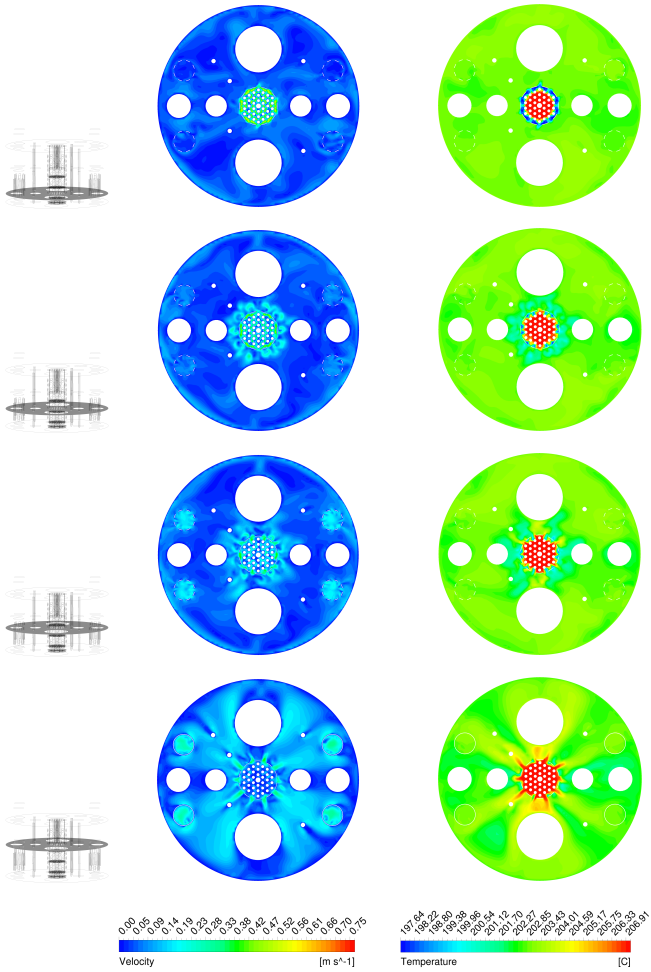

Figure 5.13: Velocity and temperature contour in the Upper Plenum in forced circulation operation at different heights of the domain.

value for the whole duration of the transient, and the secondary system remains operating in nominal conditions. In this pre-test analysis, the coupled calculation results are assessed against a full RELAP5-3D model, in order to identify eventual discrepancies due to the effect of 3D temperature profiles on natural circulation flow rates and the development of thermal stratification.

The transient evolution of the mass flow rate in the core active region and bypass following the trip of the pumps is plotted in Figure 5.14a, while the total mass flow rate leaving the upper plenum and flowing in

the external loops is plotted in Figure 5.14b.

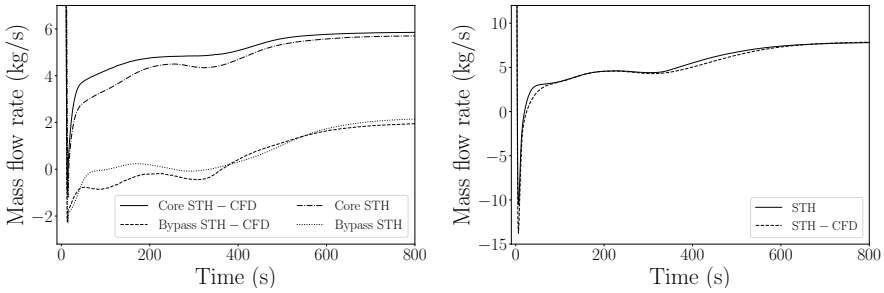

(a) Core active and bypass regions **(b)** Total HX channels

Figure 5.14: LOF transient: time evolution of the mass flow rate.

It can be observed that overall the results are in good agreement, although some difference can be observed and explained through the visualization of the 3D temperature profile computed by the coupled calculation. In particular, the LBE mass flow rate in the core active region is higher in the coupled simulation than in the 1D simulation, and the opposite is noted for the mass flow rate in the bypass region. The reason for this difference is the temperature profile in the ACS, and in particular the radial temperature gradient, which is not taken into account in the 1D model of the STH code. In the CFD calculation, the hot plume which develops above the core active region is well predicted, which leads to lighter column of fluid above it and higher mass flow rate. The opposite is observed in the bypass region, above which LBE is colder and lower mass flow rate is predicted.

The transient evolution of the temperature at the outlet of the core active region and core bypass is shown in Figure 5.15. The temperature at the outlet of the core active region tends to be lower in the coupled simulation, easily explained by the higher flow rate predicted. At the outlet of the core bypass, large deviations in the prediction of the LBE temperature between the two simulations are observed; in particular, the temperature calculated by the STH code experiences sudden increases when inversion of the flow occurs. This is a consequence of the perfect mixing formulation of the 1D code, where radial temperature profiles in the ACS region are not taken into account, therefore the temperature of the LBE re-entering the bypass is influenced by the increase of temperature at the outlet of the core active region. On the contrary, as shown in Figure 5.16, the coupled simulation reveals that the flow field in the ACS region is quite complex and of three-dimensional nature.

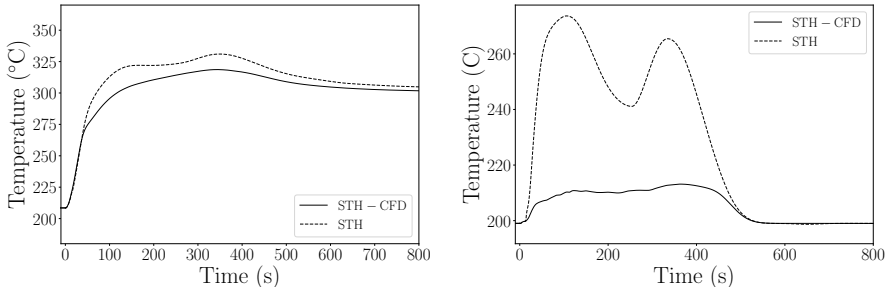

(a) Active region **(b)** Bypass region

Figure 5.15: LOF transient: time evolution of the core outlet temperature.

The observation of the vectors velocity and temperature contour in the ACS reveals that the hot LBE flowing out from the core active region does not mix well with the LBE re-entering the bypass, but forms a thin vertical plume in the central region of the ACS reaching the free surface. Cold LBE is drawn from the upper plenum by the low pressure region associated with this hot plume, and flows through the holes of the barrel at the bottom of the upper plenum towards the center of the ACS. Some of this LBE flows downwards in the bypass region during the inversion of the flow, explaining the observed lower temperature.

At the low flow conditions established in the pool after the pumps trip, thermal stratification develops, as visible in Figure 5.17 showing the evolution over time of the vertical temperature profiles at four different

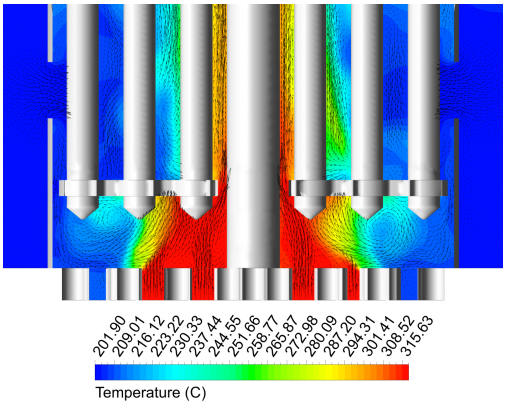

Figure 5.16: Temperature contour and vectors velocity in the above-core structure at t=300 s.

locations of the upper plenum.

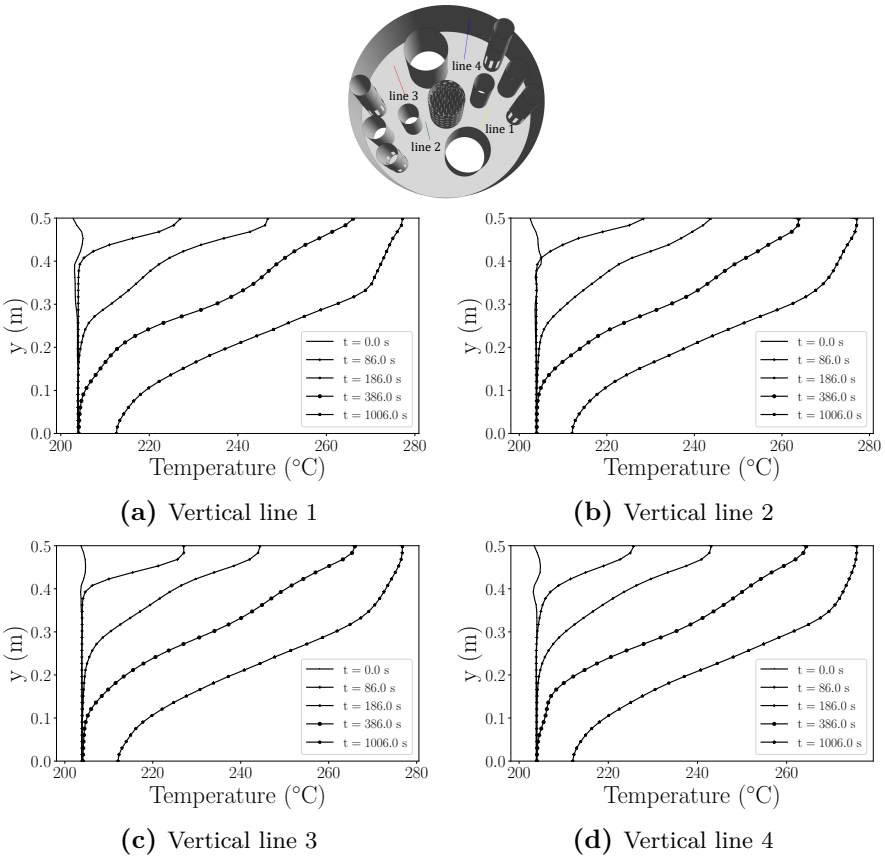

(a) Vertical line 1 **(b)** Vertical line 2

(c) Vertical line 3 **(d)** Vertical line 4

Figure 5.17: LOF transient: thermal stratification at different locations of the upper plenum.

The stratification is induced by the hot LBE plume reaching the free surface, which remains in the upper part of the plenum due to buoyancy, while cold LBE stays at the bottom of the volume. This situation leads to a gradual establishment of large vertical temperature gradients. The transient development of thermal stratification is a complex multi-dimensional phenomenon, which is not possible to be observed, due to the 1D discretization of the governing equations, with the STH code. The evolution of the temperature field in the upper plenum is also shown in Figure 5.18, in which temperature contours on a vertical cross section are plotted.

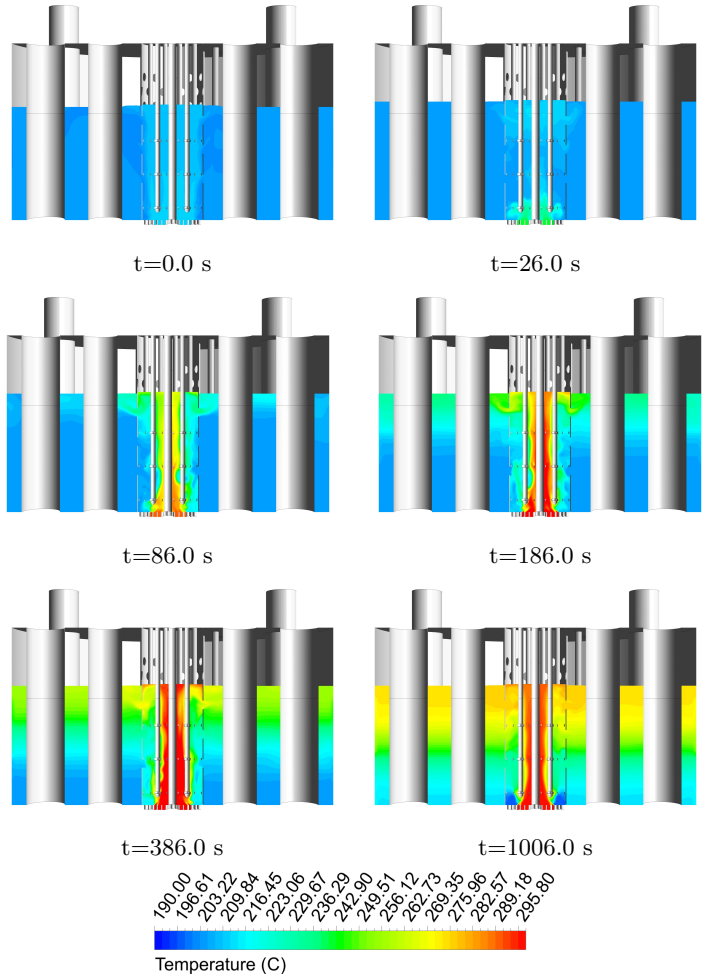

Figure 5.18: Transient evolution of the temperature field in the upper plenum during loss of flow transient.

III. Partial loss of flow transient analysis

A partial loss of flow (Partial-LOF) transient was also simulated using the same model. From forced circulation operation, one of the two circulating pumps (B-loop) is tripped while the other one (A-loop) remains working in nominal conditions. The core power (electrical heater) is maintained constant during the whole duration of the transient. Also the secondary oil system maintains constant active operation.

The transient evolution of the mass flow rates in key locations of the system are plotted in Figure 5.19. Following the pump trip, the flow rate

in the failed external circuit (B-loop) drops to negative values, indicating that recirculation in the interested loop occurs. In the A-loop, the flow rate slightly increases because of the reduction of the total hydraulic resistance of the system. As expected, the core total flow rate (active region and bypass) drops to about half of the initial value, and reaches the new steady value of 55 kg/s in about 25 s. In the new operating condition, with only one circulating pump on, a strong dissymmetric flow field establishes in the upper plenum, with LBE flowing in from the core and the failed loop, and exiting the vessel through the vertical HX channels of the unperturbed external loop.

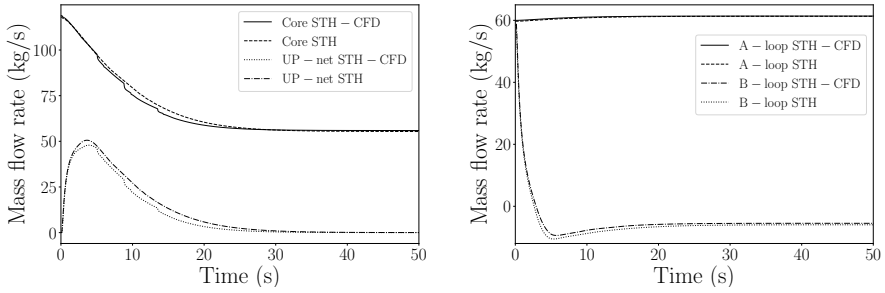

(a) Core region **(b)** External loops

Figure 5.19: Partial LOF transient: time evolution of the mass flow rate.

The evolution of the system temperatures is plotted in Figure 5.20.

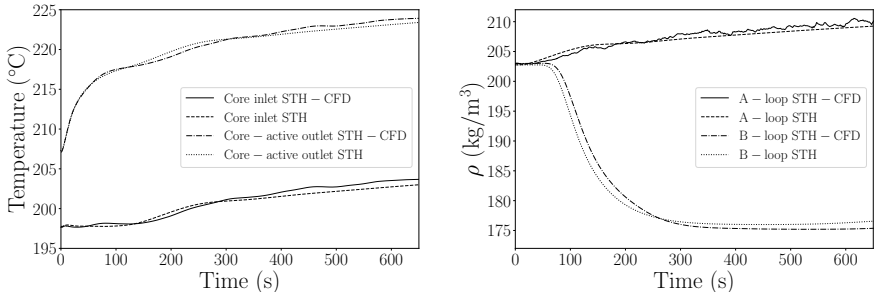

(a) Core region **(b)** External loops

Figure 5.20: Partial LOF transient: time evolution of temperature.

The core outlet temperature increases following the reduction of the flow rate, which is reflected with a certain delay at the outlet of the upper plenum (inlet of the A-loop). At the inlets of the B-loop, the

temperature suddenly drops when the fluid of the cold leg, which now flows in opposite direction and continues to be cooled by the secondary oil in the two heat exchangers, reaches the main vessel.

The temperature contours at different instants of the transient, on a vertical cross section cutting the core and two HX channels, are shown in Figure 5.21. In steady-state forced circulation, limited temperature gradients in the upper plenum are observed due to the high mass flow rate and enhanced mixing. After about 100 s from the trip of the pump in the B-loop, colder LBE begins to enter the upper plenum from the HX channels connected to the failed loop. In the meantime, temperature at

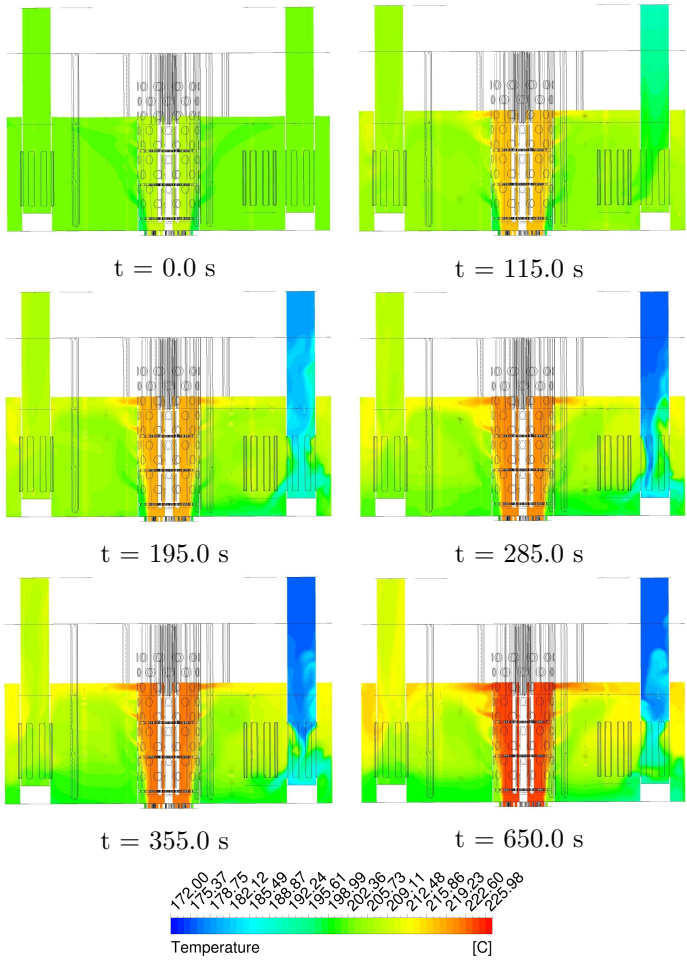

Figure 5.21: Partial LOF transient: evolution of the upper plenum temperature field in the first phase of the transient.

the core outlet continues to increase because of the reduced flow and the constant power. Three-dimensional flow and temperature fields establish in these new operating conditions: cold LBE from the failed loop flows downwards towards the bottom of the upper plenum through the holes of the two HX channels, while hot LBE flows upwards in the above-core structure and reaches the free surface. Because of the intermediate axial position of the HX channels holes, the thermal mixing between these two flow streams of LBE before leaving the upper plenum is efficient, and the temperature at the outlet (inlet of A-loop) is roughly equal to the mass flow rate – weighted average between these flow streams, explaining the overall agreement with the full 1D simulation results. However, given the complexity of this flow field, it is clear that such a conclusion is not of general validity, and that large discrepancies can be expected in different geometries and transient conditions. It is also interesting to notice that in the HX channels of the failed loop, the competition between downward cold flow coming from the external loop and the upward hot flow driven by buoyancy leads to a quite complex flow field even within the channels.

5.5 Fully coupled model development

Based on the previous results, a fully coupled model including both lower and upper plena in the CFD domain was implemented. The computational strategy is the same as discussed above, with the addition of coupling interfaces related to the lower plenum. To simplify the coupling settings and limit the number of coupling interfaces, it was chosen to include in the CFD model also the cold volumes of LBE interested by free surface, namely the annulus and the IVFHM volumes. These regions do not have an influence in the hydraulic behavior in forced circulation, but they must be taken into account during transients given the gravitational energy stored in such volumes due to the primary pumps head. The developed model is shown in Figure 5.22.

Slightly different input parameters have been chosen for the fully coupled simulation, in the light of the definition of a number of operating parameters for the experimental campaign. In particular, in this case a small power is also provided by the electrical heaters in the bypass region. This is expected to have an almost negligible impact on the overall behavior of the system, however some effects are expected in the distribution of the mass flow rate in the core channels.

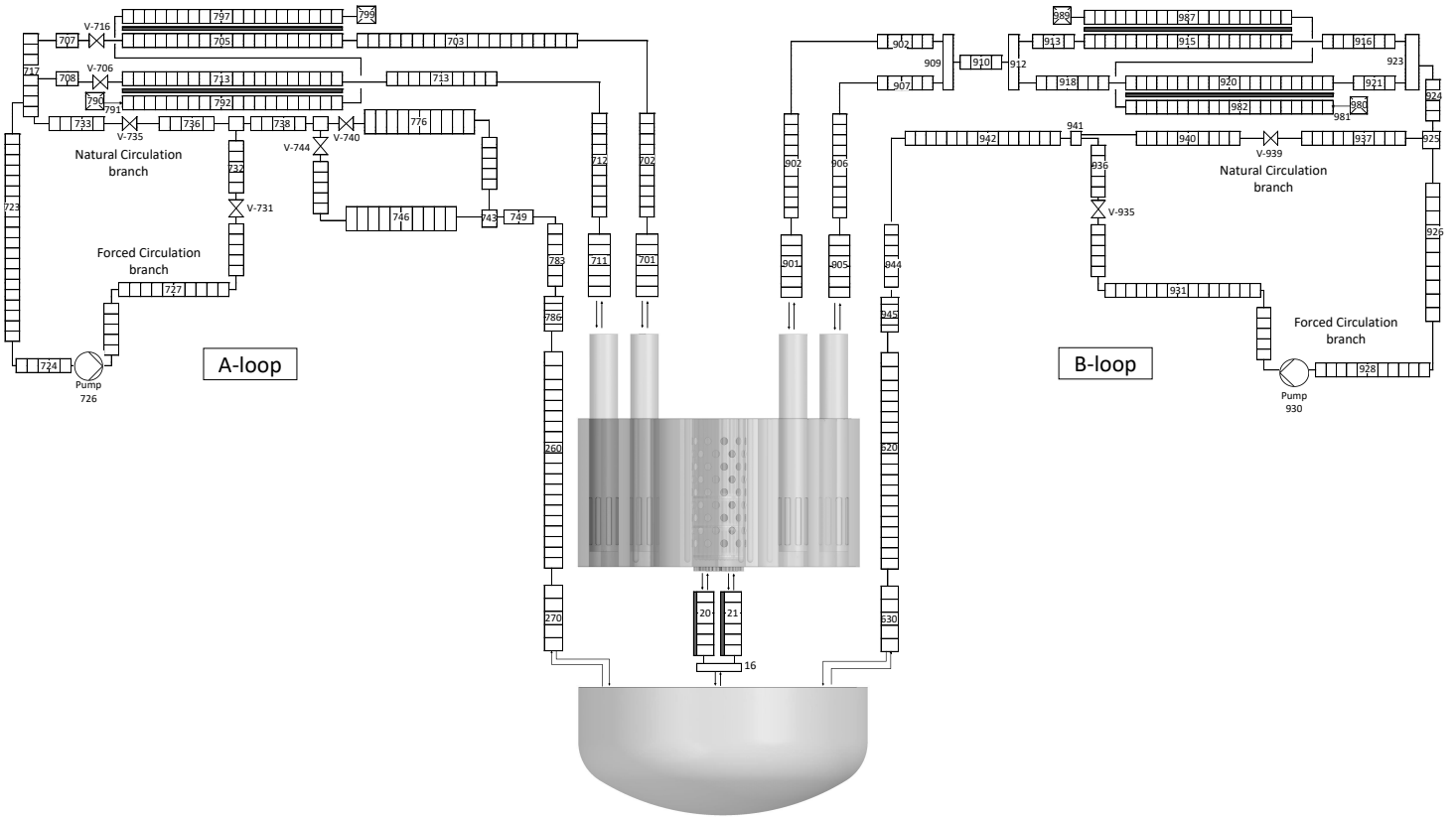

Figure 5.22: Fully coupled model of the E-SCAPE facility.

The results of the simulation of the forced circulation operating conditions are shown in Figure 5.23. As expected, the flow field in the upper plenum is the same as previously found. In the lower plenum, one can observe the pump-induced jet, with LBE flowing vertically in the plenum until impinging the vessel bottom wall, flowing then towards the central region of the volume and successively upwards towards the core. Even in this case, mesh sensitivity studies are not performed, as the main goal of the work was testing the coupling methodology and assess its performance. Such analyses will be required in the phase of post-test comparisons.

The difference in the LBE free surface levels between the cold regions and the upper plenum is also noticeable. As previously discussed, such a difference roughly corresponds to the core pressure drops. Further element of consideration on the temperature profile is the effect of conjugate heat transfer between hot plenum and annulus - IVFHM, computed this time within the CFD solver, visible in the right side of Figure 5.23.

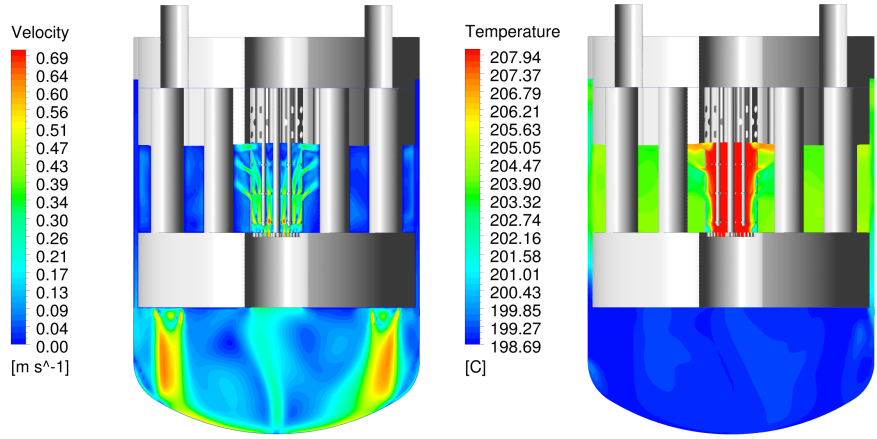

Figure 5.23: Fully coupled model: velocity and temperature profiles in forced circulation.

A transient calculation was performed on the same total LOF test, initiated by the sudden trip of both circulating pumps in the external loops. The results, shown in Figure 5.24 and Figure 5.25 are in line with the previous findings.

In the comparison with the previous analysis, a difference is observed on the temperature at the outlet of the bypass channel, as an effect

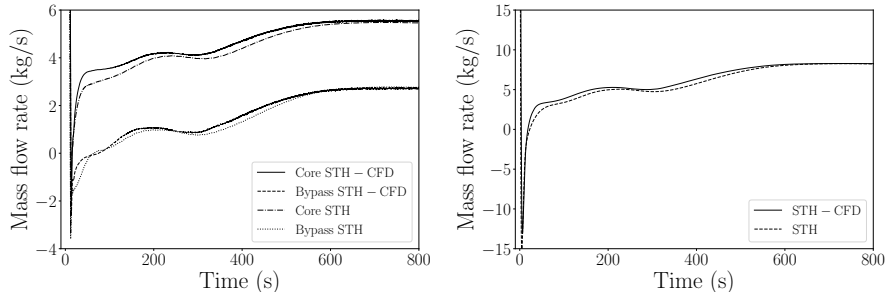

(a) Core active and bypass regions **(b)** Total hx channels

Figure 5.24: LOF transient: time evolution of the mass flow rate.

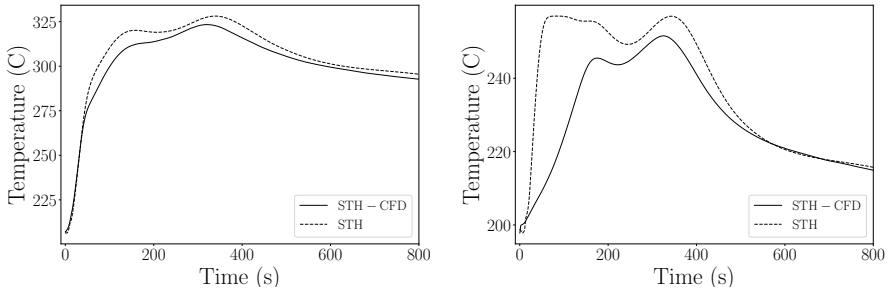

(a) Core active region **(b)** Core bypass region

Figure 5.25: LOF transient: time evolution of core outlet temperature.

of the added input electrical power. In particular, the time window of flow inversion in the bypass region is very small (about 60 s), due to the buoyancy effect induced by the heater. This is reflected on the outlet temperature, also increasing in this case, however more slowly than in the full STH simulation. This is due again to the fact that in the STH model any radial temperature gradient in the ACS is neglected, thus the temperature increase at the active region outlet is immediately reflected at the outlet of the bypass region during flow inversion. In accordance with the previous simulation, the mass flow rate in the core active region tends to be slightly higher, thus the outlet temperature lower, as the input power is identical.

The temperature profile evolution from forced to natural circulation can be observed in Figure 5.26. In particular, it can be noticed the thermal stratification established following the pumps trips, which is partially extended also to the cold regions of the vessel. Longer term studies might be required to assess more in detail the impact of such an

effect. Also, it is possible to observe the difference in the levels between forced circulation regime and natural circulation state, with the levels practically the same, as expected, in the latter.

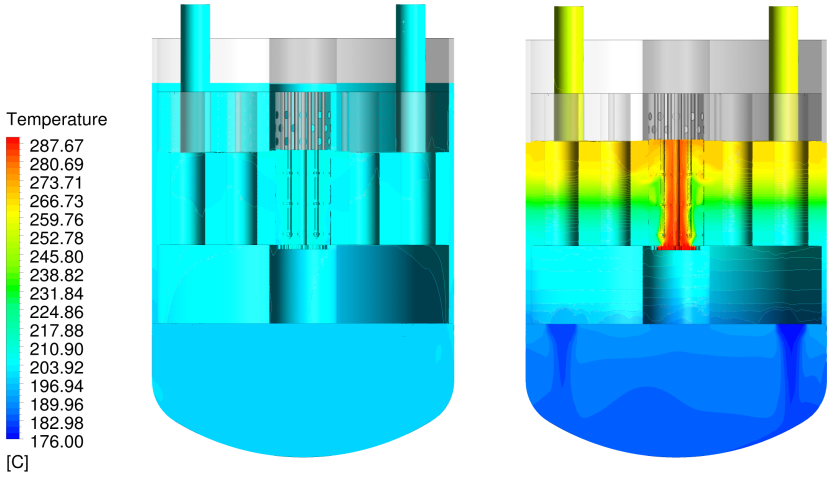

Figure 5.26: LOF transient: time evolution of the temperature field in the lower and upper plena of the vessel.

5.6 Conclusions

This chapter discussed the application of the RELAP5-3D/FLUENT coupling method to a number of pre-test transient analyses on the pool-type experimental facility E-SCAPE, built at the SCK•CEN to support the design and safety assessment of MYRRHA. The experimental installation represents a scale model of the MYRRHA primary cooling system, design version 1.2, conceived from one side to investigate thermal-hydraulic characteristics of a pool-type LBE system, and on the other side to generate high-quality experimental data to support the V&V of STH, CFD and coupled codes. The purposes of the studies presented in this chapter were to i) test the numerical method on a more complex pool-type configuration ii) identify relevant 3D transient thermal-hydraulic effects, and their impact on the system transient behavior, in view of post-test comparisons, and iii) identify potential limitations of full 1D models in pool-type reactors transient simulations.

Compared to the models discussed in chapter 3 and chapter 4, the application of the methodology to a pool-type system is more complex, as it requires the implementation of multiple hydraulic interfaces and thermal coupling for the computation of conjugate heat transfer phenomena. These two aspects, whose methodology background was discussed in section 3.2, have been tested in the analyses presented in this chapter. In particular, the developed numerical technique to reduce the degree-of-freedom of the Quasi-Newton algorithm has been adopted and showed satisfactory results.

A first model has been developed for a detailed 3D simulation of the upper plenum, which is generally characterized by pronounced 3D velocity and temperature profiles. The model was tested on the analysis of the forced circulation condition and of two transient scenarios, namely a total and a partial loss of flow transient. In these pre-test simulations, comparison between coupled and full STH models have been performed. Overall, the results were found in good agreement; however, large discrepancies on certain local temperatures were observed in the LOF simulation, particularly during flow reversal conditions in the core region. These differences can be attributed to the perfect mixing formulation of the STH code, not capable to capture radial temperature gradients in the above core structure region, which are on the contrary well predicted in the coupled simulation. Furthermore, the coupled simulation captured the development of thermal stratification in the upper plenum, established in natural circulation at low flow conditions. On the other side, it must be mentioned that, as can be expected, the computational requirements associated to the coupled simulation are rather high compared to a full STH model. To provide an idea, the full STH simulation of the loss of flow transient, computed for 1000 s of simulation time, requires few hours runtime on a single processor, while the coupled simulation executed on 12 cores runs for about 500 hours. It is however worth mentioning also that these requirements are generally smaller, in terms of both model development and computation, with respect to a full CFD model of the entire system. Based on these first analyses, a full model with the inclusion of the lower plenum in the CFD domain was developed and applied on a similar total loss of flow transient. The results were found in line with previous findings, suggesting that no particular 3D effects in the lower plenum is expected in LOF transients.

The facility E-SCAPE is currently under commissioning tests. First experiments on iso-thermal forced circulation conditions were performed, which generated data particularly useful for input model calibration,

including operational parameters, hydraulic losses characterization etc. First experimental data on integral transient tests will be used first for the validation of the single codes, in relation to the regions and phenomena related to them, and successively for the validation of coupled codes. To this purpose, detailed V&V methodologies, validation metrics and UQ methodologies will have to be defined.

Chapter 6

Coupled simulation of the MYRRHA reactor

The final part of the research activity consisted in the application of the coupling tool on a transient simulation of the MYRRHA reactor, which was the final technical goal of the thesis. This chapter provides a general description of the reactor design and main primary system components, as well as it presents the developed models and the results of the simulation of a reference transient scenario. The developments and the simulations presented in this chapter represent the content of a paper published in a peer-reviewed journal [86].

As introduced in chapter 1, the MYRRHA project is recognized as a high priority infrastructure for nuclear research in Europe. Several European FP6 and FP7 projects were established, as main target, to finalize a preliminary design of the MYRRHA reactor:

- FP6 IP-EUROTRANS, leading to the finalization of MYRRHA/XT-ADS version of MYRRHA in June 2008 [87];
- FP7 Central Design Team (CDT), defining the MYRRHA/FASTEF version in March 2012 [88];
- FP7 MAXSIMA (started in November 2012), more focused on the MYRRHA safety assessments and components qualification [89].

These projects led to the definition of the latest version of the MYRRHA design (Design Version 1.6), which was finalized in June 2014 [90, 91] and is currently in the verification phase. This system configuration represents the state of the art, but is not definitive: the MYRRHA

design is still evolving taking into account main results from the parallel R&D programme.

6.1 MYRRHA state-of-the-art configuration

MYRRHA is a pool-type accelerator driven system (ADS) cooled by LBE, able to work either in ADS or in critical mode [7]. The primary and secondary systems are designed to evacuate a maximum power of 110 MWth, generated by a MOX fueled core. A drawing of the reactor with the main internal components is shown in Figure 6.1 [91].

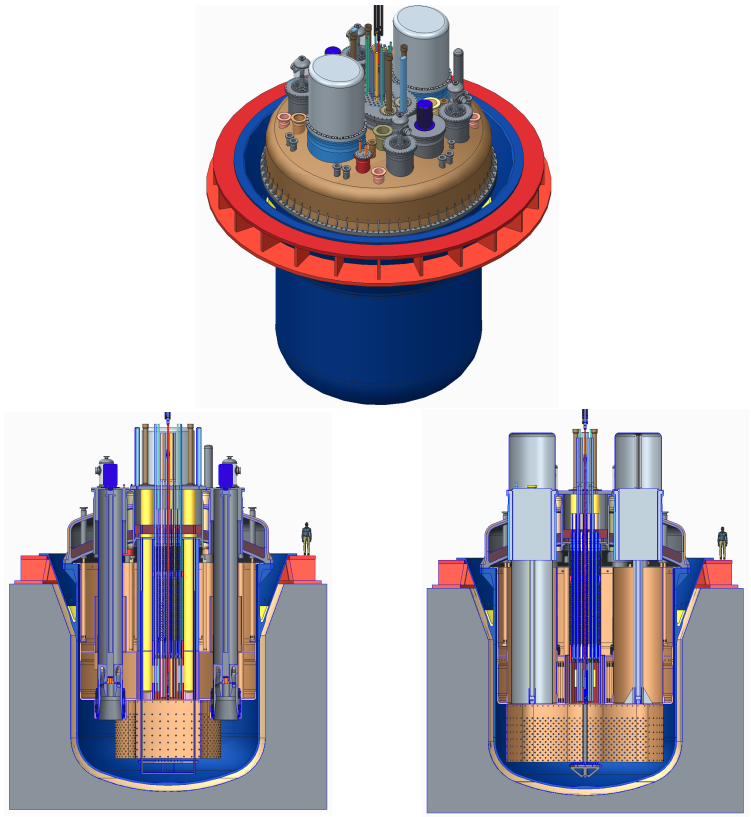

Figure 6.1: Overview of the MYRRHA-FASTEF reactor.

6.1.1 Reactor vessel

The reactor vessel houses all the safety-related primary systems and is closed by the reactor cover which supports all the in-vessel components.

The reactor vessel comprises two main components which are connected to each other:

- The reactor vessel body;
- The reactor vessel skirt.

The reactor vessel body consists of a torispherical bottom head, a cylindrical shell and a flange reinforced by gussets. The reactor vessel skirt is composed by a conical shell and a flange connected to the support ring. The reactor cover, which closes the reactor vessel from the top by means of a gas-tight connection, has the following functions:

- Primary cover gas containment;
- Radioactive products containment;
- Thermal shielding: the temperature outside the cover shall not be higher than 60 °C;
- Radiological shielding;
- Support of all the primary system in-vessel components.

6.1.2 Diaphragm

The diaphragm, located in the reactor main vessel, is a key component that separates the hot and cold LBE, supports the In-Vessel Fuel Storage (IVFS) and provides a pressure separation. More specifically, its main functions are:

- To separate the cold, high pressure plenum from the hot, low pressure plenum;
- To foresee penetrations for the components towards the cold plenum;
- To seal the components interfaces between the two plena;
- To accommodate the in-vessel fuel storage (IVFS);
- IVFS shall remain sub-critical under all normal and accident conditions;
- The neutronic coupling between the IVFS and the core shall be negligible.

In the current design, the diaphragm consists of two horizontal plates connected to each other by means of the outer shell and of the chimneys. The outer shell and chimneys have a thickening in correspondence with upper and lower horizontal plates. The two plates, the outer cylindrical shell and the chimneys separate the cold, high pressure plenum from the hot, low pressure plenum. The volume between the two plates is divided into five zones with different pressures and temperatures. The layout of these volumes and of the whole diaphragm is shown in Figure 6.2.

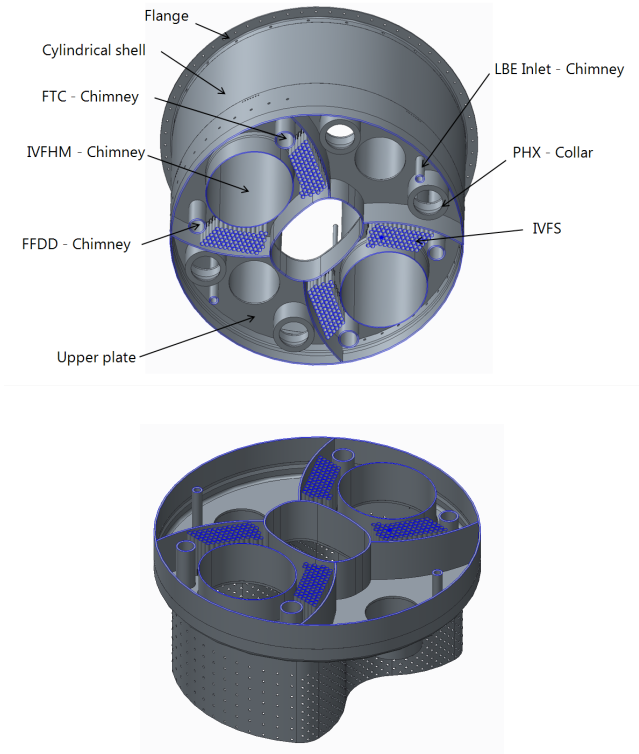

Figure 6.2: Diaphragm structure layout.

6.1.3 Core

The core is held in place by the core support structure consisting of a core barrel and a core support plate. It consists of MOX fuel pins, typical for fast spectrum reactors design. In sub-critical mode, the central hexagon houses the proton beam tube. Thirty-seven positions can be occupied by in-pile test sections (IPS) or by the spallation target

(the central one of the core in sub-critical configuration) or by control and shutdown rods (in the core critical configuration). This design gives a large flexibility in the choice of the more suitable position (neutron flux) for each experiment.

In total, 211 positions are available and subdivided as follows [92]:

- 108 fuel assemblies (FA)
- 4 In-pile structures
- 6 Control Rods
- 3 Safety Rods
- 42 Inner Dummies
- 48 Outer Dummies

The core layout is shown in Figure 6.3.

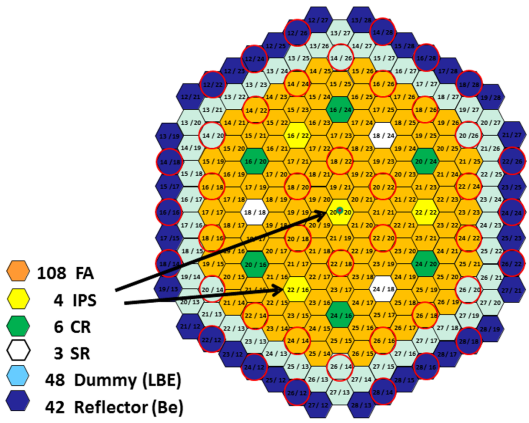

Figure 6.3: Layout of the MYRRHA core.

The in-pile sections are conceived to allow for the introduction of samples to be irradiated in different conditions and of instrumentation to monitor main core parameters. The inner dummies have the same hexagonal shape of fuel assemblies but contain no fuel, while the outer dummies include YZrO instead of fuel pellets in order to reduce the radiation damage induced by the neutron flux on the core barrel. The flow area through the inner and outer dummies is considered a bypass for the core as the LBE flows in this region without receiving any considerable heat

flux, therefore almost no temperature difference is expected between inlet and outlet of this region. The FA design is similar to the typical design used in sodium-cooled reactors; each FA contains a hexagonal bundle of 127 cylindrical fuel pins, surrounded by a hexagonal wrapper. The upper and lower ends of the wrapper are connected to the inlet and outlet nozzles guiding the LBE coolant through the FA. Each fuel pin contains fuel pellets and free space for filling and fission gases. The helical wirespacers wound on the outer surface of fuel pins keep them separated one from another in the bundle.

6.1.4 Primary Heat Exchangers (PHX)

The main thermal connection between the primary and the secondary system is provided by the Primary Heat Exchangers (PHX), operated with a water-steam mixture. The main functions of the PHXs are:

- Normal operation mode: during normal operation, the PHX must be able to remove the power generated by the reactor core and by all the other heat sources (pumps, polonium decay, IVFS). It has been designed for 110% of the nominal core power, in order to take into account these additional heat sources. The PHXs operate in forced circulation regimes on both sides (LBE and water).
- Decay Heat Removal (DHR) condition mode: in case of accidental situation, the whole reactor (primary, secondary and tertiary systems) must be able to operate in passive conditions (natural circulation) in order to guarantee the DHR function. The combined secondary and tertiary system assumes then the role of DHR-1 system.
- Maintenance mode: during shutdown periods, once the decay heat power is low enough to be compensated by the thermal heat losses through the reactor primary vessel, it is necessary to provide power to the primary LBE in order to prevent solidification. This can be done through the LBE conditioning system and/or by heating the secondary water with an external power source and then transferring power to the primary LBE through the PHX operating in a "reverse" mode.

The PHXs are designed as counter-current shell-and-tube heat exchangers. The layout of the component and the main operating parameters are shown in Figure 6.4. LBE from the hot plenum enters the PHX from

the inlet openings in the external shroud. The flow is then directed downwards, through the tube bundle, where the actual heat exchange takes place. Outlet openings, directing the LBE flow towards the primary pumps, provides the exit path for the cold (270 °C) LBE. On the secondary side, water at a pressure of 16 bar at nearly saturated conditions (200 °C) flows downward in the central down-comer pipe into the PHX bottom head, and then upwards through the tubes where it is heated by the counter-current flowing LBE, thus producing a water steam mixture with a final quality of 0.3.

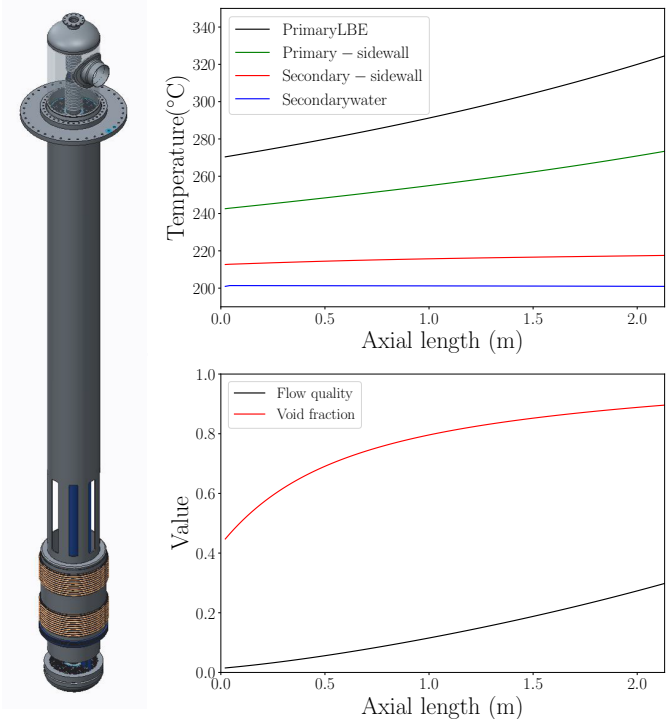

Figure 6.4: MYRRHA Primary Heat Exchanger: component layout and operating parameters.

6.1.5 Primary Pumps (PP)

The design of the primary pumps is still under development. The main requirements and constrains are related to available space, velocity of the LBE in the impeller of the pump (related to erosion issues), cavitation and the need for the flow not to be bent too much when flowing through the pump in natural circulation to avoid high pressure losses. At present,

the component is configured as axial centrifugal pump, as shown in Figure 6.5.

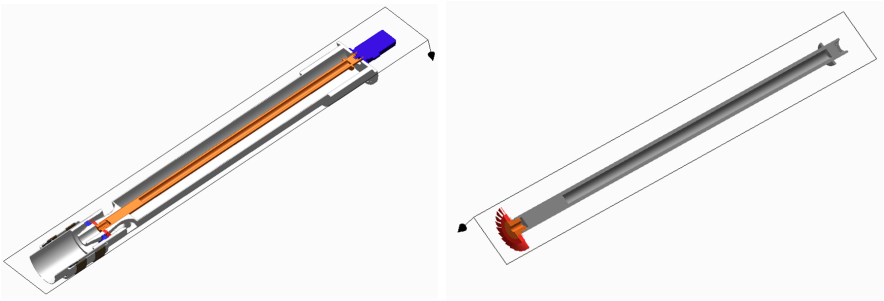

Figure 6.5: MYRRHA primary pump layout.

6.1.6 In-vessel Fuel Handling Machines (IVFHMs)

Two in-vessel fuel-handling machines, located at opposite sides of the core and covering each one side of the core, are foreseen in the current design version. Each machine is based on the well-known fast reactor technology of the 'rotating plug' concept using SCARA (Selective Compliant Assembly Robot Arm) robots. To extract or insert the FA, the robot arm can move up or down for about 2 m. A gripper and guide arm is used to handle the FAs: the gripper locks the FA, and the guide has two functions, namely to hold the FA in the vertical orientation and to ensure neighboring FAs are not disturbed when a FA is extracted from the core. An ultrasonic sensor is used to uniquely identify the FAs. The IVFHM will also perform in-vessel inspection and enentually recovery of an unconstrained FA. Incremental single-point scanning of the diaphragm can be performed by a sensor mounted at the gripper of the IVFHM. The baffle under the diaphragm is crucial for the strategy as it limits the work area where inspection and recovery are needed. It eliminates also the need of additional recovery and inspection manipulators, prevents items from migrating into the space between the diaphragm and the reactor cover, and permits side scanning.

6.1.7 Secondary and tertiary cooling systems

Each PHX unit is linked to a secondary loop operated in a forced flow regime with a two-phase water mixture at 16 bar (200 °C): the water enters the PHX in almost saturated conditions and exits with a quality

of about 0.3. The moisture is then separated in a steam drum, from where the steam is directed towards an air condenser (one per secondary loop) and the water is recirculated to the PHX. In normal operation the secondary water temperature is kept constant by the control system, letting the primary LBE conditions to change as a function of the core loading. The steam dissipates the heat to the external environment through the tertiary system air condenser and is then recirculated into the steam drum. Each tertiary system contains an air fan operated in forced circulation and logically connected to the steam drum pressure for power removal balance. A conceptual scheme of secondary and tertiary systems is represented in Figure 6.6.

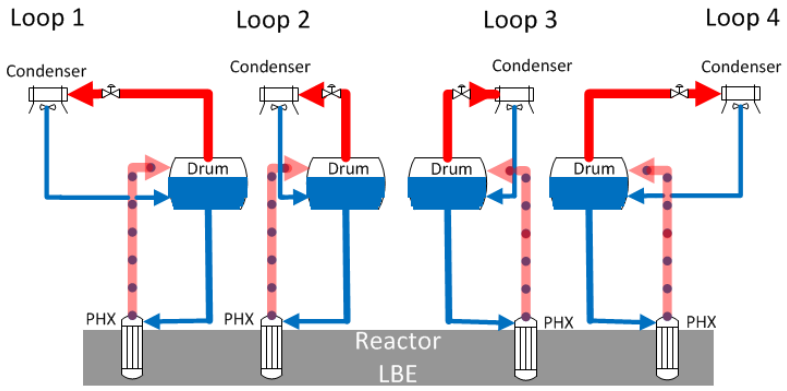

Figure 6.6: Conceptual scheme of the water/steam secondary and air tertiary cooling systems.

6.1.8 System parameters

The primary LBE coolant flows from the lower plenum (LP) into the core (270 °C) and, from there, into the upper plenum (UP) where it mixes with the cold by-pass flow. The average UP temperature is 325 °C. The four PHX units receive the LBE from the UP, which then flows into two primary pumps (PPs) (one PP serving two PHXs). From the PP boxes, the LBE is pumped back into the LP. Above the LBE free surface level an inert gas layer (Nitrogen) separates the primary coolant from the reactor cover.

Some operating parameters and characteristics of the current design version 1.6 are listed in Table 6.1

Table 6.1: MYRRHA characteristics and design values

Parameter (unit)	Value
Maximum core power (MWth)	100.0
Reactor power (MWth)	110.0
Fuel type	MOX
Core total mass flow rate (kg/s)	7710
Maximum core inlet temperature (°C)	270.0
Average core outlet temperature (°C)	360.0
Max. fuel cladding temperature (°C)	466.0
Core max. temperature difference (°C)	187.0
Upper plenum temperature (°C)	325.0
Plena temperature difference (°C)	55
Maximum core pressure drop (bar)	2.5
Primary pump mass flow rate (kg/s)	6900.0
PHX secondary pressure (bar)	16.0
PHX secondary coolant temperature (°C)	200.0

6.2 Computational models description

6.2.1 1D RELAP5-3D model

One of the main objectives of this work was to identify possible shortcomings in the analysis of LOF transients with a full STH model, by comparison against a coupled model. An ad-hoc simplified model of the MYRRHA primary system has been developed to this purpose. To allow for meaningful comparisons, the 1D code input for the components of the system computed also in the coupled model has to be identical. This introduces some constraints in the development of the 1D nodalization, which has to be such to allow for a correct implementation of the coupling hydraulic interfaces, thus it has to reflect with enough fidelity the real geometry of the regions of interest. The model of the core is certainly one of the most delicate in this regard, since hydraulic coupling interfaces are located at both core inlet and outlet boundaries, as it will be further discussed in subsection 6.2.2. In the present nodalization, the core is modeled following a homogenization approach in radial zones, originally developed for stand-alone CFD simulations [93, 94].

As depicted in Figure 6.7, the core model is structured in 5 concentric rings representing from the center: the inner FA (FA1), the combination IPS+CR+SR (IPS), the outer FA (FA2), the inner (B1) and the outer

dummies (B2).

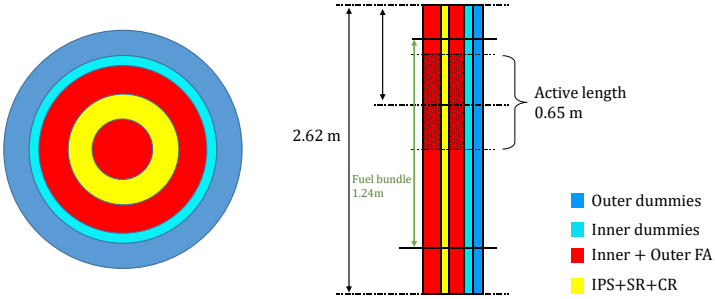

(a) Core homogenization approach in radial zones.

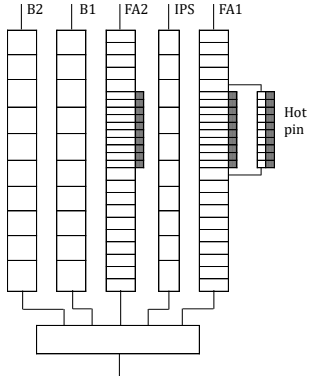

(b) RELAP5-3D nodalization of the core structured in 5 channels representing the different radial homogeneous zone.

Figure 6.7: MYRRHA core model implementation.

In the fuel assembly (FA1 and FA2) channels, the Rehme correlation is implemented for the evaluation of the Darcy friction factor f by using Reynolds-dependent junction form loss coefficients [95]. The correlation is reported below:

$$f = \left(\frac{64}{Re_{D_h}} \sqrt{F} + \frac{0.0816}{Re_{D_h}^{0.133}} F^{0.9335} \right) \frac{N_r \pi (D_r + D_w)}{s} \tag{6.1}$$

in which N_r is the number of pins, D_r is the clad outer diameter, D_w is the wire diameter, s is the wetted perimeter and F is a geometrical factor. Re_{D_h} is the Reynolds number, associated to the hydraulic diameter D_h.

The power generation in the core active region is introduced by means of heat structure components in the two channels FA1 and FA2, where a cosinusoidal power distribution is implemented. The Kazimi-Carelli correlation is used to evaluate the LBE heat transfer coefficient in the fuel bundles [96]:

$$Nu_{D_h} = 4.0 + 0.33\left(\frac{P}{D}\right)^{3.8}\left(\frac{Pe_{D_h}}{100}\right)^{0.86} + 0.16\left(\frac{P}{D}\right)^{5} \tag{6.2}$$

where P is the rod pitch, D is the rod diameter, Pe_{D_h} is the Péclet number, calculated on the basis of the hydraulic diameter D_h, already defined in chapter 5. The correlation is valid for $1.1 < P/D < 1.4$ and $10 < Pe_{D_h} < 5000$. The Nusselt number Nu_{D_h}, associated with the hydraulic diameter D_h, is defined as:

$$Nu_{D_h} = \frac{hD_h}{k} \tag{6.3}$$

where k is the thermal conductivity and h is the convective heat transfer coefficient.

The LP is modeled with the use of a single volume component. The ACS and UP are modeled by vertical pipe components, connected to each other through cross junctions in order to simulate the coolant flow through the barrel holes. Four junctions connect an intermediate volume of the UP to the PHXs which in turn are connected, in pairs, to the pump boxes and successively to the two primary pumps. At the PHX heat structure, the Ushakov correlation is used to evaluate the convective heat transfer coefficient at the LBE side, considering that the value of the ratio P/D is outside the range of validity for the application of the Kazimi-Carelli correlation (Equation 6.2). The Ushakov correlation is reported below [97]:

$$Nu_{D_h} = 7.55\frac{P}{D} - 20\left(\frac{P}{D}\right)^{-3} + \frac{3.67Pe_{D_h}^{(0.19\frac{P}{D}+0.56)}}{90(\frac{P}{D})^2} \tag{6.4}$$

Conjugate heat transfer between UP, cold annulus and IVFHM is also computed through heat structure components.

The 1D model of the whole reactor primary cooling system is shown in Figure 6.8.

In the study presented in this work, whose main objective is the application and assessment of the coupling methodology on a reactor-scale (primary cooling system) analysis, the secondary and tertiary systems

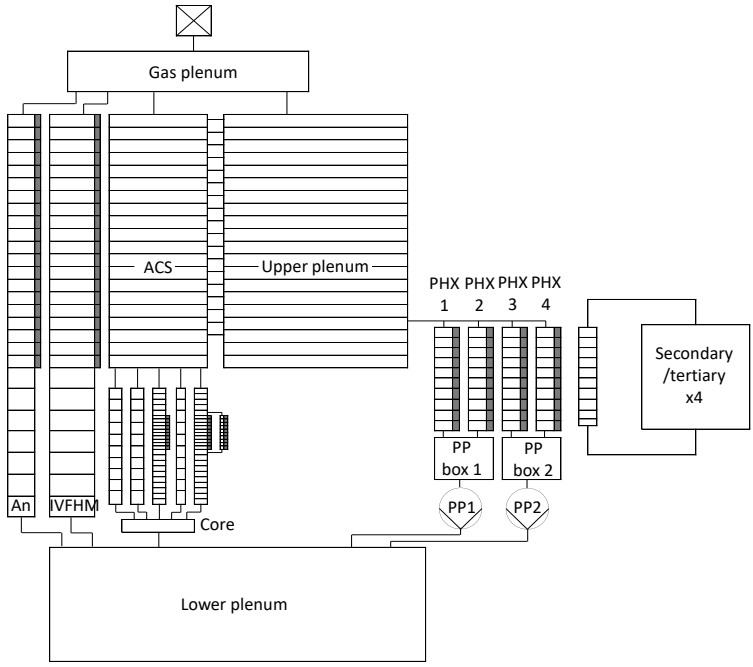

Figure 6.8: Overview of the RELAP5-3D full nodalization of the MYRRHA primary cooling system.

have been modeled by boundary conditions. For those transients in which the model of the secondary and tertiary systems is required, it can be added in the 1D nodalization without requiring any further modification of the coupling settings.

6.2.2 RELAP5-3D/FLUENT coupled model

I. Domain decomposition and models

In the MYRRHA primary system, the lower and upper plenum are coolant regions characterized by flow fields of pronounced three-dimensional nature, therefore they are modeled using the CFD code. The confined flow regions of the primary system, namely the core, PHXs and circulating pumps, as well as secondary and tertiary systems if required, remain to be computed by the system code. As it was done for the full coupled model of the pool-type facility E-SCAPE, also the annular region of the cold plenum and the IVFHM chimneys, interested by free surface flows, are computed by the CFD code to

simplify the implementation of the model and minimize the number of hydraulic coupling interfaces. The decomposition of the domain and the CFD models of the hot and cold plenum are shown in Figure 6.9.

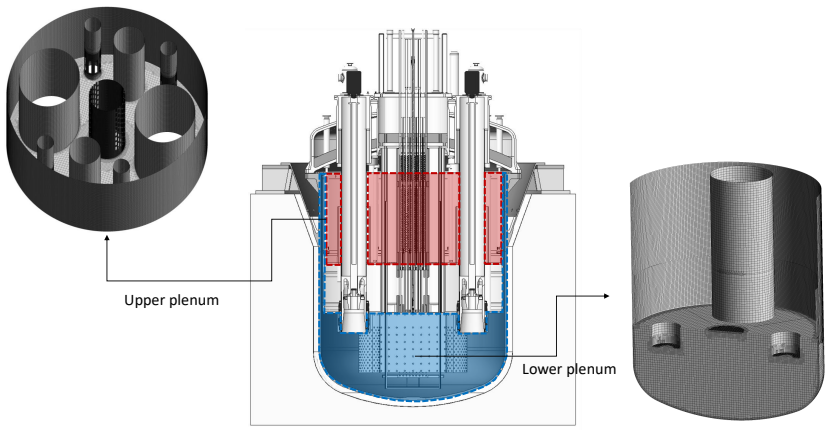

Figure 6.9: Decomposition of the MYRRHA primary cooling system, with highlighted the regions of the vessel computed by the CFD code.

It is worth remarking that the presented decomposition of the domain is such to allow for an optimal and appropriate use of both the 1D system thermal-hydraulic and the CFD codes. In particular, it enables the full exploitation of the 1D system code built-in specific modeling capabilities for core (eventually including neutronics modules to take into account reactivity feedbacks, reactor shutdown logic, etc.), secondary and tertiary loops operation, circulating pumps dedicated models etc. On the other side, the use of the CFD code is limited only to those regions interested by 3D flows, bypassing in this way the significant implementation efforts that would be required to model the entire plant.

For both the CFD domains of the lower and upper plenum, a HEX-dominant Cartesian computational grid is generated, counting about $4.0 \cdot 10^6$ cells, with a consequent optimization of cell counts as well as the improvement of solution stability for free surface flow computations. Even in this case, the two-phase VOF model is used to compute free surface level variations and the $SST\ k-\omega$ turbulence model is adopted.

In the LP, the baffle component is neglected in order to avoid an excessive size of the model which would result in significant computational power requirements. Furthermore, this component is not expected to have a

relevant impact on the global thermal-hydraulic behavior and on safety-relevant parameters. In the UP, the ACS, which is a very complex structure, is modeled as a porous medium, characterized by a value of porosity of 0.91. Porous media are modeled by the addition of a momentum source term to the standard fluid flow equations. The source term is composed of two parts, a viscous loss term and an inertial loss term [63]:

$$S_i = -\left(\sum_{j=1}^{3} D_{ij} \mu v_j + \sum_{j=1}^{3} C_{ij} \frac{1}{2} \rho |v| v_j \right) \tag{6.5}$$

Following [94], also in this model viscous losses are neglected and only the second term representing inertial resistance is considered. These coefficients are evaluated in order to obtain the expected pressure drop of 0.3 bar in normal operating conditions. Solid structures are not computed, and the conjugate heat transfer between upper plenum and cold annulus is calculated through a thin wall model approach.

For what concerns the 1D portion of the model, the regions computed by the CFD code are removed from the full nodalization and replaced by appropriate boundary condition components (time-dependent volume and single junctions). It was already remarked that the input for the components that are kept in the 1D nodalization is not modified.

II. Coupling settings

Based on the discussed decomposition of the system, hydraulic coupling interfaces are located at the core inlet and outlet sections, the inlet of the PHXs and the PP outlets, as shown in the conceptual scheme of Figure 6.10.

For all these interfaces, as it was already tested for the simulation of E-SCAPE, mass flow rate is passed from the 1D code to CFD, while pressure value averaged on the interface section is transferred in the opposite direction. As in E-SCAPE, this choice is allowed by the compressibility of the CFD domain introduced by the presence of the cover gas region, where the pressure level in the system is set through a boundary condition. Energy terms data is passed in both directions, and used by the coupled codes according to the direction of the flow.

According to the chosen domain decomposition and interface BC exchange, 12 hydraulic interfaces are implemented in the current model of MYRRHA, namely 5 core channels outlets (FA1, IPS, FA2, B1, B2), 4 PHX inlet, 2 PP outlet and the core inlet section. The method previously tested to reduce to degree-of-freedom is adopted by considering

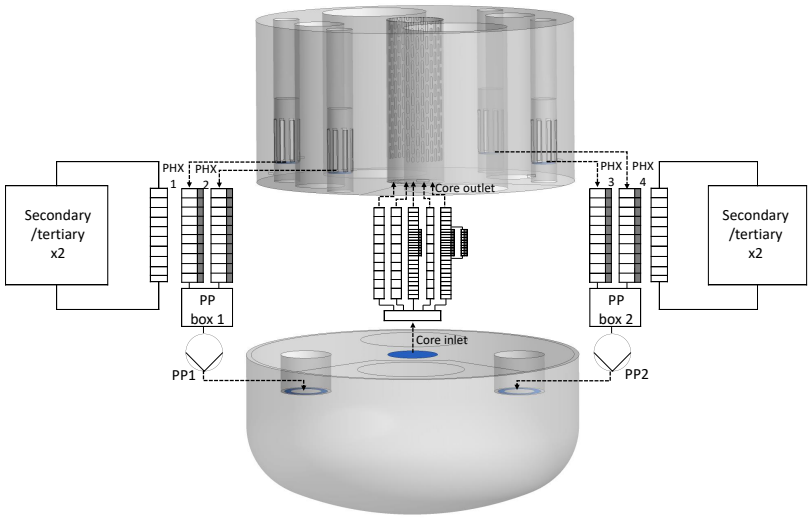

Figure 6.10: Conceptual scheme of the domain decomposition and location of the hydraulic coupling interfaces.

only total inlet and outlet flow rate in the CFD regions (upper and lower plenum). In the developed model, the CFD input vector considered for the under-relaxation algorithm is:

$$
{}^{n}\mathbf{U}^{k}_{CFD} = \begin{bmatrix}
{}^{n}\dot{m}^{k}_{c\_in} = \sum_{j=1}^{n_{c\_in}} {}^{n}\dot{m}^{k}_{c\_in_j} \\
{}^{n}\dot{m}^{k}_{c\_out} = \sum_{j=1}^{n_{c\_out}} {}^{n}\dot{m}^{k}_{c\_out_j} \\
{}^{n}\dot{m}^{k}_{phx} = \sum_{j=1}^{n_{phx}} {}^{n}\dot{m}^{k}_{phx_j} \\
{}^{n}\dot{m}^{k}_{pp} = \sum_{j=1}^{n_{pp}} {}^{n}\dot{m}^{k}_{pp_j}
\end{bmatrix} \tag{6.6}
$$

where $n_{c\_in} = 1$, $n_{c\_out} = 5$, $n_{phx} = 4$ and $n_{pp} = 2$. To approximate the $\nu \times \nu$ Jacobian, ν coupling iterations are required; in the present model, $\nu = 4$.

6.3 Simulation results

6.3.1 Forced circulation conditions

The same computational strategy discussed for E-SCAPE has been adopted, thus performing first a full STH model computation of the forced circulation condition, extracting then interface BC used in a stand-alone CFD simulation. After that, a coupled simulation is launched which leads to new steady state results. Main BC and computed parameters are summarized in Table 6.2.

Table 6.2: Forced circulation steady-state results

Parameter (unit)	RELAP5-3D	RELAP5-3D/FLUENT
Core power (MWth)	110.0	110.0
Total core mass flow rate (kg/s)	13611.4	13573.2
Active core mass flow rate (kg/s)	7669.1	7613.5
Core inlet temperature (°C)	271.5	272.9
Inner fuel assemblies outlet temperature (°C)	403.8	403.7
Hot channel outlet temperature (°C)	465.8	468.9
Primary pump head (bar)	2.42	2.53

As in E-SCAPE, in forced circulation operating conditions, due to the pressure difference between the cold and hot plenum, the free surface levels in the IVFHM chimneys and cold annulus are higher than in the UP. This difference roughly corresponds to the pressure drops in the core. Also, in the UP the free surface is slightly higher in the ACS than in the rest of volume, because of the pressure drops in the ACS and barrel holes. The velocity and temperature profiles in cold and hot plena in forced circulation operation are shown in Figure 6.11. Details of the velocity and temperature profiles at the LBE free surface are shown in Figure 6.12

6.3.2 Protected LOF transient simulation

The transient selected in this work to test the coupled model on is a protected loss of flow (PLOF) event. From normal operating conditions, the accidental transient is triggered by a sudden trip of both PPs (according to a coast-down curve) followed by immediate reactor shutdown. Studies for a unprotected event, which is characterized by a similar hydraulic behavior and progression of the transient in its first phase, were already

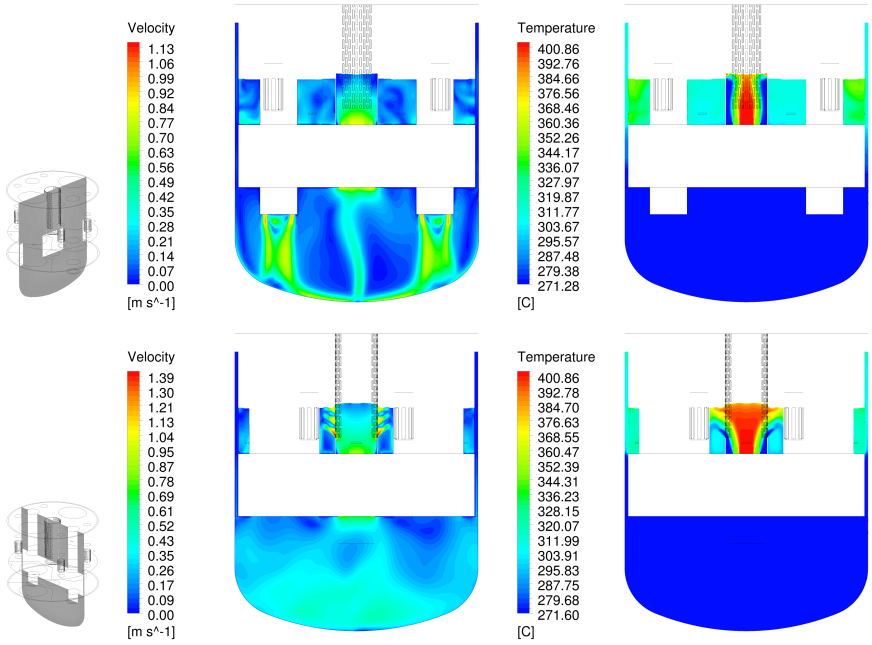

Figure 6.11: Velocity and temperature contours on the z-x (top) and z-y (bottom) planes in forced circulating conditions.

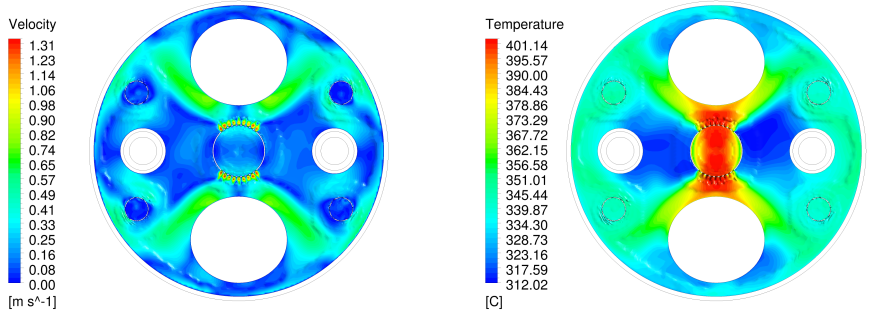

Figure 6.12: Velocity (left) and temperature (right) profiles at the LBE free surface.

carried out using stand-alone STH and CFD codes [93]. In the present analysis, a conservative value of reactor shutdown delay of 3 seconds is considered. A decay heat curve, established on the basis of the code ALEPH2 and conservative factors, is used in this transient as well as for MYRRHA DBC2, DBC3 and DBC4 safety analyses [98]. The rated power over time after the reactor shutdown is shown in Figure 6.13.

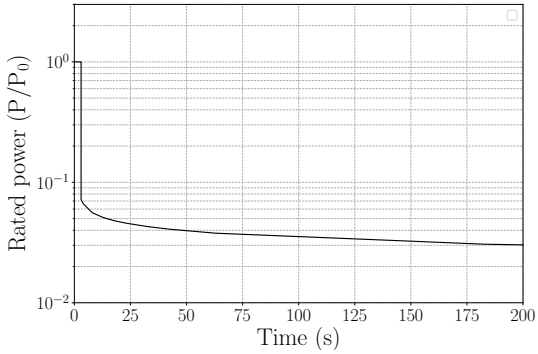

Figure 6.13: Core power after reactor shutdown during PLOF accident

After the pump trip and the insertion of the control rods, natural circulation is set in the primary pool, while secondary and tertiary systems operation continues normally. The primary pumps head over time calculated in the two simulations is shown in Figure 6.14.

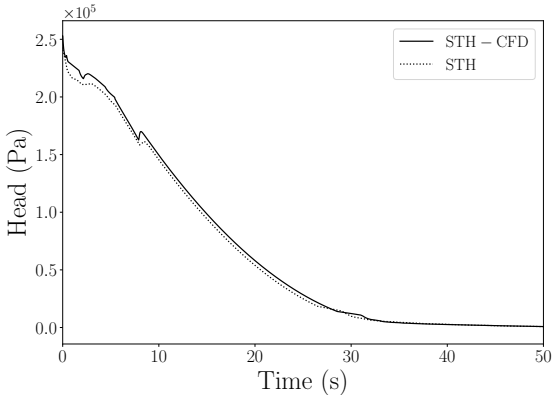

Figure 6.14: Primary pumps head during PLOF accident.

The computed time evolution of the mass flow rates in the primary system is shown in Figure 6.15. The pressure evolution at the inlet and outlet sections of the core, which reflects the free surface levels variation following the shutdown of the pumps, is shown in Figure 6.16. As it can be observed, the stand-alone system code and the coupled calculation are in a remarkable agreement, and the core flow rate in natural circulation is almost the same, only slightly lower in the coupled calculation. Flow reversal in the primary pumps after their trip occurs in the first 30 seconds of the transient, and predicted by both the simulations.

The temperature evolution in the key locations of the primary cooling

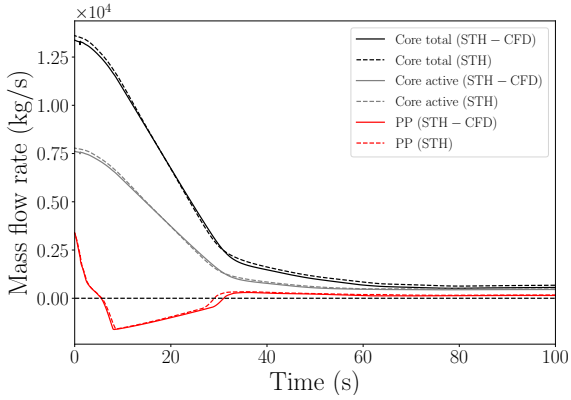

Figure 6.15: Mass flow rates evolution during PLOF accident.

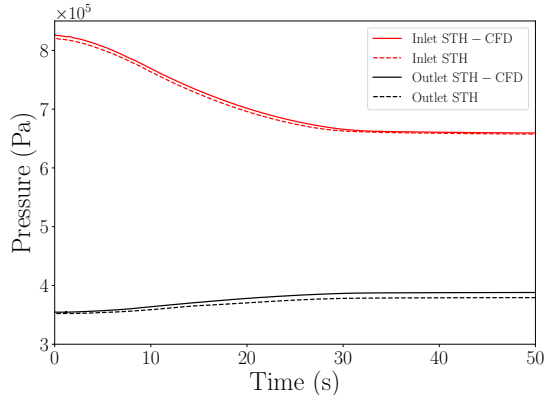

Figure 6.16: Core inlet and outlet pressure evolution during PLOF accident.

system are shown in Figure 6.17. It can be observed that the safety-relevant parameters i.e. the peak cladding temperature (PCT), is not subject to relevant discrepancies between the two calculations, remaining far from the acceptable safety limit as a result of the effective establishment of natural circulation.

Some differences can be observed at the inlet of the PHX, where flow reversal occurs. These differences arise from the fact that in the 1D code, volume averaging is computed between the hot plenum and the LBE coming from the cold plenum through the pumps. The CFD simulation shows that, within the time window in which flow reversal occurs, the cold fluid is confined within a limited region, and that the thermal mixing is scarce due to the short duration of the flow inversion. Therefore, when the flow changes direction from upwards to downwards

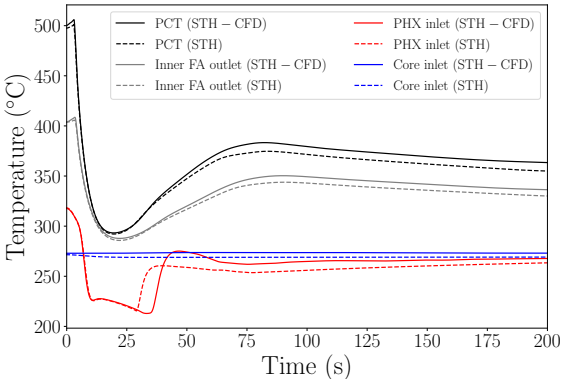

Figure 6.17: Temperatures evolution during PLOF accident.

again, the temperature at the PHX inlet remains low for a longer period of time, and higher temperature is successively observed when the hot fluid originally filling the UP reaches the PHX inlet. This effect can be visualized by observing Figure 6.18, which shows the progression of the flow and temperature profiles on a cross section cutting a PHX. Such effect, although it has not relevant impact in the safety parameters for this transient, shows the effectiveness of the coupling method in predicting complex local phenomena that may occur in a pool-type system.

The evolution of the temperature contour on a vertical cross section (plane z-y) is shown in Figure 6.19. After the reactor trip, the mass flow rate rapidly drops, and the free surface levels start decreasing in the cold annulus and IVFHM, and increasing in the UP. After about 30 s, the free surfaces have reached approximately the same level, given the very small pressure drops at such low flow conditions. The core outlet temperature begins to decrease immediately after the reactor shutdown and the reduction of the power to decay heat levels. Colder fluid starts therefore reaching the UP; due to the continued normal operation of the secondary and tertiary systems (constant BC in this simulation), after a certain time window the temperature at the outlet of the PHX entering the cold plenum decreases as well. Even in the LP, incipient development of thermal stratification can be observed. Further studies might be needed to investigate in more details the long-term thermal-hydraulic behavior of the system.

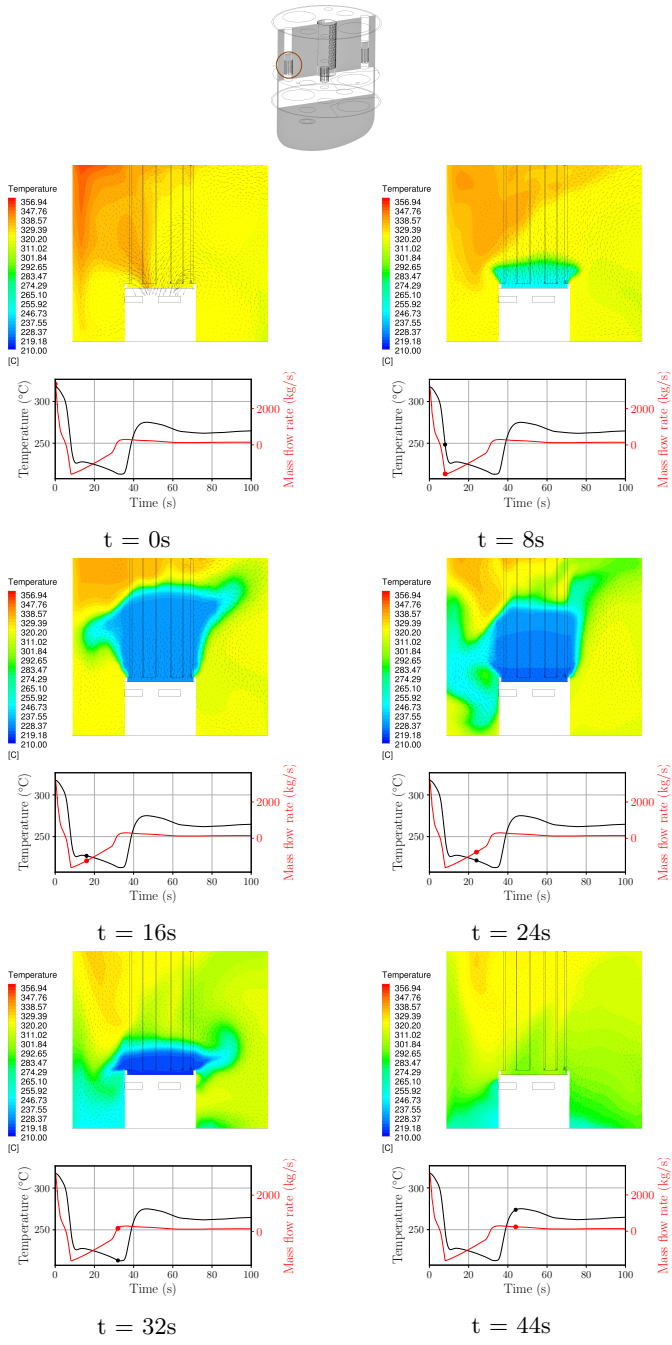

Figure 6.18: Temperature evolution at the inlet of the PHX within the flow inversion time window in the first phase of the PLOF transient.

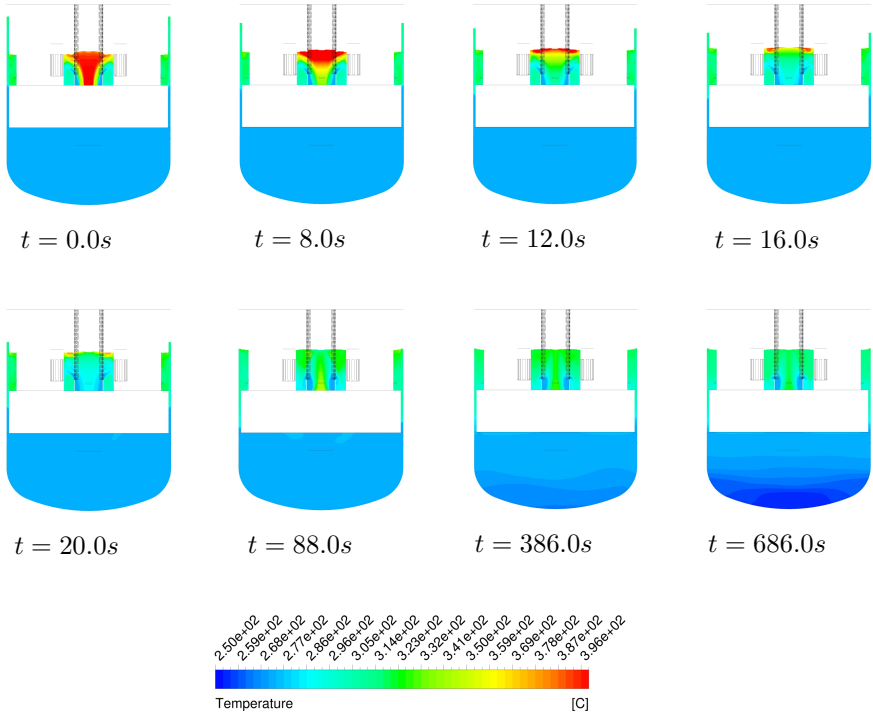

Figure 6.19: Time evolution of the temperature profile in the UP and LP following the pumps trip and reactor shutdown in a PLOF event.

6.4 Conclusions

As a demonstrative application of the developed STH-CFD coupling methodology to a reactor-scale simulation, a fully coupled model of the MYRRHA reactor has been developed as last step of the thesis. The model integrates a CFD model of the main regions of the primary vessels, namely cold and hot plenum, annulus and IVFHM, and the 1D model of the reactor core, primary heat exchangers, primary pumps and secondary/tertiary cooling systems. Such domain decomposition is conceived to exploit to the maximum extent the specific modeling capabilities of the adopted codes, and to ensure limiting the required computational costs in order to be able to compute medium- and long-term transients. Given the large number of hydraulic coupling interfaces required, the developed numerical technique to reduce the number of degree of freedom of the implicit coupling numerical algorithm has been successfully adopted.

A reference protected loss of flow transient has been simulated to assess the system behavior and to compare the results of the coupled simulation against stand-alone system thermal-hydraulic data, reference tool for licensing analyses. The simulation showed good agreement between the two models in term of integral behavior, suggesting that no particular 3D effects impact the evolution of the postulated event. Differences in local temperatures have been however observed when complex mixing effects occur, for instance in flow reversal situations at the inlet of the primary heat exchangers. Overall, this study pointed out that the developed multi-scale computational method is suitable for integral transient simulations in a nuclear reactor while taking into account the potential effect of 3D phenomena at acceptable computational costs.

Chapter 7

Conclusions and future developments

7.1 Summary and main conclusions

7.1.1 Coupling method development

The present doctoral research project has focused on the investigation, development, preliminary validation and application of a new computational methodology to perform multi-scale transient flow simulation in advanced nuclear reactors. The work addresses particular issues related to the thermal-hydraulic and safety assessment of the MYRRHA reactor, the main framework of the project, and more generally of pool-type liquid metal-cooled systems. Nevertheless, the developed computational tool has potential applications to any reactor system, including current nuclear power plants based on light water reactors. More in detail, the research has focused on the implementation of a partitioned coupling methodology which makes use of the system thermal-hydraulic code RELAP5-3D, reference tool for MYRRHA safety assessments, and the commercial CFD code FLUENT. The methodology is conceived to allow for a more accurate computation of the primary cooling system response to transient conditions, especially when impacted by three-dimensional thermal-hydraulic phenomena, generally of difficult prediction for industry-standard system codes. With regard to the MYRRHA design, the method is of particular relevance to assess effects such as flow mixing and thermal stratification in loss of flow events, dyssymmetric conditions among others.

Among the two main strategies that can be adopted for partitioned coupling implementations, namely the domain decomposition and domain overlapping techniques, the research work focused on the former, which envisages the division of the original computational domain into two or more sub-domains, coupled via the dynamic exchange of boundary conditions at coupling interfaces. To implement this technique, a new software infrastructure based on a supervisor code, written in Python language, has been developed to drive the exchange of data and compute numerical algorithms. This master process runs in parallel to and communicate with the CFD code, and executes the whole STH code block as an internal subroutine. The FLUENT code is executed via a special input file to perform the coupling instructions, and contains a UDF, written for parallel computations, to send and receive interface BC data.

An important part of the research project has been centered on the investigation of coupling numerical schemes and their testing on simple verification cases such as open and closed pipe flow configurations. The main conclusions of this part of the work can be summarized as follow:

- Exchanged boundary conditions have to be such to guarantee that fluid-transported quantities, particularly mass and energy, are conserved at the interfaces. In the developed tool, mass flow rate BC is passed in one direction, while pressure in the opposite one. Temperature BC is transferred in both forward and backward directions, and is used in the solution according to the direction of the flow. While passing data from a 3D to a 1D codes simply requires surface averaging, some physical approximations are introduced when converting 1D data to 2D profiles required by the CFD code. In this work, flat velocity profiles are used, considering that the error introduced has been proven to be small and negligible in the applications of interest.

- Explicit schemes, which imply that boundary conditions are exchanged only once in a coupling time step, are often prone to numerical instabilities, particularly in the case of fast transients in incompressible fluid systems characterized by small pressure drops. The numerical instabilities, caused by imbalance of the momentum terms at the interfaces, were found to be dependent on the characteristic size of the coupled domains and the location of the coupling interfaces.

- Implicit schemes with coupling iterations within each time step improve numerical stability and allow relaxing the constraints in

the size of the coupling time step. To improve convergence rate and reduce computational costs, advanced schemes based on dynamic relaxation algorithms have been tested. Among them, remarkable improvements were achieved with the use of a Quasi-Newton coupling scheme, whose implementation represents one of the major achievements of the research work. The algorithm is based on the approximation of the residual function through a first order Taylor expansion, with the terms of the Jacobian matrix approximated via finite differences.

7.1.2 Validation on TALL-3D

A first validation study of the coupling methodology against experimental data was based on the experimental campaign performed at the test facility TALL-3D. The LBE loop, operated at the KTH in Sweden, is particularly conceived to support the assessment of coupled STH-CFD codes by foreseeing transients with mutual feedback between 3D effects in a dedicated pool test section and the rest of the loop. The tool was applied to the analysis of the transient test T01.09, a loss of forced circulation test characterized by an oscillating transition from forced to natural circulation. The main conclusions can be summarized as follows:

- The coupled simulation led to a better agreement, compared to stand-alone system thermal-hydraulic calculation, with measured data. The analysis pointed out the capability of the multi-scale approach to predict the impact of 3D transient flow fields on monitored system parameters, and to compute more accurately the characteristic frequency and damping of the mass flow rate and temperature oscillations observed in the experimental test.

- The discrepancies observed were mostly attributed to model deficiencies in the single codes, and not to modeling choices related to the coupling method. These differences were related to the inaccurate prediction of pressure and heat losses in the STH loop, and the non sufficiently accurate simulation of a LBE impinging jet in the pool test section by the CFD model.

The overall results, in line with the main findings of a specific benchmark on TALL-3D performed within the EU project THINS, confirmed the validity of the multi-scale approach and its capability to improve standard STH analyses.

7.1.3 Pool-type systems application

Based on the TALL-3D validation analysis, the tool has been applied in the last part of the project to the simulation of pool-type systems. The implementation of such models was evidently more complex, as characterized by larger number of hydraulic coupling interfaces and more demanding modeling requirements (e.g. multi-phase flow computation in both solvers, conjugate heat transfer). To avoid significant increase of the computational costs associated with the use of the developed Quasi-Newton scheme, a novel numerical methodology to reduce the degree-of-freedom of the problem has been developed and successfully applied. The technique is based on considering in the coupling hydrodynamic algorithm only net flow rates in the coupled domains, on which the overall pressure-velocity fields coupling depends, and successively reconstructing BC values such to satisfy both new computed total flow rates and variations in the distribution of the single interface quantities. Furthermore, the modeling capabilities of the tool have been further extended through the implementation of thermal coupling interfaces to allow for the computation of conjugate heat transfer.

The pool-type system applications presented in the dissertation are the E-SCAPE facility and, final goal of the project, the MYRRHA reactor. The former, which represents a major framework for the validation of thermal-hydraulic codes on MYRRHA-relevant phenomena and transient scenarios, is a scaled model of the MYRRHA primary cooling system, aimed at investigating thermal-hydraulic behavior of a pool-type system operated with LBE, as well as at generating validation-grade experimental data. A coupled model was first built with focus on the hot plenum; a pre-test analysis of a loss of flow test was carried out and the results were compared against a full STH reference model. An overall good agreement was observed, although some discrepancies on certain local parameters were noticed, particularly when core flow reversal conditions occur. Such differences were found to be related to 3D temperature profiles in regions of the upper plenum, not possible to be correctly accounted for through the perfect mixing formulation of the STH code. A partial loss of flow transient, characterized by strong dissymmetries of the flow field in the upper plenum, was also simulated and a good agreement was observed. Successively, a fully coupled model including both upper and lower plenum in the CFD domain has been implemented. The simulation of a similar total loss of flow transient led to comparable results.

The same implementation strategy has been adopted for the develop-

ment of a fully coupled model of MYRRHA, which has been applied on the simulation of a reference protected loss of flow event, triggered by the instantaneous failure of both primary circulating pumps immediately followed by reactor shutdown. The simulation confirmed previous findings i.e. an overall agreement in transient behavior and some differences in the transient evolution of some monitored temperatures when particular flow conditions occur.

The analyses on these two systems suggest that 3D effects seem not to have a remarkable impact on the evolution of the analyzed scenarios, in terms of global system behavior. Nevertheless, significant discrepancies might be caused on local temperatures prediction in certain key locations of the system, which may result in non conservative estimations of safety-relevant parameters. Furthermore, the coupled simulations allowed for the visualization and assessment of transient phenomena such as the development of thermal stratification, which might have an impact on the long-term behavior in natural circulation.

7.2 Future work

7.2.1 Methodology/code infrastructure development

A potential improvement of the coupling methodology that will require further investigation is the implementation of more accurate boundary conditions at hydraulic coupling interfaces in the CFD domain. In this regard, more realistic velocity profiles and, if required, extrapolated inlet turbulence parameters e.g. through empirical correlations, can lead to some improvements of the simulation accuracy. However, it appears challenging to establish a general methodology for these aspects, considering that they are usually case-dependent and related to the particular location of the hydraulic coupling interfaces and the local flow characteristics.

Further domain for future developments of the computational method is certainly its software architecture. Enhanced automation of coupling settings generation will be beneficial to ensure the flexibility of the tool and to allow for its application on different systems with minimum user effect and modifications of the source code. Furthermore, at present the exchange of data between the processes is carried out by using plain text files. The implementation of more sophisticated message passing techniques e.g. parallel virtual machine (PVM) would certainly represent an improvement of the tool. However, it is worth remarking

that the overall gain in computational speed is expected to be limited, as at present the CFD code takes up most of the total computational runtime.

For what concerns numerical aspects, the research project explored several schemes that are applicable in a black-box implementation, and no drastic improvements on this aspect are to be expected. The access to the single codes' source might allow for further exploration of numerical algorithms and schemes executed through the modification of the set of governing equations. Furthermore, as the developed coupling schemes are based on black box formulation, with both the solvers represented only by an input-output operator, their application can be extended to CFD-like Reduced Order Model (ROM).

7.2.2 V&V programme

In order to apply the multi-scale tool on reactor safety and licensing analyses, a detailed V&V programme will have to be established and pursued, which will represent a major undertaking.

As discussed, the use of well validated STH and CFD codes is the fundamental pre-requisite for accurate coupled simulations, as it was directly demonstrated within the simulation work performed on the TALL-3D facility. This objective has not been fully reached yet for LBE technology, and large initiatives at national and international level are currently ongoing on this matter.

The V&V of coupled codes requires integral test data, possibly of experiments featuring mutual feedback between flow phenomena in subcomponents and the complete system behavior. It was discussed in this dissertation that a major framework for the validation of the tool is represented by the E-SCAPE experimental campaign. The experimental data-set to be generated will be used first for the validation of the stand-alone models in relation to the regions and phenomena relevant to them. Successively, integral test data will be used for the validation of the coupling tool. To this purpose, a complete validation matrix, the specification and use of validation metrics and acceptance criteria, the methodology for the quantification of uncertain input parameters and the related uncertainty will have to be further assessed and developed.

List of Figures

List of Tables

Bibliography

[1] International Atomic Energy Agency (IAEA), "Power Reactor Information System (PRIS)," .

[2] OECD Nuclear Energy Agency (NEA), "Nuclear Energy Data 2016," .

[3] International Atomic Energy Agency, *Status of Fast Reactor Research and Technology Development. IAEA TECDOC No. 1691* (2013).

[4] International Atomic Energy Agency, *Implications of Partitioning and Transmutation in Radioactive Waste Management. Technical Reports Series No. 435* (2004).

[5] US DOE Nuclear Energy Research Advisory Committee, "A Technology Roadmap for Generation IV Nuclear Energy Systems GIF-002-00," Tech. Rep. (2002).

[6] Sustainable Nuclear Energy Technology Platform, "Sustainable Nuclear Energy Technology Platform (SNETP)," .

[7] H. A. Abderrahim, P. Baeten, D. D. Bruyn, and R. Fernandez, "MYRRHA – A multi-purpose fast spectrum research reactor," *Energy Conversion and Management* **63**, 4 (2012), 10th International Conference on Sustainable Energy Technologies (SET 2011).

[8] A. Petruzzi and F. D'Auria, "Thermal-Hydraulic System Codes in Nulcear Reactor Safety and Qualification Procedures," *Science and Technology of Nuclear Installations* **2008** (2008), http://dx.doi.org/10.1155/2008/460795.

[9] INL, "RELAP5-3D Code Manuals Revision 2.3, Idaho National Lab, Idaho Falls, ID," (2005).

[10] U. S. Nuclear Regulatory Commission, "TRACE V5.0 Theory Manual," (2010).

[11] Gesellschaft für Anlagenund Reaktorsicherheit (GRS) mbH, "ATHLET Mod 3.1 Cycle A. Program Overview," (2016).

[12] D. Tenchine, R. Baviere, P. Bazin, F. Ducros, G. Geffraye, D. Kadri, F. Perdu, D. Pialla, B. R. B., and N. Tauveron, "Status of CATHARE code for sodium cooled fast reactors," *Nuclear Engineering and Design* **245**, 140 (2012).

[13] T. Höhne, E. Krepper, and U. Rohde, "Application of CFD Codes in Nuclear Reactor Safety Analysis," *Science and Technology of Nuclear Installations* **2010** (2010), https://doi.org/10.1155/2010/198758.

[14] A. Papukchiev, F. Roelofs, A. Shams, G. Lecrivain, and W. Ambrosini, "Development and application of computational fluid dynamics approaches within the European project THINS for the simulation of next generation nuclear power systems," *Nuclear Engineering and Design* **290**, 13 (2015), thermal-Hydraulics of Innovative Nuclear Systems.

[15] F. Roelofs, K. Van Tichelen, and D. Tenchine, "Status and Future Challenges of Liquid Metal Cooled Reactor Thermal-Hydraulics," *In: Proceedings of NURETH15, Pisa, Italy* (2013).

[16] IAEA, "Summary Report, Technical Meeting on Priorities in Modelling and Simulation for Fast Neutron Systems, Vienna, Austria," (2014).

[17] F. Roelofs, K. Van Tichelen, and M. Tarantino, "European Thermal-Hydraulic Progress for Sodium and Lead Fast Reactors," *In: Proceedings of NURETH17, Xi'an, Shaanxi, China, Sept. 3-8, 2017* (2017).

[18] F. Roelofs and C. Chavardes, "SESAME. Thermal hydraulics Simulations and Experiments for the Safety Assessment of MEtal cooled reactors. D6.7 version 1," Tech. Rep. (2015).

[19] O. Zienkiewicz and R. Taylor, *Finite Element Method: Volume 1 - The Basis*, 5th ed. (Butterworth-Heinemann, Oxford, 2000).

[20] H. G. and M. Steindorf, *Strong Coupling Methods* (2002).

[21] L. Mengali, M. Lanfredini, F. Moretti, F. D'Auria, "Stato dell'arte sull'accoppiamento fra codici di sistema e di fluldodlnamica computazionale. Applicazione generale su sistemi a metallo liquido pesante. Report CERSE-UNIPI RL 1509/2011." Tech. Rep. (2012).

[22] G. E. Wilson and B. E. Boyack, "The role of the PIRT process in experiments, code development and code applications associated with reactor safety analysis," *Nuclear Engineering and Design* **186**, 23 (1998).

[23] S. Yong Lee, J.-J. Jeong, S.-H. Kim, and S. Chang, "COBRA/RELAP5. A merged version of the COBRA-TF and RELAP5/MOD3 codes," *Nuclear Technology*, **99**, 177 (1992).

[24] D. Aumiller, E. Tomlinson, and R. Bauer, "A coupled RELAP5-3D/CFD methodology with a proof-of-principle calculation," *Nuclear Engineering and Design* **205**, 83 (2001).

[25] J.-J. Jeong, S. Sim, C. Ban, and C. Park, "Assessment of the COBRA/RELAP5 code using the LOFT L2–3 large-break loss-of-coolant experiment," *Annals of Nuclear Energy* **24**, 1171 (1997).

[26] J.-J. Jeong, K. Ha, B. Chung, and W. Lee, "Development of a multi-dimensional thermal-hydraulic system code, MARS 1.3.1," *Annals of Nuclear Energy* **26**, 1611 (1999).

[27] W. Weaver, E. Tomlinson, and D. Aumiller, "A generic semi-implicit coupling methodology for use in RELAP5-3D," *Nuclear Engineering and Design* **211**, 13 (2002).

[28] R. R. Schultz, "Validating and Verifying a New Thermal-Hydraulic Analysis Tool," (2002).

[29] R. R. Schultz and W. L. Weaver, "Coupling the RELAP5-3D advanced systems analysis code with commercial and advanced CFD software," *Proceedings of IAEA Technical Meeting Use of CFD Codes for Safety Analysis of Reactor Systems Pisa, Italy, November 11-13, 2002* (2002).

[30] N. Anderson, Y. Hassan, and R. Schultz, "Analysis of the hot gas flow in the outlet plenum of the very high temperature reactor using coupled RELAP5-3D system code and a CFD code," *Nuclear Engineering and Design* **238**, 274 (2008).

[31] Y. Yan and Rizwan-uddin, "Coupled CFD-System code simulation of a gas cooled reactor," *Proc. of the International Conference on Mathematics and Computational Methods Applied to Nuclear Science and Engineering (M&C 2011), Rio de Janeiro, Brazil, May 8-12, 2011* .

[32] W. Li, X. Wu, D. Zhang, G. Su, W. Tian, and S. Qiu, "Preliminary study of coupling CFD code FLUENT and system code RELAP5," *Annals of Nuclear Energy* **73**, 96 (2014).

[33] Y. Yan, Rizwan-uddin, and K. Kim, "A Coupled CFD-System Code Development and Application," *Proc. of the International Conference on the Physics of Reactors "Nuclear Power: A Sustainable Resource"* (2008).

[34] D. Bertolotto, A. Manera, S. Frey, H.-M. Prasser, and R. Chawla, "Single-phase mixing studies by means of a directly coupled CFD/system-code tool," *Annals of Nuclear Energy* **36**, 310 (2009), pHYSOR 2008.

[35] D. Bertolotto, *Coupling a System Code with Computational Fluid Dynamics for the Simulation of Complex Coolant Reactivity Effects. Doctoral thesis*, Ph.D. thesis, École polytechnique fédérale de Lausanne EPFL (2011).

[36] A. Papukchiev, G. Lerchl, C. Waata, and T. Frank, "Extension of the simulation capabilities of the 1D system code ATHLET by coupling with the 3D CFD software package ANSYS CFX," *In: Proc. The 13th International Topical Meeting on Nuclear Reactor Thermal Hydraulics (NURETH-13), Kanazawa City, Ishikawa Prefecture, Japan* (2009).

[37] B. Chanaron, C. Ahnert, N. Crouzet, V. Sanchez, N. Kolev, O. Marchand, S. Kliem, and A. Papukchiev, "Advanced multiphysics simulation for reactor safety in the framework of the nuresafe project," *Annals of Nuclear Energy* **84**, 166 (2015), multi-Physics Modelling of LWR Static and Transient Behaviour.

[38] M. Angelucci, D. Martelli, G. Barone, I. D. Piazza, and N. F. (in press), "STH-CFD codes coupled calculations applied to HLM loop and pool systems," *Science and Technology of Nuclear Installations* (2017).

[39] B. Farges, T. Sageaux, and N. Goreaud, "STAR-CD / CATHARE coupling methodology for thermal-hydraulic calculations on pri-

mary loop and heat exchangers in sodium-cooled fast reactor," *Proc. IAEA International Conference on Fast Reactors and Related Fuel Cycles: Safe Technologies and Sustainable Development (FR13), 4–7 March 2013*, (2013).

[40] J. W. T. R. Hu, E. Munkhzul, and T. H. Fanning, "Development of sfr primary system simulation capability for advanced system codes," Tech. Rep. (Argonne National Laboratory, ANL/NE-13/11, 2013).

[41] D. Wu, S. Yang, P. Wu, and L. Wang, "MOC-CFD Coupled Approach for the Analysis of the Fluid Dynamic Interaction between Water Hammer and Pump," *Journal of Hydraulic Engineering* **141**, 06015003 (2015).

[42] J. Galindo, A. Tiseira, P. Fajardo, and R. Navarro, "Coupling methodology of 1D finite difference and 3D finite volume CFD codes based on the Method of Characteristics," *Mathematical and Computer Modelling* **54**, 1738 (2011), mathematical models of addictive behaviour, medicine & engineering.

[43] G. Bella, R. Rotondi, G. Defranco, and N. Nigro, in *Mecánica Computacional Vol. XXII* (2003).

[44] A. C. I. Malossi, P. J. Blanco, P. Crosetto, S. Deparis, and A. Quarteroni, "Implicit coupling of one-dimensional and three-dimensional blood flow models with compliant vessels," *Multiscale Modeling & Simulation* **11**, 474 (2013), https://doi.org/10.1137/120867408 .

[45] L. Formaggia, F. Nobile, A. Quarteroni, and A. Veneziani, "Multiscale modelling of the circulatory system: a preliminary analysis," *Computing and Visualization in Science* **2**, 75 (1999).

[46] T. Dobroserdova, M. Olshanskii, and S. Simakov, "Multiscale coupling of compliant and rigid walls blood flow models," *International Journal for Numerical Methods in Fluids* **82**, 799 (2016), fld.4241.

[47] T. Grunloh and A. Manera, "A novel multi-scale domain overlapping CFD/STH coupling methodology for multi-dimensional flows relevant to nuclear applications," *Nuclear Engineering and Design* **318**, 85 (2017).

[48] R. Bavière, N. Tauveron, F. Perdu, E. Garré, and S. Li, "A first system/CFD coupled simulation of a complete nuclear reactor transient using CATHARE2 and TRIO_U. Preliminary validation on

the Phénix Reactor Natural Circulation Test," *Nuclear Engineering and Design* **277**, 124 (2014).

[49] M. A. Gerschenfeld, L. Simon, G. Yannick, B. Ulrich, and R. Lavastre, in *Proc. IAEA International Conference on Fast Reactors and Related Fuel Cycles: Next Generation Nuclear Systems for Sustainable Development (FR17)* (2017).

[50] T. Sageaux, O. Bernard, and N. Goreaud1, in *Proc. IAEA International Conference on Fast Reactors and Related Fuel Cycles: Next Generation Nuclear Systems for Sustainable Development (FR17)* (2017).

[51] M. Belliard, A. Gerschenfeld, and L. Simon, in *Proc. of NURETH-17* (2017).

[52] M. Jeltsov, K. Kööp, P. Kudinov, and W. Villanueva, in *Proc. 15th International Topical Meeting on Nuclear Reactor Thermal Hydraulics (NURETH-15)* (2013).

[53] A. Papukchiev, M. Jeltsov, K. Kööp, P. Kudinov, and G. Lerchl, "Comparison of different coupling CFD–STH approaches for pretest analysis of a TALL-3D experiment," *Nuclear Engineering and Design* **290**, 135 (2015), thermal-Hydraulics of Innovative Nuclear Systems.

[54] A. Papukchiev, C. Geffray, M. Jeltsov, K. Kööp, P. Kudinov, and D. Grischenko, "Multiscale analysis of forced and natural convection including heat tranfer phenomena in the TALL-3D experimental facility. Proc. of NURETH-16, Chicago, IL, August 30-September 4," (2015).

[55] D. Tenchine, D. Pialla, T. Fanning, J. Thomas, P. Chellapandi, Y. Shvetsov, L. Maas, H.-Y. Jeong, K. Mikityuk, A. Chenu, H. Mochizuki, and S. Monti, "International benchmark on the natural convection test in Phenix reactor," *Nuclear Engineering and Design* **258**, 189 (2013).

[56] J. W. Thomas, T. H. Fanning, R. Vilim, and L. L. Briggs, "Validation of the integration of CFD and SAS4A/SASSYS-1: Analysis of EBR-II shutdown heat removal test 17," (American Nuclear Society - ANS; La Grange Park (United States), 2012).

[57] A. Gerschenfeld, "Multi-scale simulations of liquid metal systems. Thermohydraulics and chemistry of liquid metal cooled reactors,

Von Karman Institute for Fluid Dynamics, Lecture Series 2017-02," (2017).

[58] A. Toti, F. Belloni, and J. Vierendeels, "Development and preliminary validation of a STH-CFD coupling method for multi-scale thermal-hydraulic simulations of the MYRRHA reactor," *In: Proc. of the 24th International Conference on Nuclear Engineering ICONE24, Charlotte, NC, USA, 26-29 June* (2016).

[59] A. Toti, J. Vierendeels, and F. Belloni, "Improved numerical algorithm and experimental validation of a system thermal-hydraulic/cfd coupling method for multi-scale transient simulations of pool-type reactors," *Annals of Nuclear Energy* **103**, 36 (2017).

[60] H. K. Versteeg and W. Malalasekera, *An Introduction to Computational Fluid Dynamics. The Finite Volume Method* (Longman Group Ltd., London, 1995).

[61] J. Ferziger and M. Perić, *Computational Methods for Fluid Dynamics*, Numerical methods : research and development (Springer, 1996).

[62] B. Launder and D. Spalding, "The numerical computation of turbulent flows," *Computer Methods in Applied Mechanics and Engineering* **3**, 269 (1974).

[63] ANSYS Inc., *ANSYS Fluent Release 12.0 Theory Guide* (2009).

[64] J. Bear, *Dynamics of Fluids in Porous Media*, Dover Civil and Mechanical Engineering Series (Dover, 1972).

[65] C. Hirt and B. Nichols, "Volume of fluid (vof) method for the dynamics of free boundaries," *Journal of Computational Physics* **39**, 201 (1981).

[66] INL, "RELAP5-3D Code Manual Volume I: Code Structure, System Models and Solution Methods," (2014).

[67] V. Ransom, "Course a—numerical modeling of two-phase flows for presentation at ecole d'ete d'analyse numerique," (1989).

[68] R. J. Wagner, "HEAT-1 – A One-Dimensional Time Dependent or Steady State Heat Conduction Code for the IBM-650, National Reactor Testing Station, 1963," Tech. Rep. (1963).

[69] U. Küttler, "Fixed-point fluid–structure interaction solvers with dynamic relaxation," *Comput Mech* **43**, 61 (2008).

[70] American Institute of Aeronautics and Astronautics, "Computational Fluid Dynamics Committee on Standards, "Guide for the Verification and Validation of Computational Fluid Dynamics Simulations"," *AIAA-G-077-1998, Reston, VA, 1998* (1998).

[71] W. L. Oberkampf and T. G. Trucano, "Verification and validation benchmarks," *Nuclear Engineering and Design* **238**, 716 (2008), benchmarking of CFD Codes for Application to Nuclear Reactor Safety.

[72] M. Jeltsov, F. Cadinu, W. Villanueva, A. Karbojian, K. Kööp, and P. Kudinov, "An approach to validation of coupled CFD and system thermal-hydraulics codes," *14th International Topical Meeting on Nuclear Reactor Thermalhydraulics (NURETH-14), Toronto, Canada, September 25-30, 2011* (2011).

[73] D. Grishchenko, M. Jeltsov, K. Kööp, A. Karbojian, W. Villanueva, and P. Kudinov, "The TALL-3D facility design and commissioning tests for validation of coupled STH and CFD codes," *Nuclear Engineering and Design* **290**, 144 (2015), thermal-Hydraulics of Innovative Nuclear Systems.

[74] P. Planquart and K. V. Tichelen, "Experimental investigation of accidental scenarios using a scale water model of a HLM reactor," *In: Proceedings of NURETH17, Xi'an, Shaanxi, China, Sept. 3-8, 2017* (2017).

[75] S. Annerel, J. Degroote, J. Vierendeels, T. Claessens, P. V. Ransbeeck, S. Kaarstad, B. Skallerud, L. R. Hellevik, P. Segers, and P. Verdonck, "Application of a strong FSI coupling scheme for the numerical simulation of bileaflet mechanical heart valve dynamics: study of wall shear stress on the valve leaflets," *Progress in computational fluid dynamics* **12(2-3)**, 68 (2012).

[76] X. Cheng, "European activities on crosscutting thermal-hydraulic phenomena for innovative nuclear systems," *Nuclear Engineering and Design* **290**, 2 (2015).

[77] R. L. Moore, "Implementation of DOWTHERM A Properties into RELAP5-3D/ATHENA," (2010), 10.2172/1037788.

[78] T. Hamidouche, "Assessment of RELAP/SCDAPSIM Mod 4.0 for LBE cooled systems application. Restricted contract report SCKCEN-R-5616," Tech. Rep. (SCKCEN, 2014).

[79] OECD-NEA, *Handbook on Lead-bismuth Eutectic Alloy and Lead Properties, Materials Compatibility, Thermal-hydraulics and Technologies* (OECD-NEA, 2007).

[80] M. Jeltsov, K. Kööp, W. Villanueva, D. Grishchenko, and P. Kudinov, in *:* (Atomic Energy Society of Japan, 2014) qC 20150427.

[81] A. Toti, J. Vierendeels, and F. Belloni, "Extension and application on a pool-type test facility of a system thermal-hydraulic/cfd coupling method for transient flow analyses," *Nuclear Engineering and Design (In press)* ().

[82] A. Toti, J. Vierendeels, and F. Belloni, "Numerical analysis of a dissymmetric transient in the pool-type facility e-scape through coupled system thermal-hydraulic and cfd codes," *In: Proceedings of NURETH17, Xi'an, Shaanxi, China, Sept. 3-8, 2017* ().

[83] H. Ait Abderrahim, "MYRRHA Technical Description. SCK-CEN/593205/42," Tech. Rep. (2011).

[84] K. V. Tichelen, F. Mirelli, M. Greco, and G. Viviani, "E-scape: A scale facility for liquid-metal, pool-type reactor thermal hydraulic investigations," *Nuclear Engineering and Design* **290**, 65 (2015), thermal-Hydraulics of Innovative Nuclear Systems.

[85] M. Greco, F. Mirelli, K. V. Tichelen, and S. Eckert, "Report on the HLM pool experiments: facility description and pre-test analysis. THINS project - Deliverable D2.1.08," Tech. Rep. (2015).

[86] A. Toti, J. Vierendeels, and F. Belloni, "Coupled system thermal-hydraulic/cfd analysis of a protected loss of flow transient in the myrrha reactor," *Annals of Nuclear Energy* **118**, 199 (2018).

[87] D. D. Bruyn, S. Larmignat, A. Woaye-Hune, and C. Artioli, "Accelerator driven systems for transmutation: Main design achievements of the XT-ADS and EFIT systems within the FP6 IP-EUROTRANS integrated project," *Proc. of ICAPP'10, San Diego, CA, USA, June 13-17, 2010* (2010).

[88] D. Castelliti and P. Baeten, "MYRRHA/FASTEF Safety Analysis in Sub-Critical and Critical Mode," *Proc. of NURETH-15, May 2013, Pisa, Italy* (2013).

[89] "FP7 MAXSIMA project Grant Agreement, SCK•CEN, August 2012," Tech. Rep. (2012).

[90] H. A. Abderrahim, "Multi-purpose hybrid research reactor for high-tech applications a multipurpose fast spectrum research reactor," *International Journal of Energy Research* **36**, 1331 (2012).

[91] M. Iamele, "MYRRHA Technical Description Rev.1.6. SCK•CEN/1148931," Tech. Rep. (2014).

[92] M. Sarotto, "Possible working range of the MYRRHA core and basic neutronic parameters for safety analyses," *Deliverable 2.1, EC FP7 MAXSIMA project* (2014).

[93] F. Andreoli, D. Bisogni, F. Belloni, and G. Scheveneels, "Influence of the 3D phenomena on the safety parameters during ULOF accident in the MYRRHA reactor," *Proc. of NURETH-16, Chicago, IL, August 30 - September 4, 2015* (2015).

[94] L. Koloszar, S. Buckingham, P. Planquart, and S. Keijers, "MyrrhaFoam: A CFD model for the study of the thermal hydraulic behavior of MYRRHA," *Nuclear Engineering and Design* **312**, 256 (2017), 16th International Topical Meeting on Nuclear Reactor Thermal Hydraulics.

[95] K. Rehme and G. Trippe, "Pressure drop and velocity distribution in rod bundles with spacer grids," *Nuclear Engineering and Design* **62**, 349 (1980).

[96] N. E. Todreas and M. Kazimi, *Nuclear Systems I-II* (Taylor and Francis, 1990).

[97] P. Ushakov, A. Zhukov, and M. Matyukhin, "Heat transfer to liquid metals in regular arrays of fuel elements," *High Temperature* **15**, 868 (1977).

[98] T. Hamidouche, "Envelop decay curves for MYRRHA safety studies," *Internal report SCK•CEN/1719280* (2016).